NTNU – Trondheim
Norwegian University of
Science and Technology

Dynamic Model Predictive Control for Load Sharing in Electric Power Plants for Ships

Torstein Ingebrigtsen Bø

Marine Technology
Submission date: June 2012
Supervisor: Roger Skjetne, IMT
Co-supervisor: Tor Arne Johansen, ITK

Norwegian University of Science and Technology
Department of Marine Technology

Learn from yesterday, live for today,
hope for tomorrow. The important thing
is to not stop questioning.

ALBERT EINSTEIN

NTNU Trondheim
Norwegian University of Science and Technology
Department of Marine Technology

PROJECT DESCRIPTION SHEET

Name of the candidate:	Torstein Ingebrigtsen Bø
Field of study:	Marine control engineering.
Thesis title (Norwegian):	Dynamisk modellprediktiv regulering for lastdeling i elektriske kraftsystem om bord i skip.
Thesis title (English):	Dynamic model predictive control (MPC) for load sharing in electric power plants for ships.

Background
During the last 20 years, maritime electric installations have increased in size and scope ranging from only few systems and installations to become an industry standard. Several research groups have addressed this topic from different perspectives both nationally and internationally. The Norwegian maritime industry is having a leading role in the development of advanced technology improving safety and performance of DP operated offshore vessels.

In advanced ships and offshore installations the main power consumers are connected to the energy sources through an electric distribution network. The trend is towards more complex electric networks and more diverse energy sources that may combine small and large diesel engines, fuel cells, batteries, gas turbines/engines, and others. The complexity of the network, and the diversity in dynamic behavior, offers many opportunities for optimizing energy consumption and maintenance costs due to tear and wear through automatic control based on numerical optimization and dynamic models. Safety requirements to the system and its operation, such as limiting dimensions, fault isolation, and reconfiguration in terms of acceptable transient and steady-state responses to normal load variations and abnormal fault events in the electric power generation and distribution system, should be implemented as constraints.

Work description
1. Perform a literature study on dynamic load sharing control using numerical optimization and dynamic models in the context of vehicles (not only ships) and isolated installations (weak grids).
2. Formulate the dynamic load sharing control problem as an MPC problem.
3. Implement a constrained MPC strategy in Matlab using numerical optimization.
4. Demonstrate the loadsharing MPC using a simulation case study that incorporates a number of energy sources with different dynamics, generators, and an electric distribution network.
5. Develop and demonstrate a method for handling of failure cases.

Guidelines
The scope of work may prove to be larger than initially anticipated. By the approval from the supervisor, described topics may be deleted or reduced in extent without consequences with regard to grading.

The candidate shall present his personal contribution to the resolution of problems within the scope of work. Theories and conclusions should be based on mathematical derivations and logic reasoning identifying the various steps in the deduction.

The report shall be organized in a rational manner to give a clear exposition of results, assessments, and conclusions. The text should be brief and to the point, with a clear language. The report shall be written in English (preferably US) and contain the following elements: Abstract, acknowledgements, table of

contents, main body, conclusions with recommendations for further work, list of symbols and acronyms, references and (optional) appendices. All figures, tables, and equations shall be numerated. The original contribution of the candidate and material taken from other sources shall be clearly identified. Work from other sources shall be properly acknowledged using quotations and a Harvard citation style (e.g. *natbib* Latex package). The work is expected to be conducted in an honest and ethical manner, without any sort of plagiarism and misconduct. Such practice is taken very seriously by the university and will have consequences. NTNU can use the results freely in research and teaching by proper referencing, unless otherwise agreed upon.

The thesis shall be submitted in 3 printed copies, each signed by the candidate. The final revised version of this project description must be included. The report must appear in a bound volume or a binder according to the NTNU standard template. Computer code and a PDF version of the report should be included electronically.

A 15 min. presentation (conference style) on your status, intermediate results, and plan for completion is expected to be delivered at a scheduled time midway into the project period.

Start date: January 15, 2012 **Due date:** As specified by the administration.

Supervisor: Roger Skjetne
Co-advisor(s): Tor Arne Johansen (Prof., ITK) and Aleksander Veksler (Ph.d. cand., ITK)

Trondheim,

_____

Roger Skjetne
Supervisor

Summary

The main contribution of this thesis is an investigation of model predictive control (MPC) for marine diesel electric power plants. Recommendations and new ideas for further development are emphasized.

The motivation of the thesis is to develop a controller for diesel electric power plants that can control the plant in a more efficient way. This includes reducing wear and tear, fuel consumption, and emissions. However, the safety aspect is always the most important factor and must be handled with care.

The case plant to be studied is a diesel electrical power plant consisting of several diesel driven generators (genset). These gensets produce electrical power to serve the electrical demands on a marine vessel. The consumers can be propulsion units, heave compensators, drilling equipment, and hotel loads. These highly dynamic consumers are large compared with the producers. This gives unwanted fluctuation of frequency. In some vessels this effect is so large that more gensets are required for transients than for peak demands. This can be avoided with better control strategies.

The controller developed in this thesis adjusts the local controllers on the diesel engines. The objective is to keep the genset at a given load sharing, while keeping the frequency within rules and regulations. In addition is the plant controlled to a state where a single point failure does not lead to blackout.

Blackout is prevented by calculating a failure case in addition to the normal case. The failure case may be a disconnection of the largest genset on the power bus segment. The case is calculated in the controller to make sure that if the case occurs the plant is able to handle the failure without a blackout. A normal case, where everything goes as normal, is calculated to optimize the current operation.

The controller is verified by simulation done in MATLAB/Simulink. The implemented controller performs well during all of the simulated cases. However, the predictions made by the controller are in some cases conservative. This is due to the choice of the fuel rate constraints. Lastly, suggestions for how to improve the performance of the controller are included. The most important suggestions are to include a model of the turbocharger in the control plant model and to include more failure cases.

Sammendrag

Hovedbidraget for denne masteroppgaven er å undersøke bruk av modell prediktiv kontroll (model predictive control) for marine diselelektriske kraftverk. I tillegg er det lagt vekt på ideer og forslag for videre utvikling av kontrolleren.

Denne avhandlingen er motivert av ønsket om å utvikle en kontroller som kan regulere diselelektriske kraftverk mer effektivt. Dette inkluderer reduksjon av slitasje, utslipp og drivstoffforbruk. Sikkerheten er den viktigste faktoren og blir derfor behandlet spesielt.

Tilfellet som blir studert er et dieselelektrisk kraftverk bestående av flere dieseldrevne generatorer (genset). Disse gensetene produserer strømmen som blir brukt av fartøyet. Forbrukerne kan være propulsjonsmotorer, hivkompensatorer, boreutstyr og hotellforbrukere. Disse forbrukerne er både store sammenlignet med produsentene og svært dynamiske. Ved noen kraftverk er denne effekten så stor at det kreves flere genset for å ta hånd om transienter, enn det kreves for å ta hånd om maksimum last. Dette kan bli unngått med bedre kontrollstrategier.

Kontrolleren i denne avhandlingen justerer de lokale kontrollerne på diesel motorene. Målet er å holde en gitt lastfordeling, samtidig som frekvensen holdes innenfor klassekrav. I tillegg reguleres kraftverket til en tilstand som gjør at punktfeil ikke fører til strømavbrudd (blackout).

I kontrolleren beregnes to hendelsesforløp, både en normal situasjon og en punktfeil. Den normale situasjonen brukes for å optimalisere nåværende situasjon. Mens punktfeilen er brukt for å sikre at strømavbrudd blir unngått etter punktfeilen. For å illustrere kontrollmetoden er en frakobling av den største generatoren brukt som punkfeil.

Kontrolleren er verifisert ved simulering gjort i MATLAB/Simulink. Den implementerte kontrolleren fungerer godt i alle simulerte situasjoner. På grunn av valget av drivstoffbegrensninger, gir kontrolleren konservative prediksjoner i noen tilfeller. Imidlertid er forslag for ytelsesforbedringer inkludert. De viktigste forslagene er å inkludere en modell av turboladeren i kontrollerens modell og å inkludere flere feilforløp.

Acknowledgment

The work of this thesis was done between January and June 2012, as a part my master's degree in Marine Technology at Norwegian University for Science and Technology (NTNU).

This thesis is a continuation of the project reported in Bø (2011), where a comparison study of models for marine power plants was presented and a new nonlinear governor developed. However, this thesis is standalone and reading the previous report is not necessary for understanding the content of this report. The comparison study and the governor presented in Bø (2011) are not included in this thesis.

The work has been supervised by Professor Roger Skjetne, from the Department of Marine Technology; Professor Tor Arne Johansen and Ph.D. candidate Aleksander Veksler, both from Department of Engineering Cybernetics.

I would like to thank Eirik Mathiesen, at Kongsberg Maritime, for inspiring discussions and for giving me insight in current marine power plants. To Professor Roger Skjetne, I would like to give thanks for introduced me to marine electrical systems and guiding me through this thesis. Thanks are given to Ph.D. candidate Aleksander Veksler for discussions of great value and inspiration.

I would like to thank my office colleagues and good friends for a good working environment. Especially would I like to thank Pål Levold, for valuable discussions regarding scientific writing.

I would like to give a special thanks to Professor Tor Arne Johansen, for introducing me to model predictive control and guiding me through the process of making the controller presented in this thesis.

Trondheim, June 10th, 2012 Torstein Ingebrigtsen Bø

Contents

List of Tables

List of Figures

Glossary

AVR Automatic voltage regulator, controls the reactive power and terminal voltage of a generator by changing the field excitation in the generator.

Bus An electrical utility that distributes the electrical power.

DP Dynamic Positioning, a control system that tries to keep a vessel at the same position and heading, by counteracting external forces from waves and wind. This is done by using thrusters to generate forces.

Fuel rate The amount of fuel flowing into engine, denoted u. In a car this is given by the position of the throttle pedal.

Genset A diesel motor connected to a generator, which delivers the power to the bus.

Governor Controls the power and speed of a genset by changing the fuel rate.

List of Acronyms

AVR Automatic Voltage Regulator

DC Direct current

DP Dynamic positioning

FLR Fast Load Reduction

LQR Linear Quadratic Regulator

MPC Model predictive control

PMS Power Management System

pu Per unit

rms Root mean square

Nomenclature

η_c	Combustion efficiency.
$\mathcal{R}$	Cost matrix for change of control input.
ω	Per unit angular velocity of diesel engine, $\frac{\omega_m}{\omega_{m,b}}$.
ω_b	Base electrical angular velocity (e.g., 120π rad s^{-1}).
$\bar{\omega}$	Per unit average frequency of the gensets connected to the bus.
ω_m	Angular velocity of diesel engine.
ω_t	Per unit speed of turbocharger.
$\omega_{m,b}$	Base mechanical angular velocity, $\frac{2}{N}\omega_b$.
ϕ_0	Difference between electrical angle of the bus and mean electrical angle of the gensets.
ϕ_i	Difference between electrical angle of Genset i and mean electrical angle of the gensets.
θ	Electrical rotor angle.
θ_m	Mechanical rotor angle.
$\boldsymbol{\omega}_{NL}$	Per unit no-load frequency.
$\boldsymbol{\varepsilon}$	Error between control output and desired output, for one time instant.
$\boldsymbol{E}$	Error between control output and desired output, for all time instant in prediction horizon.
$\boldsymbol{f}_k$	Time derivative of state variables at update time.
$\boldsymbol{u}$	Fuel rates into engines.
$\boldsymbol{x}$	State vector.
$\boldsymbol{x}_k$	State vector at update time.
$\boldsymbol{Z}$	Control output for all time instant in prediction horizon.

$\boldsymbol{z}$	Control output for one time instant.
$\boldsymbol{Z}_d$	Desired control output for all time instant in prediction horizon.
$\boldsymbol{z}_d$	Desired control output for one time instant.
$\xi_{\omega,i}$	Value of integrator in governor for Genset i.
$\xi_{v,i}$	Value of integrator in AVR for Genset i.
A	State matrix.
(A/F)	Air-to-fuel ratio, ratio between the mass flow of air and fuel into the engine.
$(\mathrm{A/F})_{high}$	Lower air-to-fuel ratio for full combustion.
$(\mathrm{A/F})_{low}$	Lower air-to-fuel ratio for any combustion.
$(\mathrm{A/F})_n$	Air-to-fuel ratio at rated power and maximum turbocharger speed.
B	Input matrix.
C	State to control output matrix.
D	Input to control output matrix.
D_f	Per unit damping constant, due to friction and windage.
$du_{max,now}$	Maximum increase of fuel rate for full combustion at time of update.
du_{max}	Maximum increase of fuel rate between two consecutive samples.
H	Inertia constant, $\frac{J_m \omega_{m,b}^2}{2S_b}$.
J	Cost function.
J_m	Moment of inertia of diesel engine and generator.
k_u	Gain from fuel rate input to per unit mechanical torque
m	Number of samples in prediction horizon.
$m_{a,0}$	Ratio between the air flow into the engine when the turbocharger is at zero speed and when it is running at full speed.
N	Number of poles of the generator.
n	Number of gensets.
p_i	Per unit active power delivered from Genset i.
p_{FLR}	Load reduced by the fast load reduction.
Q	Cost matrix for error in control output.
q_i	Per unit reactive power delivered from Genset i.
$S_{b,i}$	Base power of Generator i.
T_b	Base mechanical torque, $= \frac{S_b}{\omega_{m,b}}$.

t_D	Per unit damping torque, due to friction and windage.
t_e	Per unit electrical torque, torque from generator.
t_k	Time instant for update.
t_m	Mechanical torque from diesel engine to generator.
T_t	Time constant of turbocharger.
u_{max}	Maximum fuel rate.
u_{min}	Minimum fuel rate.
v	Per unit line-to-line bus voltage.
V_b	Base electric voltage (line-to-line).

Notation

In this thesis most of the equations are given in per unit, since it implies good numerical properties, and gives values that are easy to interpret. Variables given in upper case are given with units, and lower case variables are in per unit. All per unit variables have a base value, which gives the factor between the per unit variable and the variable with unit. For example:

$$S = sS_b. \tag{0.1}$$

Capital delta, Δ, is used to denote the difference between the value at the linearization time, t_k, and the time t:

$$\Delta x(t) = x(t) - x(t_k). \tag{0.2}$$

Lower case delta, δ, denotes the difference between two consecutive discrete time instants:

$$\delta x[i] = \Delta x[i] - \Delta x[i-1]. \tag{0.3}$$

Bold letters, for example $\boldsymbol{x}$, denotes that the variable is a vector. Matrices are written with capital letters. The root mean square (rms) value of signal $x(t)$ is defined as:

$$\lim_{T\to\infty} \sqrt{\frac{1}{T}\int_{t=0}^{T} x(t)^2 \,\mathrm{d}t}. \tag{0.4}$$

The time derivative of vector $\boldsymbol{x}(t)$ is denoted $\dot{\boldsymbol{x}}(t)$. The transpose of a vector or matrix is denoted superscript $\top$. The operator $\mathrm{diag}(a_1, a_2, \ldots, a_n)$ produces an $n \times n$ diagonal matrix, with the diagonal entries a_1,a_2,...,a_n. The vectors $\mathbf{0}$ and $\mathbf{1}$ are respectively vectors of only zeros and ones. Subscript w denotes that the predicted value is given for the failure case.

Chapter 1

Introduction

1.1 Background

A diesel electrical power system replaces the conventional diesel mechanical system. Instead of having a diesel engine directly connected to a propeller, the engine is connected to a synchronous generator which produces electric power. The power is then distributed to all consumers, for example, propulsion units, drilling system, and hotel loads. Instead of having only a few prime movers, a vessel with diesel electric propulsion often has between 2 and 10 pairs of diesel engines and synchronous generators (called a genset). This means that gensets can be started and stopped as needed.

Advantages of diesel electric power system (Ådnanes; 2003):

Lower fuel consumption With a diesel electric power system the gensets can run in configurations that minimize fuel consumption. During transit the demand for power is usually large, but during DP-operations the demand can be small. When the power demand is low some gensets can be shut down, so that the rest can run closer to an optimal load sharing.

Maintenance during operation Not all the gensets need to run all the time, therefore a gensets can be shut down for maintenance while the other gensets are running.

Flexible location of engine room With a conventional diesel mechanical system, the engine room needs to be located in front of the propeller. With a diesel electric system only an electric motor is needed near the propeller, while the engine room can be located wherever it is most convenient.

Increase robustness for single point failure Diesel electrical system has often redundancy. This means that if one single point failure occurs, another component can replace the failed component.

Less maintenance cost The gensets in a diesel electric system must run at constant speed and can run at a steadier load than a conventional system. This gives lower wear and tear, thus lower maintenance costs.

Improved maneuverability In some vessels, azimuth thrusters are used as the main propulsion. They can direct the force in any direction, this gives increased maneuverability.

No power consumption at zero thrust If no thrust is needed but thrust must be available, the pitch is set to neutral for mechanical system with variable pitch propellers. This makes noise and consumes power. With a variable speed drive (frequency converter and electrical motor), the propulsion motor can be stopped when no thrust are needed. In addition the propeller can run at an optimal speed for any desired thrust.

Disadvantages of diesel electrical power system (Ådnanes; 2003):

More complex system A diesel electric system adds complexity compared with a diesel mechanical system. This also means that more personnel with knowledge in electrical systems need to be hired.

Higher fuel consumption during transit A diesel electric system adds components between the shaft of the diesel engine and the propeller shaft. The combined loss of all these components is in order of 10%. During transit, nearly full power is needed; the advantage of more optimal load sharing for gensets is small compared with the added losses of the extra electrical components.

Increased investment cost As mentioned, more components are needed in a diesel electric system than a conventional system. These components are expensive and make the complete vessel more expensive to build.

In the last years, new concepts have also been developed. Rolls-Royce has a system called Hybrid Shaft Generator (see Figure 1.1, Rolls-Royce (2011)). With this system the main propeller can be driven by a diesel engine directly via a reduction gear (diesel mechanical propulsion), only by an electrical motor (diesel electrical propulsion), or by both the diesel engine and the electrical motor.

When the system is used as a diesel mechanical system it has the same efficiency as a conventional system, this means that during high load periods (e.g., transit) the losses are smaller than a diesel electric system. Similarly in low demand periods, either the diesel engine connected to the propeller can be shut down and the system is a diesel electric system, or the diesel engine can drive the motor as a synchronous generator and produce power to other units. In this way the main diesel engine does not need to run with low power at a low efficiency. Compared with a normal diesel electrical system it has all the benefits from a diesel electric system, except that with this concept there must be an engine room near the propeller.

During the last years electrical power system with direct current (DC) distribution has positioned itself as the *next big thing* in the world of marine power plants.

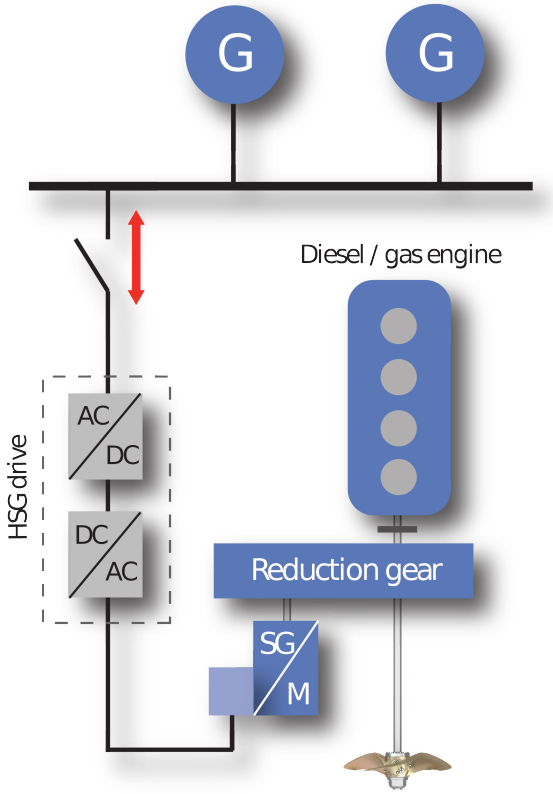

Figure 1.1: Rolls-Royce Hybrid Shaft Generator. Courtesy: Rolls-Royce (2011).

Hansen et al. (2011) claims that with DC, fuel consumption and emissions can be reduced with 20%. This is mostly due to the feature that the frequency is not locked at the rated frequency. This can be utilized to run the engines at lower speeds during periods of low demand, which gives a higher efficiency than at rated speed. Another possibility is to use the gensets as energy storage. Since the frequency is decoupled, it is allowed to vary in a much larger range than with a conventional diesel electric system. This variation can be used to store kinetic energy, which can be used for transients in load demands. Lastly, other DC technologies can easily be added to the DC-grid, such as fuel cell and batteries. These technologies can help improving efficiency and reduce wear and tear. The technology is very fresh, with the technology today it is suitable for vessels with installed power less than 20 MW (Hansen et al.; 2011). The first vessel with DC-distribution delivered by ABB, is expected to be delivered first quarter of 2013 (ABB; 2012).

1.2 Motivation

Today the controllers used in marine diesel electrical power plants do not utilize the full potential of the diesel engines. For example, during periods where the load is highly varying, the frequency varies so much that it is a problem to synchronize more gensets to the bus. During such periods the number of gensets required to take care of transients can be higher than what is required to take care of the peaks. With better controllers the number of gensets can be reduced, so that the gensets can operate at higher fuel efficiency. Also problem such as emission of soot could be avoided by a better control strategy.

In some advance vessels the Power Management System (PMS) adjust settings on the governors to optimize the performance. In such systems the governors are in charge of the low level control, while the PMS optimizes the governors to achieve better overall performance.

With increasing fuel prices and the movement for more green technology, the demand for more efficient marine power plants has raised. Improving the performance of marine power plants will give large impacts, both on economy and environment. However, risks connected to failures of the power system of a vessel are severe.

1.3 Previous Work

During the last decade there have been made some studies on modeling of marine power plants. Among them are Hansen (2000), who made a complete model from diesel engines to propellers. Later Radan (2008) also presented a model. Ådnanes (2003) gave an introduction to diesel electric propulsion and a description of the important components. Pedersen (2009) did a new approach by using bond graphs. He made a module based library consisting of models of the important electrical component. He also included models of upcoming technologies, such as fuel cells.

There are some researcher groups around the world who are working on marine power plants. Among them are the Royal Institute of Technology (KTH), Department of Electrical Engineering in Sweden (with e.g., Nord (2006) and Djagarov et al. (2011)). At University of Texas a model of a marine power plant has been developed by Ouroua et al. (2005). This model was implemented in MATLAB/Simulink.

There are also many studies on land-based power grids; often they use a stiff grid assumption. This means that they assume that the voltage and frequency are constant. For a marine power plant the voltage and frequency will vary since there are components that produce or consume power in the same order of magnitude as the complete system. The plant or bus is therefore called weak. Kundur et al. (1994) gives a description of a general power plant and analyzes the stability of such a plant.

For diesel engines there is also presented many models. Guzzella and Amstutz (1998) present a process plant model which includes the air- and fuel-system. This model is far too complicated to be used as a control plant model. Therefore, a literature study on both control methods and control models is included. Jiang (1994) used system identification to identify the parameters of a diesel engine. He used an ARMA process to describe the process. Blanke (1981) presents a model for medium speed diesel engines.

With concern to control of marine power plants, Veksler et al. (2012) presented a thruster allocation where the goal is to smooth out power fluctuations by using the thruster allocation. This utilizes the vessel as energy storage. They also suggest using feed forward from the power demand to the governor of the diesel engines.

Radan (2008) did a study on Power Management System (PMS). He presented industry standards and new method for blackout prevention control. Algorithms for choosing the correct size of gensets are included, which did show that the fuel efficiency can be increased if the sizes of the gensets are chosen optimally. For thrusters, he established observers based on *Luenberger observer*. He also included integral action to the observers, which improved the rejection of noise. For control, he did show that inertia control increase the performance of the thruster. He stated that the observers and the control methods can be applied to any rotating machinery, including prime movers.

McGowan et al. (2006) used fuzzy control with measurements from the terminal voltage and speed, instead of active power and speed, to control the genset. This gives better performance during changes of active loads, but gives frequency variations during changes of reactive load.

In the field of wind turbine generators, there have been some studies on wind turbine generators connected to diesel driven generators and batteries. Khalid and Savkin (2010) did a study on using model predictive control (MPC) to control the storage of energy in the batteries. Sebastián and Alzola (2010) also added a resistor bank and did a study where the diesel engine could be disconnected with a clutch. The resistor bank also takes care of excess energy from the wind turbine generators.

For standalone diesel engines there have been some studies on the design of the governor. Florián et al. (2006) presented an MPC that controls the fuel flow and a variable-geometry turbocharger. They did show that this approach can reduce emissions during transient periods. A governor based on H-infinity is presented by Kuraoka et al. (1990). They showed that this method can robustly control a diesel engine. Arfolini and Bloisi (2007) presented controllers for fuel rate and waste gate. They presented an LQ-controller which gave better disturbance rejection and easier tuning than PID. An MPC was implemented using a toolbox in MATLAB; however, this controller became hard to tune. They suggest that using MPC seems to be a good solution to the problem, as long as nonlinearities are taken care of in the implementation.

1.4 Outline of the Thesis

In Chapter 2, current control strategies are presented, some of these controllers will work as low level controllers for the plant. A short introduction to model predictive control (MPC) is given in Chapter 3. In Chapter 4, the process plant and control plant model are presented.

The controller is established in Chapter 5, this controller is the main contribution of the study. The presented controller includes a method for preparing the system for failures. With the method the controller calculates internally two cases, a normal case and a failure case. This is done to make sure that it can handle both cases without blackout.

A case study is done in Chapter 6, to show the performance of the controller. The last contributions are recommendations for further development of the controller, presented in Chapter 7.

During the process of writing this thesis, the goal has been to make it readable for both readers who only seek an overview and those who looks for details. Instead of putting all the math in the main part of the thesis, most of it is attached. So for the reader who seeks an overview it may be enough to read the main part. For those who would like to implement the controller or develop it further, would I suggest to read the main part first, and then look for the details in the appendices.

Chapter 2

Industrial State of the Art Load Sharing Techniques

Today there are mainly two types of control system for active power sharing of gensets that are used in the industry: speed droop and isochronous load sharing (Ådnanes; 2003). There is also a third configuration where both methods are combined. For control of the reactive power an Automatic Voltage Regulator (AVR) is used.

2.1 Speed Droop

With speed droop, the reference frequency of the genset is decreased with increasing delivered active power by the genset. This is the equation for droop (Woodward; 2011):

$$\% \text{ Droop} = \frac{\text{no-load frequency} - \text{full-load frequency}}{\text{full-load frequency}} \times 100, \tag{2.1}$$

and the reference frequency is:

$$\omega_{ref} = \text{no-load frequency} - \frac{\text{Delivered Power}}{\text{Rated Power}} \times \text{Droop}. \tag{2.2}$$

In Figure 2.1, a droop curve is shown. It illustrates the dependency between the setpoint of the frequency and the delivered active power.

The reference frequency is then compared with the actual frequency in per unit, ω. This gives the frequency error:

$$e_\omega = \omega_{ref} - \omega. \tag{2.3}$$

This error is given to a PID-controller, which computes the fuel rate, u. This is summarized in Figure 2.2, where a typical implementation of speed droop control is illustrated.

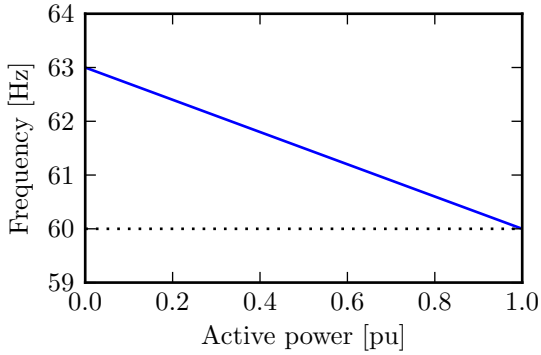

Figure 2.1: Example of droop curve, with 5% droop and *no-load frequency* of 63 Hz

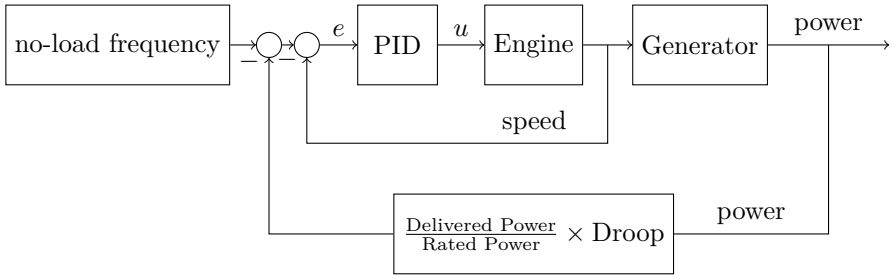

Figure 2.2: Schematics of droop control of genset, all variables are in per unit.

The advantage of speed droop is that it is very easy to implement, and if multiple gensets are connected to the same bus with the same droop curve they deliver the same load in per unit. Skjetne (2010) showed that the active power load sharing is mainly dependent on the rotor angle, while reactive power is dependent on the internal voltage in the generator. The governor controls therefore the active power sharing.

If multiple gensets run on the same bus, they can achieve a constant difference in produced power by selecting different no-load frequencies. If a certain ratio is wanted between the produced power of the gensets (e.g., Genset 1 should produce twice the power as Genset 2), the Droop must be adjusted (e.g., Genset 2 has twice the Droop as Genset 1). This is useful when a new genset is connected to a bus; then set the *no-load frequency* of the new genset to the current frequency of the

bus, synchronize the genset, and connect it. To make it take a part of the load sharing, increase the *no-load frequency* slowly until it reaches the desired level.

Another advantage of speed droop is that it requires no communication between the gensets.

The disadvantage of speed droop is that it requires a change of net frequency as the load of the bus changes. This is especially a problem if two buses should be connected to each other. This can in some extent be counteracted by modifying the droop curve during operation.

2.2 Isochronous Load Sharing

With isochronous load sharing the control is done without change of reference frequency. Instead it requires a *load sharing line*. This line consists of two wires, the difference in voltage between those two wires represents the average power in percent of rated power, produced by the gensets connected to the bus. There exists also more modern implementations where digital communication is used (ComAp; 2009).

If a genset produces more power than the average of all gensets, it reduces the speed which next reduces the produced power. If a constant difference in load sharing is desired, a bias can be added to the reading of average power for the gensets (Woodward; 2011). This makes the genset "believe" that all the other gensets deliver more power, and it will increase the delivered power to match it. Also subtract the bias from the "reported" power.

In this configuration a ratio between the produced powers of each genset can be achieved. The average power and reference power for Genset j is defined as:

$$\tilde{p} = \frac{1}{n} \sum_{i=1}^{n} \frac{p_i - b_i}{c_i} \tag{2.4}$$

$$p_{ref,j} = \tilde{p} c_j + b_j, \tag{2.5}$$

where p_i is the produced active power of Genset i, c_i is the load gain, and b_i is the bias. A constant difference between gensets can be set by tuning b_i. Similarly, a ratio between the produced power of each genset can be achieved by tuning c_i. However, with commercial governors, only one governor can be tuned at a time. The reason for this is unclear, but it seems to be a design choice made by the makers. In Table 2.1 some example of different configurations are given.

In the governor, a PID-controller receives the error of frequency and power, and from this it sets the fuel rate of the engine. The received error is:

$$e = K_1(p_{ref} - p) + K_2(\omega_{ref} - \omega), \tag{2.6}$$

where K_1 and K_2 are constant gains.

Table 2.1: Example of configurations during isochronous load sharing for a plant with two equally sized gensets.

Case	1	2	3
$\frac{P_{bus}}{S_{b,bus}}$	50%	45%	50%
b_1	10%	0	15%
b_2	0	0	0
c_1	1	2	2
c_2	1	1	1
$\tilde{p}$	45%	30%	30%
p_1	55%	60%	70%
p_2	45%	30%	30%

The drawback with isochronous load sharing is that it is more complex than droop and requires communication of the average produced power. A failure that influences the load sharing line might result in a common mode failure for all the gensets connected to the line. Special attention is therefore required for making such a system fail-safe. For example, when a plant consist of multiple buses it is important to split the load sharing line when the bus tie breaker is opened, and similarly connect the line when the breaker is closed.

2.3 Combination of Droop and Isochronous

The last type of configuration is to run some gensets in speed droop and some in isochronous mode. The isochronous gensets will make sure that the frequency stays constant (e.g., 60 Hz) and from the droop curve the other gensets will deliver constant power. This means that the gensets in isochronous mode, often called swing machines (Woodward; 2011), are the only gensets which changes delivered power.

This can be utilized when the consumed load is large and the variation is small relatively to the absolute load. The power can then be produced by having one or multiple large gensets taking up most of the load, while a big genset takes up the variations and is the one that will be subject for wear and tear due to change of load.

2.4 Automatic Voltage Regulator

For control of reactive power sharing and bus voltage, an Automatic Voltage Regulator (AVR) is used. It changes the field excitation of the generator, which affects both the terminal voltage and the reactive power. Also in this case droop

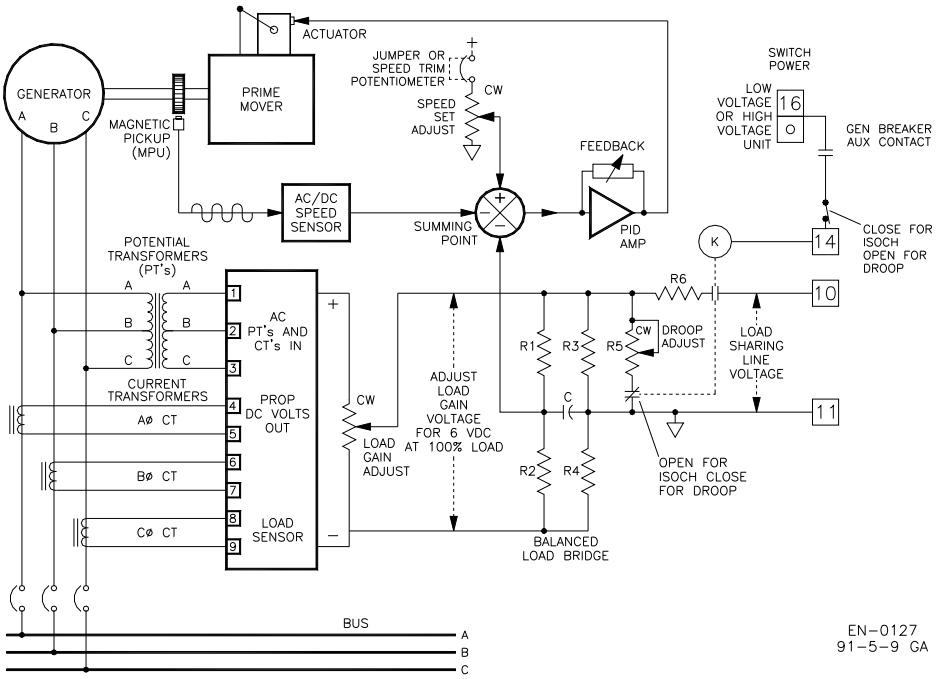

Figure 2.3: Woodward balanced load bridge, with both isochronous load sharing mode and speed droop. Courtesy: Woodward (2011)

is commonly used, by letting the setpoint for the terminal voltage be dependent on the produced reactive power (similarly as in speed droop where the setpoint of frequency is dependent on active power). In some plants droop compensation is used to adjust the droop curve to minimize the deviation of the voltage from the rated values (Ådnanes; 2003). Another method is to use an overall controller for all gensets, for example one AVR or the PMS can control the field excitation of all generators.

Chapter 3

Model Predictive Control

In this section a brief overview of model predictive control is given. It is mainly based on Maciejowski (2002) and Imsland (2007).

With Model Predictive Control the input to a system is calculated by optimizing a cost function with constraints. A model is used to predict how the plant will behave to different inputs. The controller uses this model to calculate the inputs, that are within the constraints and minimize the cost function.

The state equations for a linear system are:

$$\dot{\boldsymbol{x}} = A\boldsymbol{x} + B\boldsymbol{u} \tag{3.1}$$

$$\boldsymbol{z} = C\boldsymbol{x} + D\boldsymbol{u}, \tag{3.2}$$

where $\boldsymbol{x}$ is a vector of state variables, $\boldsymbol{u}$ is the input, $\boldsymbol{z}$ is the controlled output, and A, B, C, and D are matrices.

The control objective of the controller is to get the controlled output to their desired value, with as small as possible changes of the control input. These objective are weighted in a cost function:

$$J = \sum_{i=0}^{m} (\boldsymbol{z}_d[k+i] - \boldsymbol{z}[k+i])^\top Q[i](\boldsymbol{z}_d[k+i] - \boldsymbol{z}[k+i]) + \boldsymbol{\delta u}[k+i])^\top R[i]\boldsymbol{\delta u}[k+i] \tag{3.3}$$

where $\boldsymbol{z}_d$ is desired control output. Brackets denote that the values are given in discrete time. Q and R are cost matrices, and

$$\boldsymbol{\delta u}[i] = \boldsymbol{u}[i] - \boldsymbol{u}[i-1]. \tag{3.4}$$

A cost on the input, $\boldsymbol{u}$, can also be added, for example by defining it as control output.

Note that the cost function is given in discrete time and with a finite number of time samples. This is needed since this is implemented on computers, which can

only handle a finite number of variables. The time interval for the sum is called *prediction horizon* and the length of it is denoted m. The length must at least be comparable with the timescale of the slowest dynamics. The discretization is accurate as long as the time between each sample is small compared with the time constant of the system.

In addition to the cost function are there constraints. Often are the inputs constrained by slew rate constraints:

$$\boldsymbol{\delta u}_{min} \leq \boldsymbol{\delta u}[i] \leq \boldsymbol{\delta u}_{max}. \tag{3.5}$$

Other constraints can also be added, such as constraints of the range of input and control output.

The plan is now to find the solution of (3.3), within the constraints of (3.5). To calculate the optimal input, the cost function must be found as a function depending only on the inputs. First write the cost function on matrix form:

$$J = (\boldsymbol{Z}_d - \boldsymbol{Z})^\top \mathcal{Q}(\boldsymbol{Z}_d - \boldsymbol{Z}) + \boldsymbol{U}^\top \mathcal{R}\boldsymbol{U}, \tag{3.6}$$

where $\boldsymbol{Z}$ is a vector of all the controlled outputs, $\boldsymbol{U}$ are all controlled inputs.

$$\mathcal{Q} = \mathrm{diag}(Q[0], Q[1], \ldots, Q[m]) \tag{3.7}$$
$$\mathcal{R} = \mathrm{diag}(R[0], R[1], \ldots, R[m]) \tag{3.8}$$
$$\boldsymbol{Z} = \begin{bmatrix}\boldsymbol{z}^\top[k] & \boldsymbol{z}^\top[k+1] & \ldots & \boldsymbol{z}^\top[k+m]\end{bmatrix}^\top \tag{3.9}$$
$$\boldsymbol{U} = \begin{bmatrix}\boldsymbol{\delta u}^\top[k] & \boldsymbol{\delta u}^\top[k+1] & \ldots & \boldsymbol{\delta u}^\top[k+m]\end{bmatrix}^\top. \tag{3.10}$$

Since this is a linear plant the error of the controlled outputs can be predicted by a linear function:

$$\boldsymbol{E} = \boldsymbol{Z}_d - \boldsymbol{Z} = \mathcal{T} - \Psi\boldsymbol{U}, \tag{3.11}$$

where $\mathcal{T}$ is a vector, consisting of the *tracking error*, the error that will occur if the input is kept constant. Ψ is the matrix which describe the change of control output due to change of control input. $\mathcal{T}$ and Ψ are established in Appendix C.

Using (3.11), the cost function can be written depending only on the inputs.

$$J = \boldsymbol{E}^\top \mathcal{Q}\boldsymbol{E} + \boldsymbol{U}^\top \mathcal{R}\boldsymbol{U} \tag{3.12}$$
$$= (\mathcal{T} - \Psi\boldsymbol{U})^\top \mathcal{Q}(\mathcal{T} - \Psi\boldsymbol{U}) + \boldsymbol{U}^\top \mathcal{R}\boldsymbol{U} \tag{3.13}$$
$$= \mathcal{T}^\top \mathcal{Q}\mathcal{T} + \boldsymbol{U}^\top(\Psi^\top \mathcal{Q}\Psi^\top + \mathcal{R})\boldsymbol{U} - 2\mathcal{T}\mathcal{Q}\Psi\boldsymbol{U}. \tag{3.14}$$

Note that minimizing J under the constraint of (3.5) is a linear quadratic problem (LQ-problem). From the solution of this LQ-problem the input for the first time step is used. At each time step the problem is solved again, and the new optimal input is used.

If the stationary solution is not affected by any constraints, it is possible to avoid using finite horizon. This can be done by adding an extra cost for the last prediction time step to the finite horizon cost function. This is due to the fact that after some time the states will go into an area where they never will be affected by the constraints again. The solution to the unconstrained problem with infinite horizon is the solution of the Linear Quadratic Regulator (LQR). If the end cost is set to the truncated cost, found by the LQR, the cost function with finite horizon and end cost is equal to a cost function with infinite horizon (Imsland; 2007). They will then calculate the same optimal inputs.

3.1 Soft Constraints

Some constraints are more important than others. For instance, class rules demands that the electrical frequency stays within ±10% of the rated frequency (DNV; 2012). This can be given as a constraint for the controller. However, there can be situations where the controller cannot satisfy both the constraints on the fuel rate and frequency for the whole prediction horizon.

This can occur if the load on the genset increases too much, which gives a rapid decrease of the frequency. If the frequency constraint is applied in addition to the fuel rate constraint, the mathematical problem is infeasible. However, the constraints on the diesel engine are physical and cannot be broken, while the constraints on the frequency are artificial. The future can changes in respect to what is predicted (e.g., the load reduces), so that the frequency stays within the limit. It is therefore desired to have a solution that violates the frequency constraints as little as possible.

Such a solution can be found by using *soft constraints*. These constraints can be violated, but a penalty is added to the cost function when the constraints are violated. This is often done by adding a *slack variable*, which is constrained to always be nonnegative.

Soft constraints on the frequency can be modeled as shown below:

$$\omega(t) \leq \omega_{max} + \epsilon \tag{3.15}$$

$$\omega_{min} - \epsilon \leq +\omega(t) \tag{3.16}$$

$$0 \leq \epsilon, \tag{3.17}$$

where ϵ is the slack variable. To minimize the slack variable, hence the violation of the constraints, $\rho\epsilon^2$ is added to the cost function.

3.2 Failure Tolerant Control

The controller predicts a case where the plant behaves as normal, but what if a failure occurs? In a vessel it occurs that genset must disconnect, switchboards

short circuits, and loads starts both suddenly and with large load demands. A controller must be able to handle such cases.

To deal with this, the controller calculates failure cases in addition to the normal case. The controller calculates different inputs for all cases; however, the inputs for the first time instant are equal for all of the cases. This makes sure that the controller chooses inputs that will work for all cases. The cost function will only consider the normal case, while the hard and soft constraints make sure that the failure cases avoid blackout. The controller will therefore proactively reduce the consequences of certain failures.

In this thesis the simulations will be done with three gensets, where the first two are equally sized and the size of the last is doubled. The failure case is chosen to be a sudden disconnection of the third genset. Other than a short circuit of the switchboard this case may be the worst single point failure. The goal with choosing this case, is to illustrate that the consequence of this failure can be reduced by using this method.

Figure 3.1 shows predictions for both the normal case and the failure cases. The normal case is that three gensets continues to operate at a constant load. The input to the system is no-load frequency (the full model will be presented later)- Note that the first change of no-load frequencies is equal for both cases.

3.3 Linearization

Linear model predictive control assumes a linear model. However, a diesel electric power plant is nonlinear. A linearization is therefore done at each update instant. An alternative is to use nonlinear model predictive control; however, this requires more computational power.

The linearization is done around the actual value at the instant when the controller updates the no-load frequency. In Figure 3.2, an illustration shows the linearization point. Another choice of linearization point is discussed in Section 7.5.

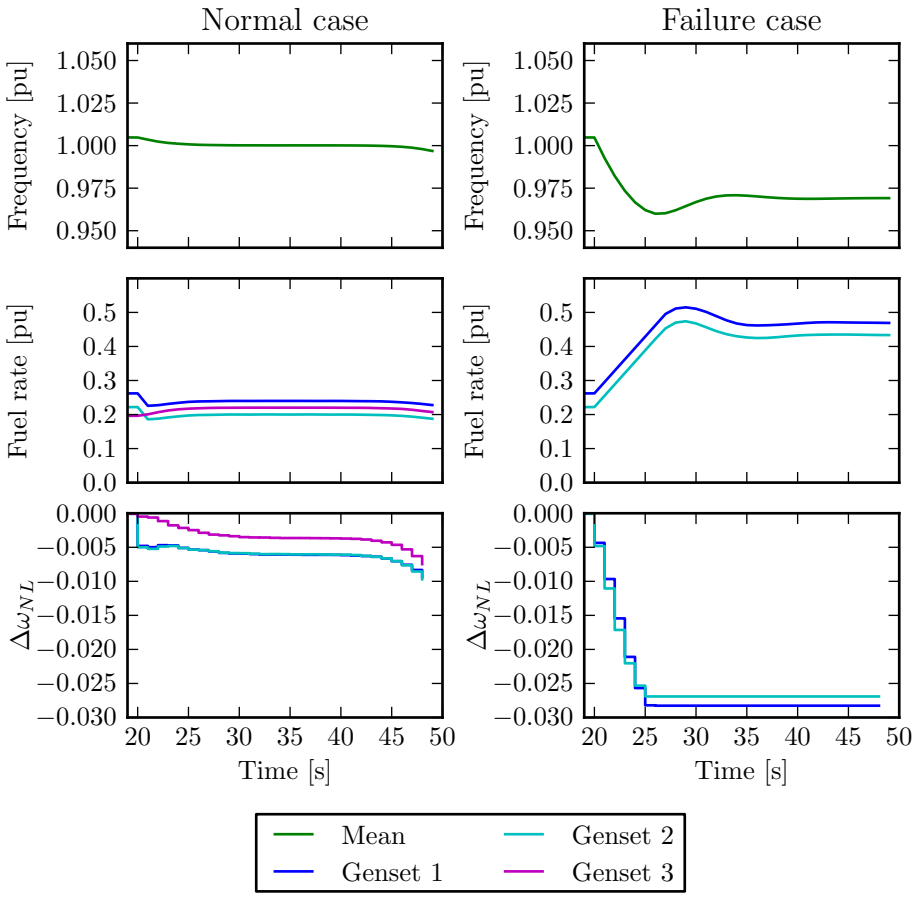

Figure 3.1: Two prediction for further development of frequency and fuel rates. To the left, the normal case is plotted, and to the right, the failure case is plotted (disconnection of Genset 3). $\Delta\omega_{NL}$ denotes the difference between the current and predicted no-load frequencies. Note that the first changes of no-load frequencies are equal for the two cases.

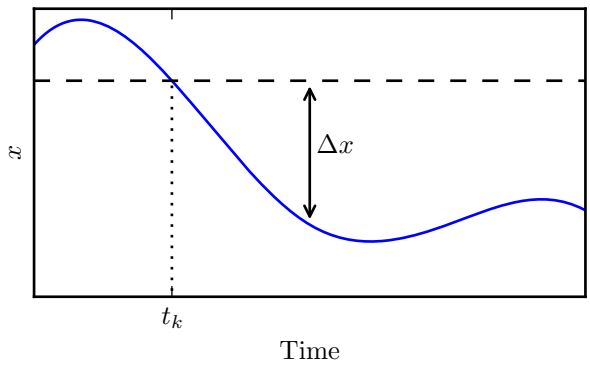

Figure 3.2: Illustration showing the linearization point for update of controller at t_k. The blue line shows how the value actually evolves with time and the dashed line shows the value that is linearized around at t_k.

Chapter 4

Modeling

In this chapter, two models are presented.

- Process plant model, which is used for simulation purposes.
- Control plant model, which is used internally in the controller.

Only a brief overview of the models are presented in this chapter, more details are given in Appendices A and B.

The control objective, which will be presented in the next chapter, states that frequency, fuel rate, and load sharing are the important states for this application. The high-level MPC shall control the plant by adjusting the governors. The models are therefore chosen with this in mind. The electrical system is therefore simplified and is mainly modeled for power flow and frequency. The model is therefore only valid as long as the plant is in a normal state. However, cases such as short circuit and connection of direct-on-line motors give transients that are not modeled. For the model of the diesel engine, it is most important to calculate speed, fuel rate, and delivered power. The model is cycle averaged, so the model cannot be used for analyzing of for example harmonic distortions or stationary efficiency. Lastly, the loads dynamics are not modeled at all, this is done since the controller cannot modify them and there is not made any predictions for the loads, other than it may stay constant. For testing, different time series of loads are used.

4.1 Process Plant Model

For simulation of the complete system, a process plant model is used. This model should be as accurate as possible, since the model is used for evaluation and testing of the performance of the controller.

In Figure 4.1, the single-line diagram for the simulation case is given. As seen consists the case plant of three genset of respectively, 5 MW, 5 MW, and 10 MW. The voltage on the bus is 11 kV.

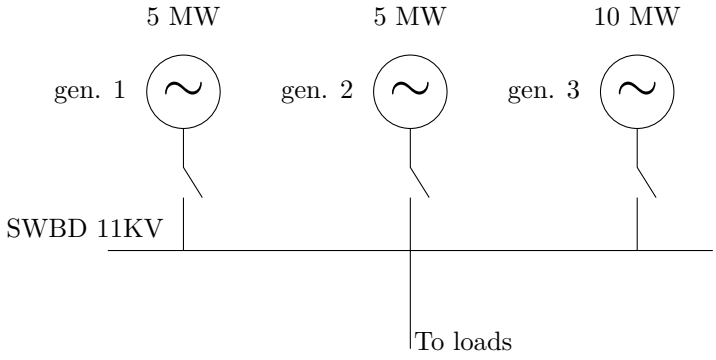

Figure 4.1: Single-line diagram of the producers for the simulation plant.

4.1.1 Diesel Driven Generator Set

A diesel driven generator set (genset) consists of a generator and a diesel engine. The dynamics of a generator is fast compared with a diesel engine, so it is reasonable to approximate it as a static system (Bø; 2011).

The response of a diesel engine is dominated by the inertia, the fuel system, and the turbocharger. The turbocharger consists of a compressor, which compresses air into the cylinders, and a turbine, which utilizes exhaust energy to spin the compressor. The amount of air in the cylinders, limits the amount of fuel that can be burned in the cylinders. When the fuel rate is increased the turbocharger must therefore also increase its speed. Then more air is compressed and injected into the cylinders, and next more fuel can be burned.

The turbocharger is modeled as a first order process, with the power as input and speed as output (Veksler et al.; 2012). Further the air flow is set to linearly depend on the speed of the turbocharger. The air-to-fuel ratio, (A/F), sets how much of the fuel that is burned. If the air-to-fuel ratio is above a certain limit, $(A/F)_{high}$, all of the fuel will be burned. Similarly, under a certain limit, $(A/F)_{low}$, nothing of the fuel will burn. In the region between these two air-to-fuel ratios, will some of the fuel burn. Xiros (2002) suggests that a linear function is used in this region. This gives a rapid decrease of the torque if the air-to-fuel ratio decreases under $(A/F)_{high}$. The fuel rate is therefore saturated so that the air-to-fuel ratio always is above $(A/F)_{high}$. Hence, the turbocharger contributes with a saturation of the fuel rate, u. The equations for the turbocharger are given in Appendix A.1.

In addition to the dynamical constraints due to the turbocharger, a static constraint is used to constraint the range of the fuel rate to a minimum and maximum fuel rate.

The equations of the rotational dynamics are (see Appendix A.1):

$$\dot{\theta} = \omega\omega_b \tag{4.1}$$

$$\dot{\omega} = \frac{1}{2H}\left[-D_f\omega + k_u u - \frac{1}{\omega}\left(p + r_s\frac{p^2+q^2}{v^2}\right)\right], \tag{4.2}$$

where the symbols denotes:

θ	Per unit electrical angel.
ω	Per unit angular velocity.
ω_b	Base angular velocity.
D_f	Windage friction constant.
H	Inertia constant.
k_u	Gain from fuel rate input to per unit mechanical torque.
p	Delivered active power from the genset.
q	Delivered reactive power from the genset.
r_s	Resistance in the stator windings.
v	Bus voltage.

4.1.2 Load Sharing

The load sharing is mainly set by the difference of rotor angles between the generators (Skjetne; 2010). The load sharing is calculated by assuming that the electrical system is in steady state. Then the alternating current system can be written on complex phasors form. During normal operation (i.e., not during short circuits, etc.) this is reasonable, since the electrical system is much faster than the mechanical.

See Appendix A.2 for more details and equations for load sharing.

4.1.3 Governor and Automatic Voltage Regulator

The governors used in the process plant model is a saturated PID-controller with droop. The Power Management System (PMS) controls the no-load frequency of the droop curve (see Section 2.1), to indirectly control the frequency and load sharing. When changing the no-load frequency, spikes are induced on the fuel rate. This occurs since the reference frequency changes discontinuously and the D-part of the governor tries to remove these sudden changes. To remove some of this effect, the time derivative of the frequency error is set to:

$$\dot{e} = -\dot{\omega} - \text{Droop}\dot{p}. \tag{4.3}$$

The actual derivation is done in the PID-controller, and the derivative is filtered.

For the Automatic Voltage Regulators (AVRs) a saturated PI-controller with droop is used in the process plant model.

4.2 Control Plant Model

In this study the focus is to use linear model predictive control (MPC). The process plant must therefore be linearized as mentioned in Section 3.3.

4.2.1 Linearization

Since the linearization is done about the value at the time of update (see Figure 3.2 on page 18), the states are calculated by using the sum of the current value, $\boldsymbol{x}_k$, and the deviation from it:

$$\boldsymbol{x}(t) \approx \Delta\boldsymbol{x}(t) + \boldsymbol{x}_k, \tag{4.4}$$

where $\boldsymbol{x}_k = \boldsymbol{x}(t_k)$ and $\boldsymbol{x}(t)$ is the exact solution of the nonlinear system:

$$\dot{\boldsymbol{x}} = \boldsymbol{f}(\boldsymbol{x}, \boldsymbol{\omega}_{NL}), \tag{4.5}$$

where the control input $\boldsymbol{\omega}_{NL}$ is the per unit no-load frequency.

$\Delta\boldsymbol{x}(t)$ is the solution of:

$$\begin{aligned}
\boldsymbol{\Delta}\dot{\boldsymbol{x}} =& \frac{\partial}{\partial \boldsymbol{x}} \boldsymbol{f}(\boldsymbol{x}(t_k), \boldsymbol{\omega}_{NL}(t_k))\boldsymbol{\Delta x} && (4.6)\\
&+ \frac{\partial}{\partial \boldsymbol{\omega}_{NL}} \boldsymbol{f}(\boldsymbol{x}(t_k), \boldsymbol{\omega}_{NL}(t_k))\boldsymbol{\Delta\omega}_{NL} + \boldsymbol{f}(\boldsymbol{x}(t_k), \boldsymbol{\omega}_{NL}(t_k)) && (4.7)\\
=& A\boldsymbol{\Delta x} + B\boldsymbol{\Delta\omega}_{NL} + \boldsymbol{f}_k, && (4.8)
\end{aligned}$$

where $\boldsymbol{\Delta x}(t_k) = \boldsymbol{0}$ and $\boldsymbol{\Delta\omega}_{NL}(t) = \boldsymbol{\omega}_{NL}(t) - \boldsymbol{\omega}_{NL}(t_k)$. The state matrix, A; input matrix, B; and initial derivative, $\boldsymbol{f}_k$; are:

$$A = \frac{\partial}{\partial \boldsymbol{x}} \boldsymbol{f}(\boldsymbol{x}(t_k), \boldsymbol{\omega}_{NL}(t_k)) \tag{4.9}$$

$$B = \frac{\partial}{\partial \boldsymbol{\omega}_{NL}} \boldsymbol{f}(\boldsymbol{x}(t_k), \boldsymbol{\omega}_{NL}(t_k))\boldsymbol{\Delta\omega}_{NL} \tag{4.10}$$

$$\boldsymbol{f}_k = \boldsymbol{f}(\boldsymbol{x}(t_k), \boldsymbol{\omega}_{NL}(t_k)) \tag{4.11}$$

Note:

$$\begin{aligned}
\dot{\boldsymbol{x}} &\approx A(\boldsymbol{x} - \boldsymbol{x}_k) + B(\boldsymbol{\omega}_{NL} - \boldsymbol{\omega}_{NL,k}) + \boldsymbol{f}(\boldsymbol{x}_k, \boldsymbol{\omega}_{NL,k})\\
&= A\boldsymbol{\Delta x} + B\boldsymbol{\Delta\omega}_{NL} + \boldsymbol{f}_k && (4.12)\\
&= \boldsymbol{\Delta}\dot{\boldsymbol{x}}.
\end{aligned}$$

From now on Δ denotes the difference from the value at the point of linearization, t_k, and the time, t.

4.2.2 Governor

Since the governor is a part of the loop it needs to be included in the model. One of the purposes of this study is to consider transient behaviors. This means that saturation and rate saturation of the fuel rate will occur.

The governor is modeled as an ideal PID controller in the control plant model. To make sure that no saturation occurs, the MPC is aware of the saturation limits. The MPC will therefore command no-load frequencies so that no or little saturation will occur. However, the governors updates the fuel rate faster than the MPC updates the no-load frequencies. This means that the MPC cannot check for saturation for the complete time interval between two updates, since it only gives *one* no-load frequency for the time interval. As long as the MPC updates fast enough, the error due to saturation between updates will be small.

To ease the calculation, the time derivative of the frequency error is approximated as:

$$\dot{e}_\omega = \dot{\omega}_{ref} - \dot{\omega} \approx -\dot{\omega} \tag{4.13}$$

It means that the derivative part of the PID-controller depends only on changes of frequency. This is in contrast to the process plant, where it is also dependent on the change of power. The error introduced by this simplification is usually small, except during disconnection of gensets. In that case, the error will usually only last in a period shorter than one update interval.

The equations for the governor are attached in Appendix B.1.

4.2.3 Automatic Voltage Regulator

The AVR is modeled as an ideal PI-controller. For simplicity saturation of the field excitation is neglected. This should give accurate results, since the periods of saturation occur seldom and are short. Equations are given in Appendix B.2.

4.2.4 Mapping of Angles

Numerical problems can occur due to the electrical angle, θ_i, increasing unbounded. However, it is only the difference between the gensets rotor angles which is of interest, since it gives the power sharing. To make the variable bounded a new angle is defined, ϕ_i. It is the difference between the electrical angle of Genset i and the mean electrical angle of all the gensets (where all the electrical angles are defined with a maximum difference of $\pm\pi$). Mathematically it is defined as:

$$\phi_i = \theta_i - \bar{\theta} = \theta_i - \frac{1}{n}\sum_{j=1}^{n}\theta_j, \tag{4.14}$$

where n is the number of gensets connected to the bus. The time derivative is:

$$\dot{\phi}_i = \dot{\theta}_i - \frac{1}{n}\sum_{j=1}^{n}\dot{\theta}_j \tag{4.15}$$

$$= \omega_b \left(\omega_i - \frac{1}{n}\sum_{j=1}^{n}\omega_j \right). \tag{4.16}$$

An equivalent angle for the bus is defined as:

$$\phi_0 = \theta_0 - \bar{\theta}, \tag{4.17}$$

where θ_0 is the electrical angle of the bus.

The definition of the load angle, δ_i, is easy to express as a function of the new angles:

$$\delta_i = \theta_i - \theta_0 = \phi_i + \bar{\theta} - \phi_0 - \bar{\theta} = \phi_i - \phi_0. \tag{4.18}$$

Note that if all angles starts with a difference smaller than 2π, then the difference cannot exceed 2π, since this can only occur if a generator is forced out of synchronization. The sum of all gensets is also always zero, from definition. This implies that ϕ_i is bounded.

4.2.5 Dynamics of the Genset

For the dynamics of the diesel engine, the equations used in the process plant are used. These equations are linearized and put on matrix form. The consumed load is also assumed to stay constant, since we do not have any better predictions.

The linearization gives:

$$\boldsymbol{\Delta\dot{x}} = \tilde{A}\boldsymbol{\Delta x} + B\boldsymbol{\Delta\omega}_{NL} + \boldsymbol{f}_k + K\boldsymbol{\Delta p}. \tag{4.19}$$

For a case with n gensets, the vectors are:

$$\boldsymbol{\Delta x} = \begin{bmatrix} \Delta p_{bus} \\ \Delta q_{bus} \\ \Delta \phi_1 \\ \Delta \omega_1 \\ \Delta \xi_{\omega,1} \\ \Delta \xi_{v,1} \\ \vdots \\ \Delta \phi_n \\ \Delta \omega_n \\ \Delta \xi_{\omega,n} \\ \Delta \xi_{v,n} \end{bmatrix} \tag{4.20}$$

$$\boldsymbol{\Delta \omega}_{NL} = \begin{bmatrix} \Delta \omega_{NL,1} & \dots & \Delta \omega_{NL,n} \end{bmatrix}^\top \tag{4.21}$$

$$\boldsymbol{\Delta p} = \begin{bmatrix} \Delta \phi_0 & \Delta v & \Delta p_1 & \Delta q_1 & \dots & \Delta p_n & \Delta q_n & \end{bmatrix}^\top, \tag{4.22}$$

where the symbols are:

p_{bus}	Per unit consumed active power.
q_{bus}	Per unit consumed reactive power.
ξ_ω	Value of integrator in PID controller in governor.
ξ_ω	Value of integrator in PID controller in AVR.
p_i	Per unit delivered active power from Genset i.
q_i	Per unit delivered reactive power from Genset i.
v	Per unit voltage on bus.

Values of the matrices and more details are given in Appendix B.3.

4.2.6 Load Sharing

The equation for load sharing used in the process plant model can be written on this form (Skjetne; 2010):

$$\sum_i p_i \frac{S_{b,i}}{S_b} = p_{bus} \tag{4.23}$$

$$\sum_i q_i \frac{S_{b,i}}{S_b} = q_{bus} \tag{4.24}$$

$$p_i = \frac{v_{f,i} v}{x_s} \sin \delta_i \tag{4.25}$$

$$q_i = \frac{v}{x_s} \left(v_{f,i} \cos \delta_i - \frac{v}{\omega_i} \right), \tag{4.26}$$

where $v_{f,i}$ is per unit field excitation voltage of Genset i.

The expression for the field voltage given by the AVR and the expression for load angles are inserted into (4.25) and (4.26). These equations are then linearized using Maple, and put on matrix form:

$$E\boldsymbol{\Delta p} = F\boldsymbol{\Delta x}. \tag{4.27}$$

The values of E and F are given in Appendix B.4.

The goal is to express the electrical variables as a function of the state variables. Therefore E consists of all derivatives with respect to the electrical variables and F consist of the derivatives with respect to the state variables. With this method the electrical variables in the state space equation, (4.19), can be substituted by using (4.27), so that the equation only depends on input and state variables.

4.2.7 Full Model

A complete state space model can now be derived by substituting the electrical variables, $\boldsymbol{\Delta p}$, using (4.27).

By combining (4.19) and (4.27), the state space equation is complete:

$$\boldsymbol{\Delta \dot{x}} = \tilde{A}\boldsymbol{\Delta x} + K\boldsymbol{\Delta p} + B\boldsymbol{\Delta \omega}_{NL} + \boldsymbol{f}_k \tag{4.28}$$

$$\boldsymbol{\Delta \dot{x}} = (\tilde{A} + KE^{-1}F)\boldsymbol{\Delta x} + B\boldsymbol{\Delta \omega}_{NL} + \boldsymbol{f}_k \tag{4.29}$$

$$A = \tilde{A} + KE^{-1}F \tag{4.30}$$

$$\boldsymbol{\Delta \dot{x}} = A\boldsymbol{\Delta x} + B\boldsymbol{\Delta \omega}_{NL} + \boldsymbol{f}_k. \tag{4.31}$$

It is not proved that E is invertible, but in Appendix B.4 this topic is discussed and the conclusion is that it is plausible that E is invertible as long as the states are within the limits of the protection relays. As long as there is no proof, a test should be implemented to check if E is invertible and a fail-to-safe strategy should be used when E is singular.

4.2.8 Control Output

The control outputs are the average frequency and the fuel rates before the no-load frequencies are changed.

This is written as a function of the states and input:

$$\Delta \boldsymbol{z} = C\Delta \boldsymbol{x} + D\Delta \boldsymbol{\omega}_{NL}. \tag{4.32}$$

More details are given in Appendix B.6

Chapter 5

Controller

In this chapter the algorithm for the model predictive control (MPC) used in this thesis will be presented. The equations for the MPC are attached in Appendix C. The controller is based on linear MPC theory; however, as noted in the previous chapter the system is nonlinear. To deal with this the system is linearized at each time step, by using the control plant derived in the previous chapter. The controller tries to calculate a safe control input by calculating two alternative cases. The normal case, where everything works as normal; and a failure case, where the largest genset disconnects.

Since this is not a standard setup the equations for the controller are tailor made for this purpose.

Briefly the main steps of the controller are:

1. States are measured or computed.
2. A linearized model is calculated for both the cases.
3. The models are converted from continuous time to discrete time, by using `c2d` in MATLAB with zero-order hold.
4. The cost function and constraints are calculated as a function of the no-load frequency.
5. The optimal no-load frequency is calculated and commanded to the (simulated) plant.

5.1 Control Objectives

The first control objective is to keep the frequency within given limits. In a marine power plant, the main concern is to maintain the frequency within the limits given

by protection relays, in order to avoid blackout. However, the frequency does not need to stay close to the rated values, as long as they are within the limits given by the protection relays.

An important task of the controller is to make sure that if a failure occurs it does not escalate into a blackout. An example of a failure case is that one generator must disconnect from the bus, without any pre-warning. The scope of this study is to present and demonstrate a method that proactively handles some given cases.

Rapid load changes on the gensets will increase wear and tear. The next control objective is therefore to minimize the changes of no-load frequency, since it changes the fuel rate.

The last control objective is that the controller should manage to obtain any desired load sharing. This gives the possibility to run the plant at maximum efficiency for a given genset combination, or to burn off soot.

To achieve these control objectives the controller adjusts the no-load frequencies of the governors. It is assumed that the no-load frequency can be adjusted to any value (infinite resolution) and at any time (infinite update rate). There may not exist such governors today; however, this is assumed to show the potential of switching to such governors.

To summarize, the control objectives are:

1. The controller should keep the frequency within rules and regulation.
2. The controller should be ready for a disconnection of the largest genset. Such that the frequency stays within given limits after the disconnection.
3. Wear and tear should be reduced to a minimum.
4. The controller should control the load sharing to any desired sharing.

Control objective 3 and 4 can be summarized to minimize the cost function:

$$\begin{aligned} J[k] = \sum_{i=1}^{m} \Big[& (\bar{\omega}[k+i] - \omega_d) Q_\omega (\bar{\omega}[k+i] - \omega_d) \\ & + (\boldsymbol{u}^\top[k+i] - \boldsymbol{u}_d^\top[k+i]) Q_u (\boldsymbol{u}[k+i] - \boldsymbol{u}_d[k+i]) \\ & + \boldsymbol{\delta\omega}_{NL}^\top[k+i] R \boldsymbol{\delta\omega}_{NL}[k+i] \Big] \end{aligned} \tag{5.1}$$

where $\boldsymbol{u}$ is fuel rate, $\boldsymbol{u}_d$ is desired fuel rate, and $\bar{\omega}$ is the average frequency of the gensets connected to the bus. Q_ω is the cost of frequency error, Q_u is the cost of load sharing error, and R is the cost of changing the no-load frequencies

5.2 Frequency Constraints

As mentioned in Section 3.1, there are class rules on the deviation of frequency. DNV (2012) states that the frequency shall stay between 90% and 110% of rated frequency during transients, and between 95% and 105% for steady state.

In this study only the rule for transient frequency are explicitly taken care of in term of constraints. This is done as suggested in Section 3.1:

$$\bar{\omega}[i] \leq \omega_{max} + e[i] \tag{5.2}$$

$$\omega_{min} - e[i] \leq \bar{\omega}[i] \tag{5.3}$$

$$0 \leq e[i], \tag{5.4}$$

where $k + 1 \leq i \leq k + m - 1$.

The rule for steady state frequency error could be addressed by using another soft constraint. It is expected that with suitable tuning, both rule can be enforced with such a method.

5.3 Fuel Rate Constraint

As mentioned in Section 4.1.1, the fuel rate is constrained to a given range. It was also highlighted that the fuel rate is also constrained by the dynamics of the turbocharger. These constraints set how fast the fuel rate can be increased. To increase the fuel rate as fast as possible from minimum to maximum, the fuel rate must first be increase in a step and then increased slowly.

Two methods for constraining the fuel rate are used, and both methods are illustrated in Figure 5.1. *Rate based fuel rate constraint* uses the current fuel rate as initial point for a ramp that constraints the fuel rate. The *air dependent fuel rate constraint* uses the current maximum allowed fuel rate for the initial point of a ramp that constraints the fuel rate. The maximum allowed fuel rate is based on the available air from the turbocharger, and is the maximum fuel rate that gives full combustion.

During maximum increase of fuel rate, the rate based constraint gives the best prediction of these two methods. Since the predictions of the constraints are very close to the applied constraint. However, with the air dependent constraint the actual constraint is often less strict than predicted. This gives a conservative prediction of the fuel rate which affects the prediction of frequency. The air dependent constraint gives better control performance, since more of the available air is used.

The rate based constraints on the fuel rate are:

$$u_{min} \leq u[i] \leq u_{max} \tag{5.5}$$

$$u[i] - u[i-1] \leq du_{max}, \tag{5.6}$$

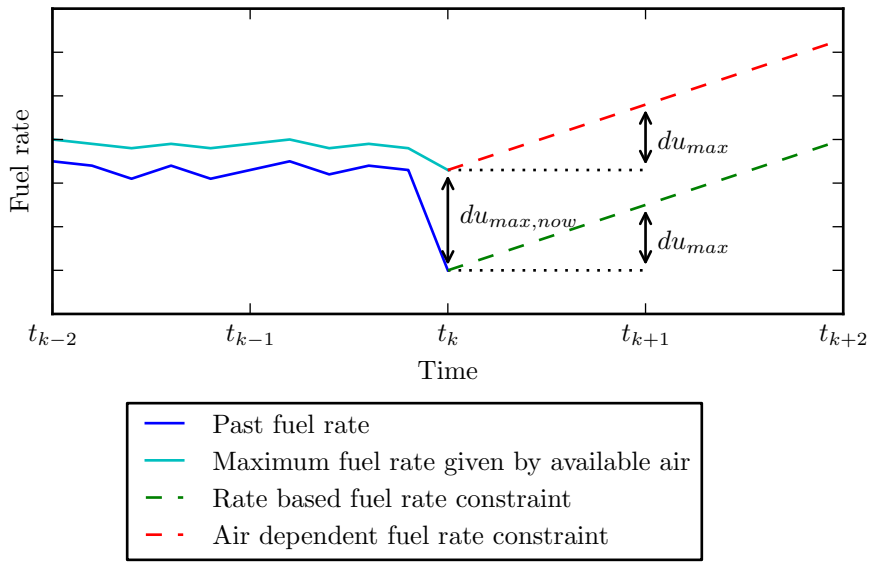

Figure 5.1: The figure is illustrating the two types of fuel rate constraints used. For rate based fuel rate constrain, the current fuel rate is set as initial point of the constraining ramp. For air dependent fuel rate constraint, the current maximum allowed fuel rate (given by the amount of available air) is used instead.

where $k+1 \leq i \leq k+m-1$. Note that there is no lower limit of how fast the fuel rate can decrease, but there is a lower limit of the amount of fuel rate. This is used since the fuel rate can be decreased fast in an engine with direct injection, and at least as fast as the update rate used in the case study (one second).

For the air dependent constraint, the constraints (5.5) and (5.6) are used for the complete prediction horizon, except the first sample where the increase is constrained by:

$$u[k+1] - u[k] \leq du_{max} + du_{max,now}, \tag{5.7}$$

where $du_{max,now}$ is the maximum allowed increase of fuel rate at the update time.

For the failure case, the rate based fuel rate constraints are similarly as for the normal case. With air dependent fuel rate constraints, the fuel rate is allowed to increase with the same amount during the first step and the step after disconnection. However, it can only take a full step once, either during the first step, from $u[k]$ to $u[k+1]$, or the step after the disconnection, from $u[k+1]$ to $u_w[k+2]$. It is also possible to utilize a combination of the steps. This is illustrated in Figure 5.2. The reason for this is that the step is given by the available airflow from the turbocharger. If the fuel rates utilize all the airflow from $u[k+1]$, then the extra airflow is only given by the extra speed the

turbocharger has managed to obtain between $k+1$ and $k+2$. Next, the extra amount of fuel that can be burned is given by the extra airflow, and it is estimated to be a constant equal to du_{max}.

The constraints for fuel rate for calculation of failure case with air dependent fuel rate constraints are:

$$u_w[k+2] - u[k+1] \leq du_{max} + du_{max,now} \tag{5.8}$$

$$u_w[k+2] - u[k] \leq 2du_{max} + du_{max,now}. \tag{5.9}$$

When the no-load frequency is changed, the fuel rate changes in a step. In Figure 5.3, this problem is illustrated. Note that each time the no-load frequencies are changed, the fuel rates are changed instantly. It is chosen to apply the constraints to the fuel rate before the change, and not after. This is done since it is believed that the fuel rate will change smother than modeled. The reason is that it is assumed that there is some dynamics in the governor and the fuel system that is not modeled, and will smooth out the changes of no-load frequencies.

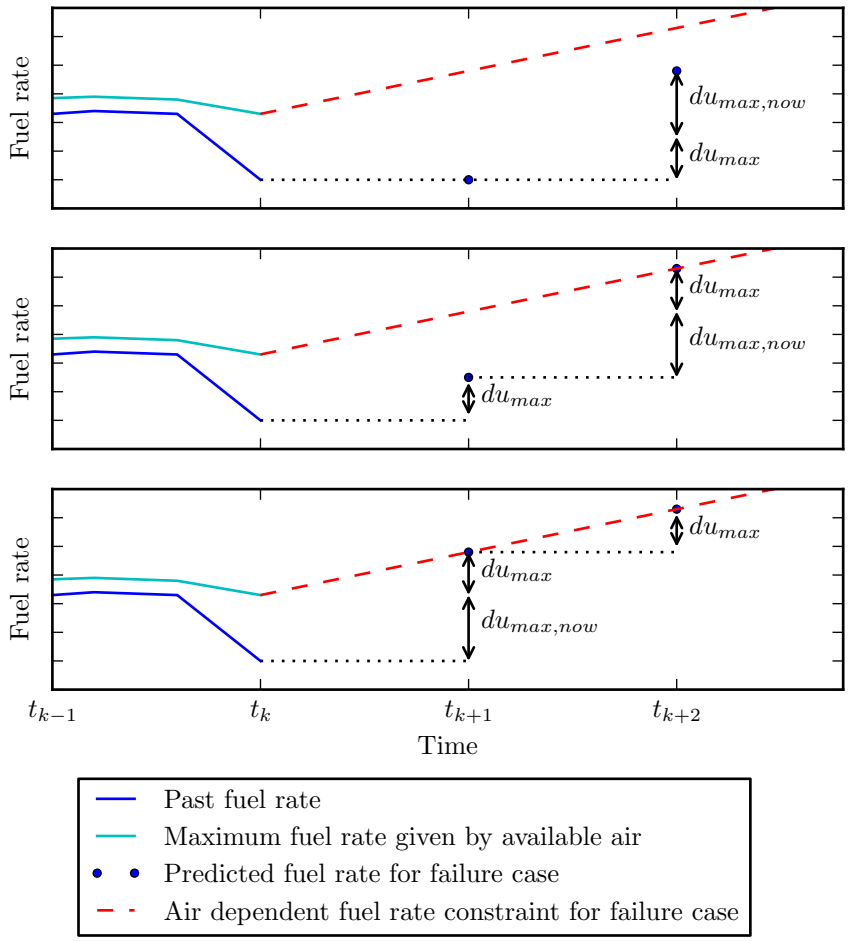

Figure 5.2: Three examples of constrained prediction of fuel rates for the failure case using air dependent constraint. In the upper plot $u[k+1]$ is predicted to be equal to $u[k]$, this means that $u_w[k+2]$ is only constrained by (5.8). Next plot, utilizes the maximum fuel rate at $k+2$, but with a minimum fuel rate at $k+1$. This is constrained by (5.8) and (5.9). At the bottom maximum fuel rate for both $k+1$ and $k+2$ are used, this is constrained by (5.7) and (5.9).

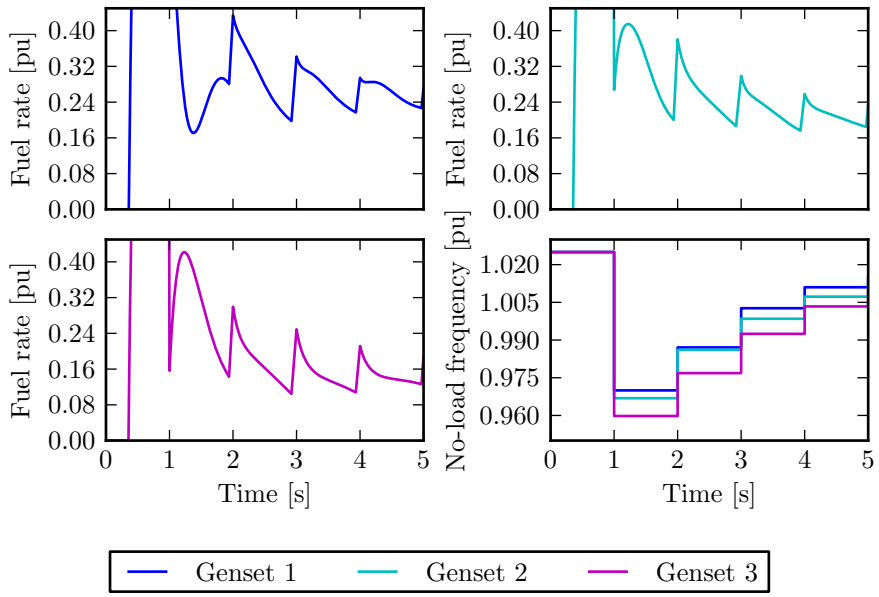

Figure 5.3: Fuel rate during changes of no-load frequency. The figure illustrates the jagged fuel rate, due to discontinuous changes of no-load frequency.

5.4 Fault Tolerant Control

One of the most important tasks for a Power Management System (PMS) is to react to faults, so that failures do not escalate to an even more critical failure mode, such as blackout. To make sure that the controller *can* handle failures, it is important that the power plant is in a state that makes it feasible to avoid blackout. The failure case used in this study is a sudden disconnection of the largest generator (Genset 3). For this case it is necessary to maintain a high enough frequency before the disconnection, such that the frequency does not drop below the underfrequency limit, which gives blackout. Other cases, not considered here, may lead to other risks, such as overfrequency.

The problem is solved by calculating responses and no-load frequency for both the normal case and the failure case. The idea is that the controller cannot be sure which of the cases that will happen. It calculates therefore both cases where the first inputs are equal, while thereafter the inputs (no-load frequency) can diverge. In practice this means that the first input is subject to the constraint that the input should give a feasible solution for the failure case.

The disconnection is predicted to occur at $k+1$. Since the no-load frequency is equal for both cases, the MPC prepares the plant for disconnection. If a disconnection occurs between updates of no-load frequency, will the no-load frequency not be changed until the end of the interval. This means that in the time between, a no-load frequency that is not optimal is used. However, this time period is small and the intermediate no-load-frequency will often give saturated or close to saturated fuel rate.

Another approach is to set the predicted time for disconnection to right after the update of no-load frequency. This is the worst time for disconnection, since the time before the disconnection is reacted to is as long as possible. If the predicted time of disconnection is changed, will the MPC give a no-load frequency that handles both the normal case and a case where Genset 3 disconnects right after the time of update. However, this was tested and did not work well. The reason is that the predicted decrease of frequency, in the failure case, requires that the no-load frequency is reduced. This is required so that the fuel rate does not exceed its range at the end of the update interval (i.e., $k+1$). This decrease leads the system into a blackout due to underfrequency.

5.4.1 Sequence of Events After Disconnection of Genset

After a disconnection the delivered power from the disconnected generator is shared among the remaining generators. Since diesel engines can only do a small increase of the torque, the diesel engine will generate only some more power than before. As a consequence the frequency will drop. To recover the power systems frequency, a Fast Load Reduction (FLR) is commonly used. The FLR reduces the consumed power, by demanding reduction of for example variable speed drives.

The reduction takes about 200 milliseconds (Mathiesen; 2012). Some FLRs reduce the consumed load to the level where all gensets produces the same power as before the disconnection. Radan (2008) summarizes other methods to reduce the loads with more intelligence.

After the load has been reduced, the load is increased slowly, so that the diesel engines can manage to ramp up in the same speed. The load consumption increases until it has reached the required load or the gensets reach their maximum continuous rating.

Since the effect of ramp up is rather small, compared with the changes due to the overload in the beginning, the ramp up of the load is neglected. The simulated case in the controller is:

1. One genset disconnects from the bus, while the power consumption stays constant.
2. After some time (e.g., 200 milliseconds) the load is reduced to the value where all connected genset delivers the same power as before the disconnection. The load is then kept constant.

5.4.2 Load sharing

To make the prediction model as good as possible, an accurate load sharing for the failure case is needed for linearization.

The accurate load sharing can be hard to find. As a rough approximation it is assumed that the load is shared equally (in Watts) among the gensets. This seems to be reasonable, as long as the different in size is not very large, since small gensets (in power) are faster (i.e., inertia constant smaller) and will therefore take up a larger share relative to the size. For a plant with three gensets, this gives:

$$P_{excess} = p_3 S_{b3} - p_{FLR} S_b \tag{5.10}$$

$$p_1' = p_1 + \frac{P_{excess}}{2S_{b1}} \tag{5.11}$$

$$p_2' = p_2 + \frac{P_{excess}}{2S_{b2}}, \tag{5.12}$$

where p_{FLR} is the load reduced by the FLR and p_i' is the produced power after the disconnection of Genset 3.

Similarly for reactive power:

$$q_1' = q_1 + q_3 \frac{S_{b3}}{2S_{b1}} \tag{5.13}$$

$$q_2' = q_2 + q_3 \frac{S_{b3}}{2S_{b2}}. \tag{5.14}$$

5.5 Tuning

The tuning process is not documented in detail is this report, since it was quite complex.

The idea used during tuning was to follow the control objectives as prioritized in the first section of this chapter. Since it is most important to have frequencies within the constraints for both cases, the costs on the slack variables are high. The load sharing is important, so the cost on the fuel rate is therefore medium-high. To avoid wear and tear a small cost is added on changes of no-load frequency. A small cost is also added to the frequency; else the frequency has a tendency to stay low. This occurs since the total desired fuel rate does not always match the total consumed power.

Lastly, for the failure case, no cost is added on frequency and fuel rate errors. This is done since it is only important that the frequency stays within the limits and neither to get the rated frequency nor an optimal fuel rate.

Chapter 6

Case Study

This chapter presents some simulations done with the controller.

All of the simulations are done with three genset with the parameters shown in Table 6.1 to 6.3. Parameters for generators are found in Krause et al. (2002). The turbocharger parameters are found in Xiros (2002).

The simulation is implemented in Simulink/MATLAB, the QP-solver used is SQOPT (Gill et al.; 2008) through TOMLAB (TOMLAB; 2011). As ordinary differential equation solver ode15s is used, it is based on the numerical differentiation formulas. The program used for simulation is attached digitally.

The limit for underfrequency is set higher for the failure case than for the normal case. This is done to have a higher safety margin. However, there are no restrictions for these limits, so the limits could have been chosen opposite.

Table 6.1: Parameters of the genset used in simulations.

	Symbol	Unit	Genset 1	Genset 2	Genset 3
Rated power	S_b	MW	5	5	10
Inertia constant	H	s	10	7	6
Friction	D_f	–	0.02	0.025	0.03
Resistance	r	–	0.003	0.0025	0.002
Synchronous reactance	x_s	–	1	1.5	2

Table 6.2: Parameters for MPC used in simulations.

	Normal case	Failure case
Update rate mpc	1 s	1 s
Prediction horizon	30 s	30 s
Frequency error cost	0.1	0
Fuel rate error cost (Genset 1 & 2/ 3)	0.01/0.02	0
Slack variable error cost (frequency constraint)	100	100
No-load frequency change cost	0.1	0.1
Frequency constraint, high	1.05	1.05
Frequency constraint, low	0.95	0.96
Ramp time fuel rate constraint	25 s	25 s
Minimum fuel rate constrained by MPC	0.01	0.01
Maximum fuel rate constrained by MPC	1.1	1.1

Table 6.3: Parameters for gensets used in simulations.

Turbocharger time constant	5 s
Minimum fuel rate	0
Maximum fuel rate	1.1
Minimum air-to-fuel ratio for complete combustion	23
Air-to-fuel ratio at rated power	27
Reactive load	0
Number of poles	2
Base voltage	11 kV
P-gain in governor	10
I-gain in governor	5
D-gain in governor	5
Filter constant in governor	10
Droop in AVR	5%
P-gain in AVR	400
I-gain in AVR	100
Droop in AVR	5%

6.1 Disconnection of Genset 3

The first case to be studied is the performance when the failure case occurs.

6.1.1 Disconnection Without FLR

In Figure 6.1, results from a simulation are shown. In this case the consumed load is 35% of installed power and the rate based constraint is used. At $t = 19.99$

seconds, Generator 3 is disconnected, this is right before an update of the no-load frequencies. As seen in the figure, the electrical frequency (equal to the frequency of Genset 1 and 2) drops to a frequency above the lower limit of 96%. It is clear that the MPC proactively controls the frequency to a level that is high enough to recover the frequency after disconnection.

After the disconnection the frequencies splits in two paths. Generator 1 and 2 take the same path, since the electrical power grid will synchronize them. However, since Genset 3 is disconnected, its frequency will take another path (dotted line). The frequency of Genset 3 will often increase, due to the sudden decrease of delivered power. The predicted frequency is the average frequency of the connected of gensets.

The fuel rate increases slowly in a ramp as demanded. However, there is a bias between the prediction and actual fuel rate, for the frequency error of the prediction grows with the difference between the frequency and the linearization point. This prediction seems to be conservative, which is good for safety. The reason for the errors is not found, but these errors may be reduced by linearizing around the predicted path instead of linearizing around the current states.

It can also be noted that after the disconnection, the fuel rate does not converge to the desired value. This is due to the tuning, as mentioned in Section 5.5, no penalty is applied to the load sharing after disconnection. This is done to make sure that the load sharing during the normal case is not affected by the failure case. Also note that before the disconnection the load share for Genset 3 is much lower than desired, and Genset 2 and 3 have a higher fuel rate than desired. This happens since the MPC prepares for a possible disconnection of Genset 3. To avoid such “favoring” of one genset, each genset should have its own failure case.

In Figure 6.2, results from the case are plotted with air dependent fuel rate constraint. It is clear that it uses more of the available air. This gives faster ramp-up of the fuel rate and better performance, while the error of the prediction is even larger. The predictions are even more conservative, since the predicted ramp-up of fuel rates are too gentle.

In Figure 6.3, results are plotted for the case with air dependent fuel rate constraint and the time for the disconnection is moved to right after an update of no-load frequency. This give poorer performance and the frequency decreases under the given limit. This happens since the MPC cannot increase the no-load frequency, and hence the fuel rate, until nearly the time of an update interval after the disconnection. However, the plant will still be safe if the underfrequency limit is set with some safety margin.

Lastly in Figure 6.4, results are plotted from a simulation with constant no-load frequency (i.e., the MPC is turned off). It is clear that the plant does not manage to avoid blackout, since the frequency drops under the given limit. In such cases an FLR must be used.

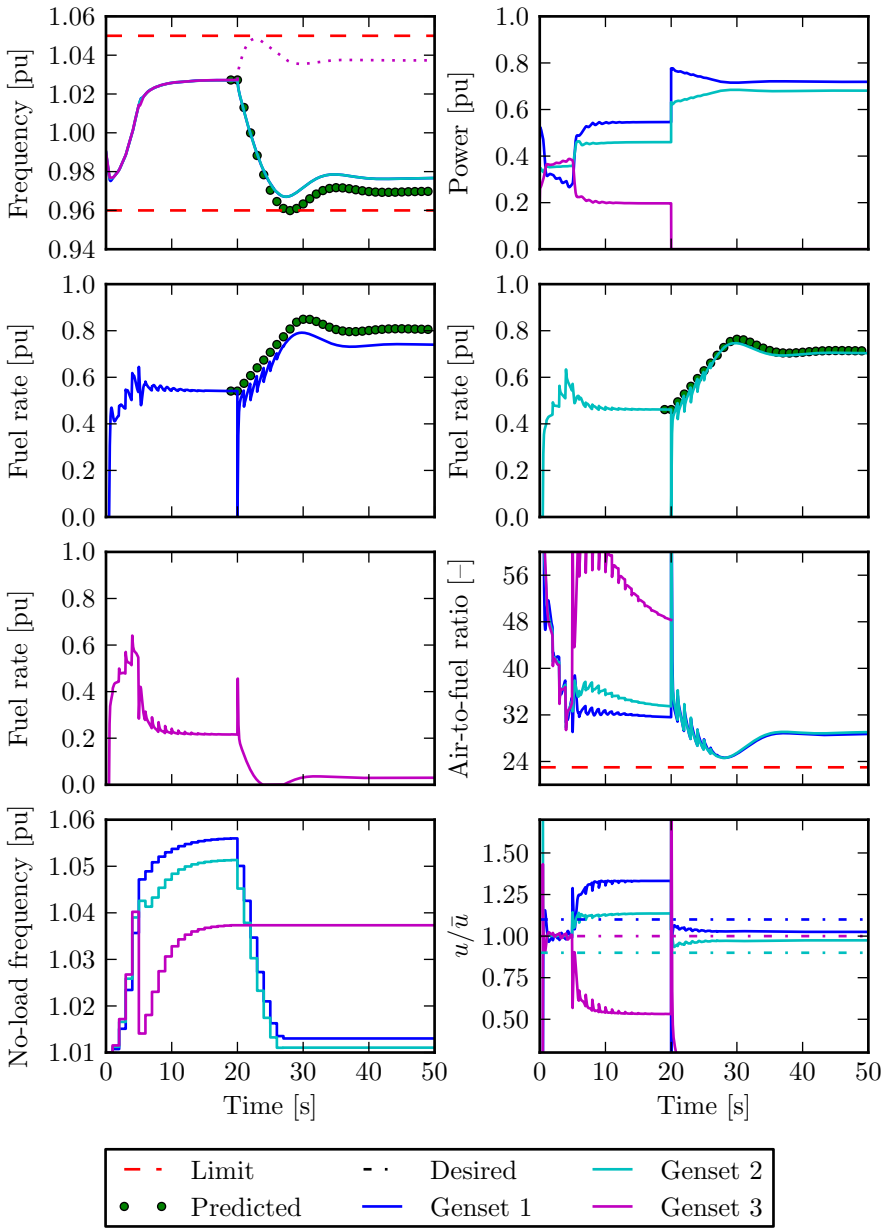

Figure 6.1: Results from simulation of sudden disconnection of Genset 3, with rate based fuel rate constraints. The load is 35% of installed power and the simulation is done without FLR. Note that after disconnection the frequency for Genset 3 separates from the other gensets (dotted).

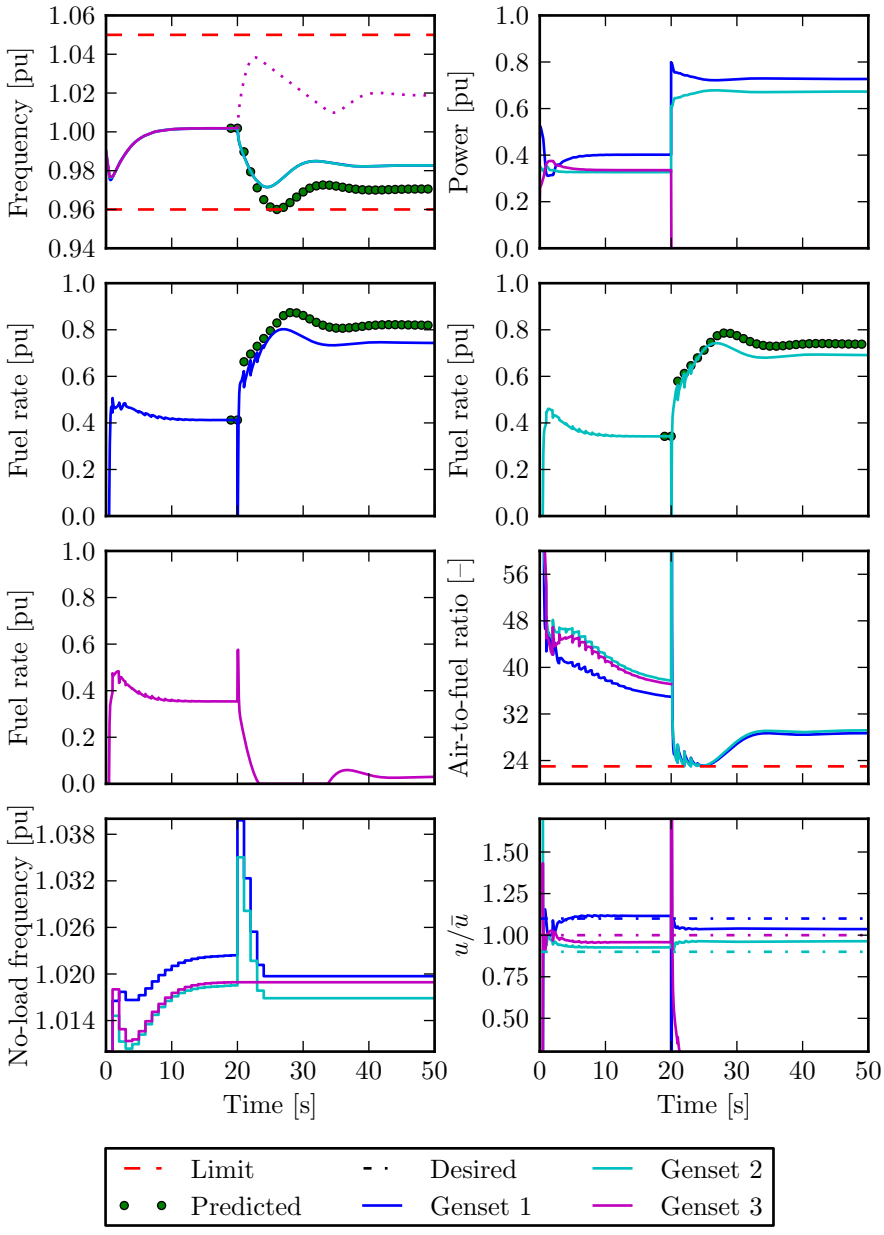

Figure 6.2: Results from simulation of sudden disconnection of Genset 3, with air dependent fuel rate constraints. The load is 35% of installed power and the simulation is done without FLR. The disconnection occurs right before an update of no-load frequency. The dotted line denotes the frequency of Genset 3 after disconnection.

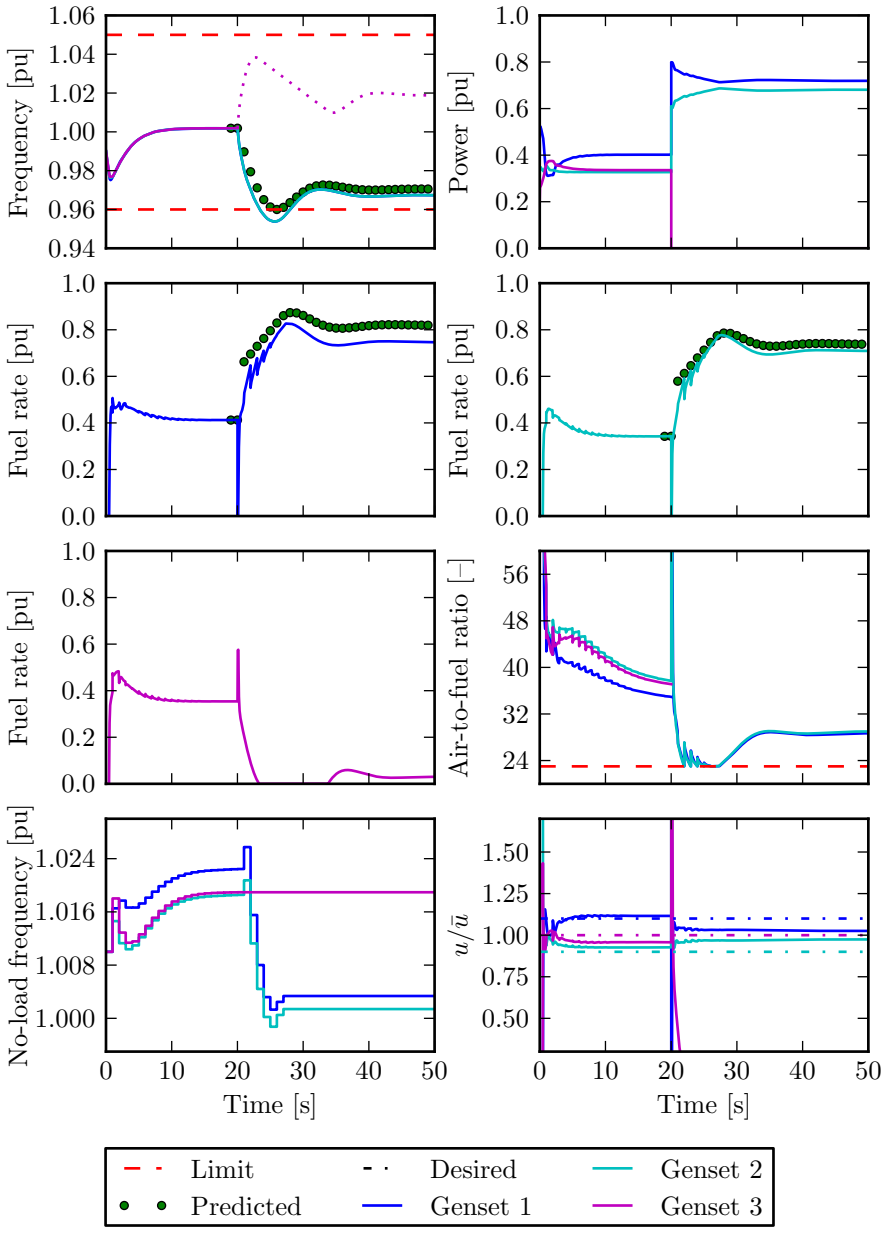

Figure 6.3: Results from simulation of sudden disconnection of Genset 3, with air dependent fuel rate constraints. The load is 35% of installed power and the simulation is done without FLR. The disconnection occurs right after an update of no-load frequency. The dotted line denotes the frequency of Genset 3 after disconnection.

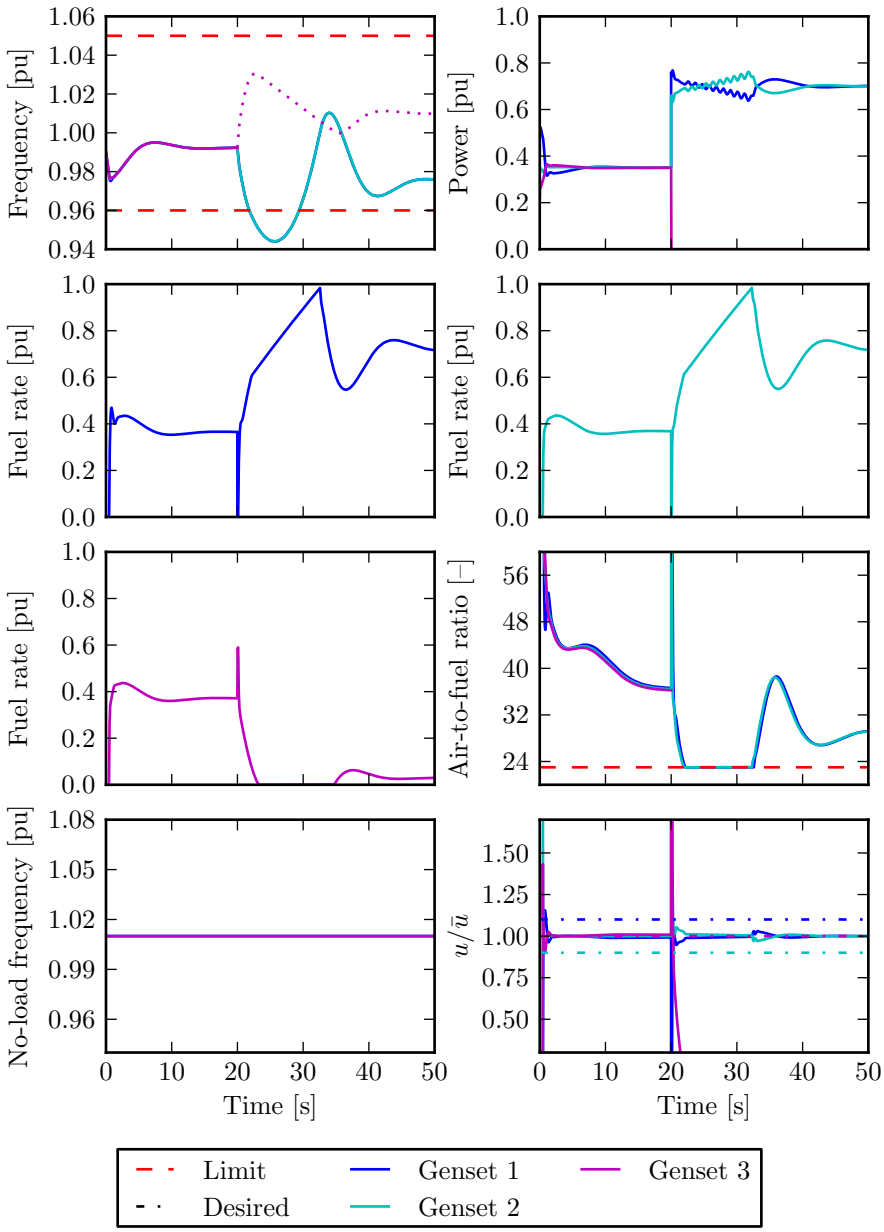

Figure 6.4: Results from simulation of sudden disconnection of Genset 3, with constant no-load frequency. The load is 35% of installed power and the simulation is done without FLR. The dotted line denotes the frequency of Genset 3 after disconnection.

6.1.2 Disconnection With FLR

In Figure 6.5, a similar case as the previous is plotted. However, the load is increased to 80% of installed power and the FLR reduces the load to 40% of installed power, 200 milliseconds after disconnection. This figure shows a simulated done with rate based fuel rate constraint.

Here the predictions fail, and the frequency dips much more than predicted. This is due to the fuel rate constraints are set too low. This occurs since the fuel rate decreases after the disconnection and this fuel rate is used to constrain the predicted fuel rates. The decrease of fuel rate occurs due to the power-derivative term in the governor, which tries to reduce variations in the power.

It can be questioned if the drop of fuel rate will occur with an industrial governor. This drop can be removed by adding some logic to the governor, for example can the derivative term in the governor be limited. However, the drop is not important. What is more important is to note that a sudden drop of fuel rate confuses the MPC to set too low constraints on the fuel rate.

In Figure 6.6, the case is simulated with air dependent fuel rate constraints. This gives much better response and blackout is avoided. However, the errors in the predictions are quite large, since the predicted constraints are too conservative.

Note that the frequency is at some point close to the overfrequency limit. This happens since the MPC updates the no-load frequency between the disconnection and the reduction of consumed load done by the FLR. When all gensets are connected, the FLR is modeled in the controller, to give a good description of the failure case. However, when Genset 3 is disconnected, the FLR is not modeled in the controller. The MPC will therefore command too high no-load frequencies if it updates in the time between the disconnection and the reduction of load, since the MPC will predict that the load will stay constant. At the following updates, the MPC reduces the no-load frequency so that overfrequency is avoided.

In Figure 6.7, the disconnection occurs at $t = 20.01$ seconds, this is right after an update of no-load frequency. This gives much better performance, with only a small error in the prediction. Before the disconnection, the MPC predicts that if the disconnection happens the no-load frequency should be kept constant. Since the actual no-load frequency is kept constant, the prediction and response is much better.

In Figure 6.8, the case is simulated with constant no-load frequency. This gives similar response as the previous in Figure 6.7, as expected.

From this it is concluded that the FLR should be included also after disconnection. The system frequency is mainly rescued by the FLR. However, the MPC can be used to estimate the decrease of frequency after the disconnection, which can be used to check if the system is in a safe state.

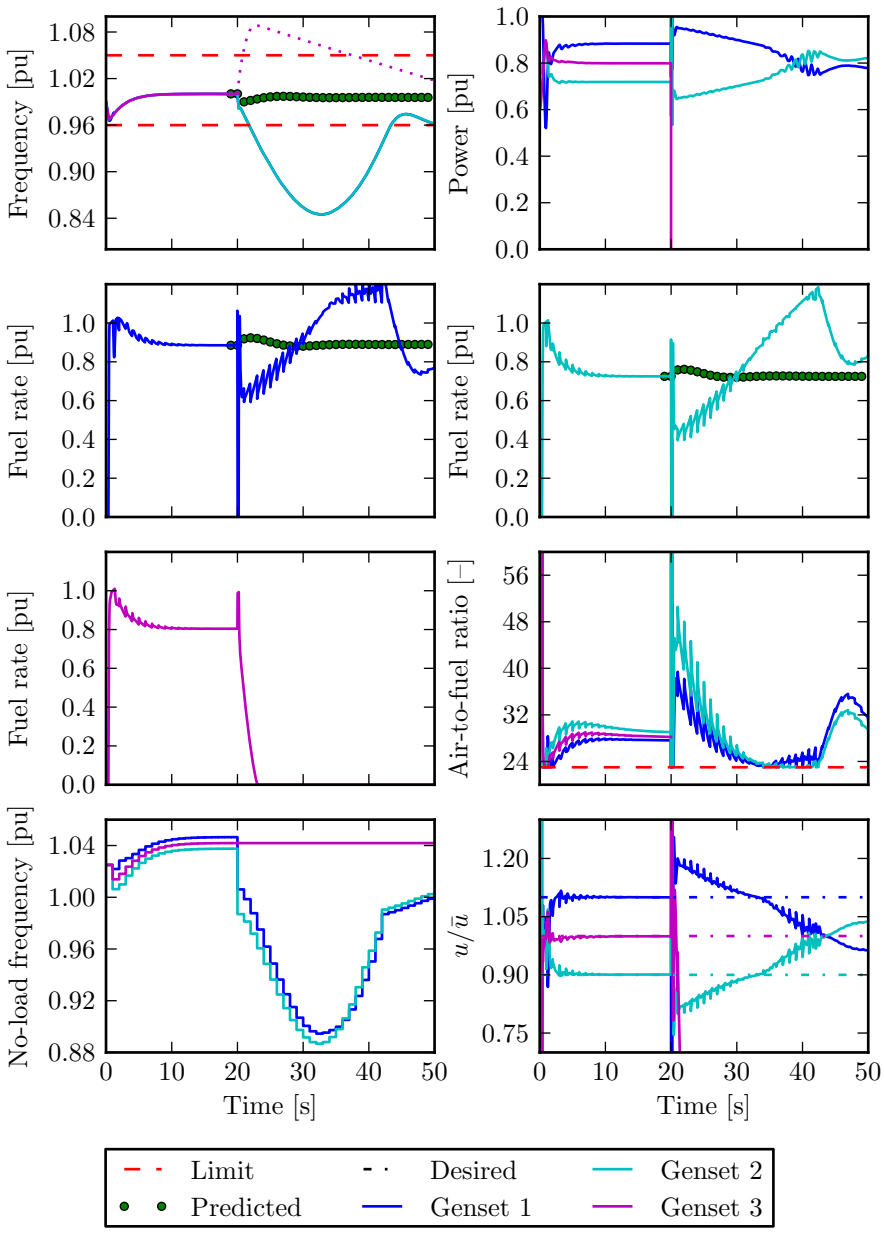

Figure 6.5: Results from simulation of sudden disconnection of Genset 3, with FLR and rate based constraint. Load start with 80% of installed power and reduces to 40%. The dotted line denotes the frequency of Genset 3 after disconnection.

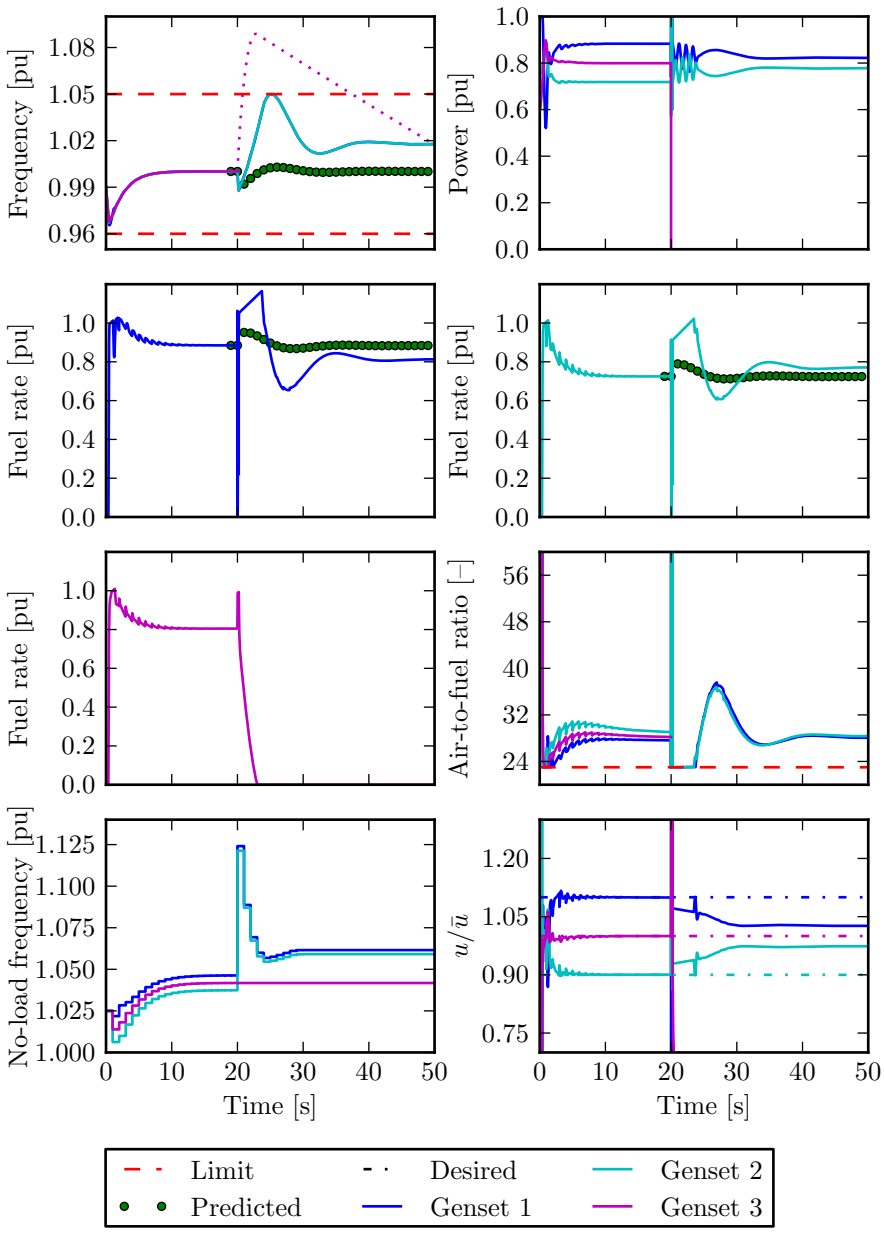

Figure 6.6: Results from simulation of sudden disconnection of Genset 3, with FLR. Simulated with air dependent fuel rate constraints. The disconnection occurs at $t = 19.99$ seconds. The dotted line denotes the frequency of Genset 3 after disconnection.

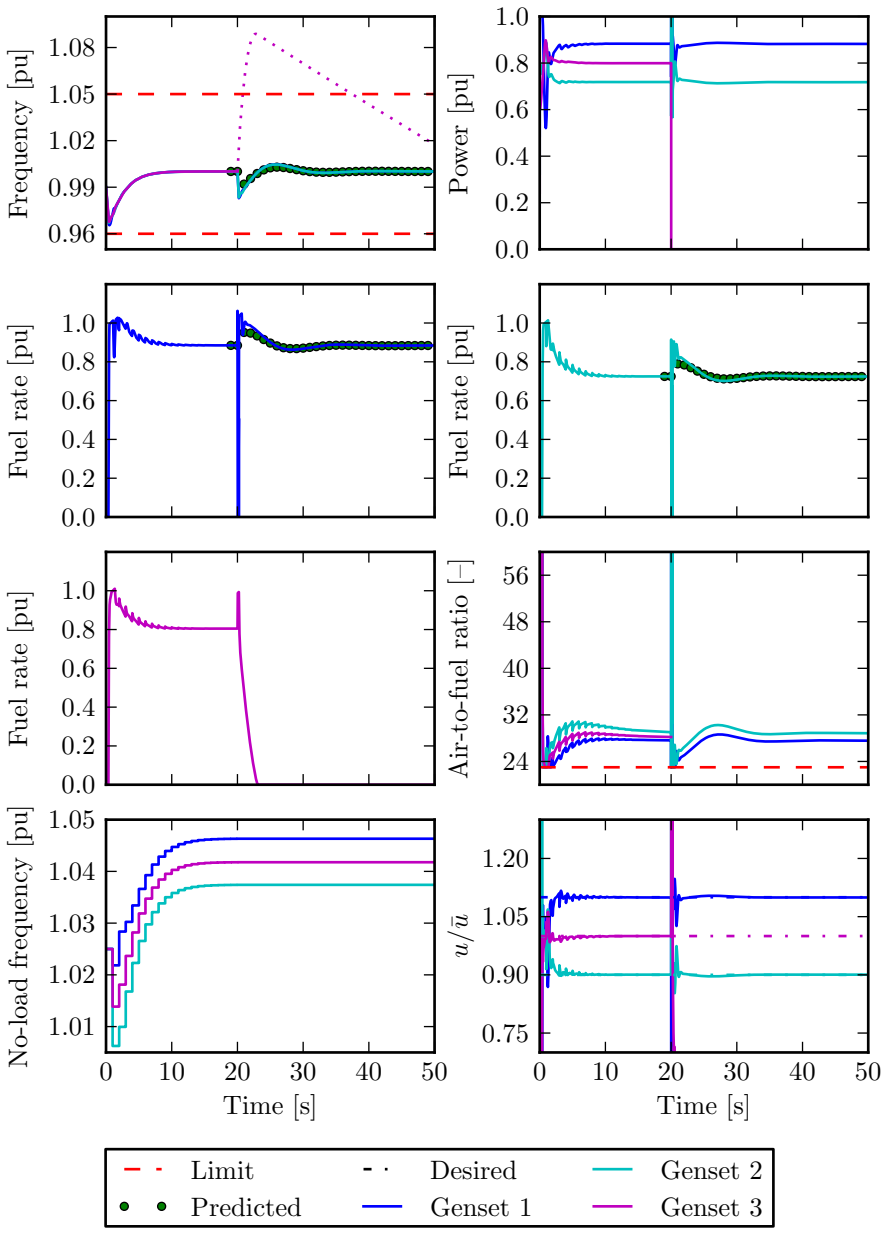

Figure 6.7: Results from simulation of sudden disconnection of Genset 3, with FLR. Simulated with air dependent fuel rate constraints. The disconnection occurs at $t = 20.01$ seconds. The dotted line denotes the frequency of Genset 3 after disconnection.

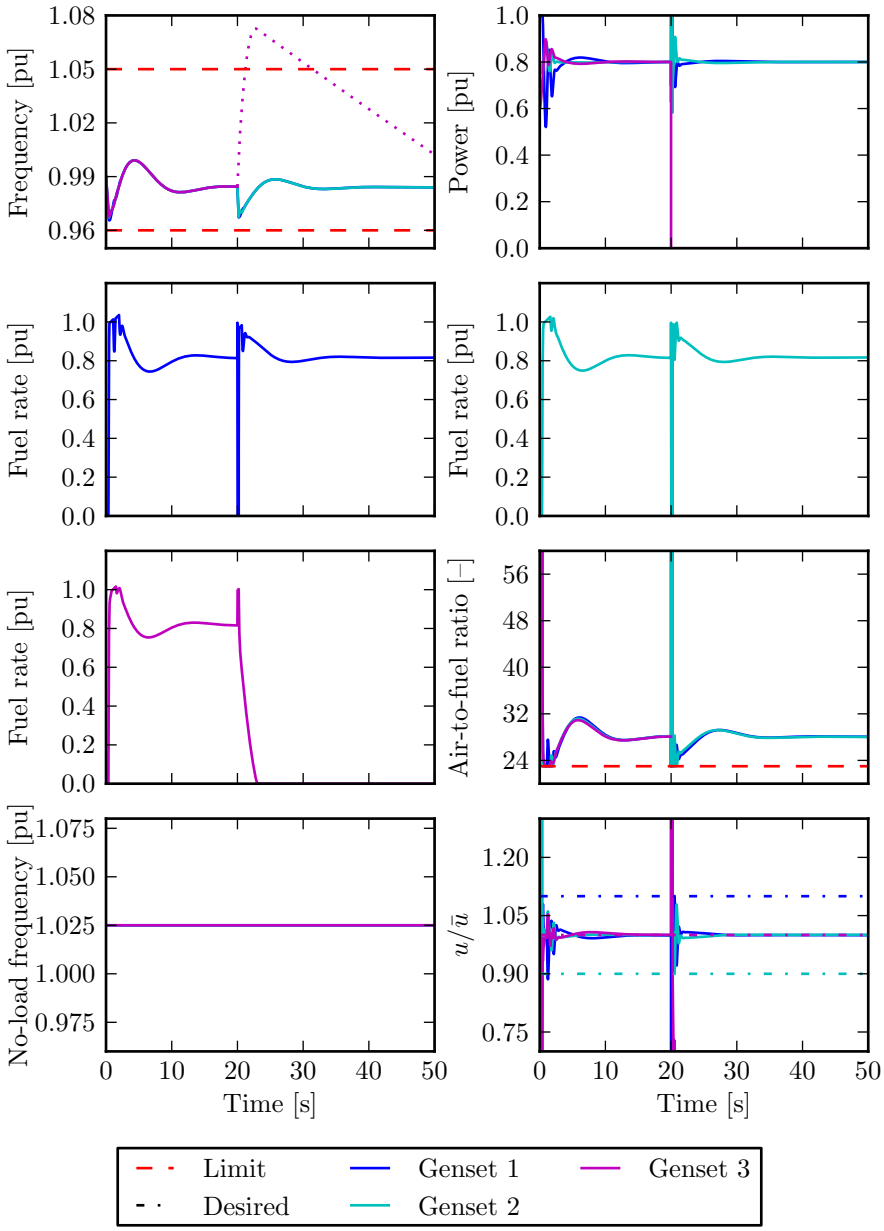

Figure 6.8: Results from simulation of sudden disconnection of Genset 3, with constant no-load frequency. The dotted line denotes the frequency of Genset 3 after disconnection.

6.2 Varying Load

One of the most demanding load cases for a marine power plant is varying load with high amplitude. They are often due to waves, where the consumption by the heave compensators or dynamic positioning (DP) will vary with the wave.

6.2.1 Slowly Varying Load

In Figure 6.9, results are shown where the load is varying with a period of 100 seconds and varying between 5% and 75% of installed power. The controller handles this case very good. The frequency is kept fairly constant and the load is shared as desired. Also note that the predictions for fuel rate are wrong, since the load is assumed to stay constant. The case is simulated with the rate based constraints. Air dependent fuel rate constraints would give the same results, since the constraints are not active.

In Figure 6.10, the simulation is done with constant no-load frequency. It is clear that the MPC mainly reduces the variation of the frequency in this case.

6.2.2 Wave Load

Next a similar simulation is done with a period of the load of only 10 seconds. This is a period that can occur due to waves. Note that this corresponds to a ramp time (i.e., time from 0 to 100% load) of around five seconds, this is much faster than the ramp time used in the rate based fuel rate constraints, which is 25 seconds.

In Figure 6.11, results of simulation with the rate based constraints are plotted. As expected the controller does not work. The problem is that during intervals of low load demand, the controller sets too low constraints on the fuel rate, because the current fuel rate is used to constrain the next fuel rates. The controller decreases the no-load frequency to reduce the fuel rate, which ends up leading the system into underfrequency.

Figure 6.12, shows the case with the air dependent constraints. With these constraints the frequency stays within the limits. However, the average frequency is very low, excessive air at the periods of low load should be used to increase the average frequency.

At last a simulation is done with the MPC turned off (i.e., constant no-load frequency), this is shown in Figure 6.13. This gives larger variations of frequency than with the MPC turned on and with air dependent fuel rate constraints. This shows that with better control technology than used today, it should be possible to reduce the variations of frequency for this case.

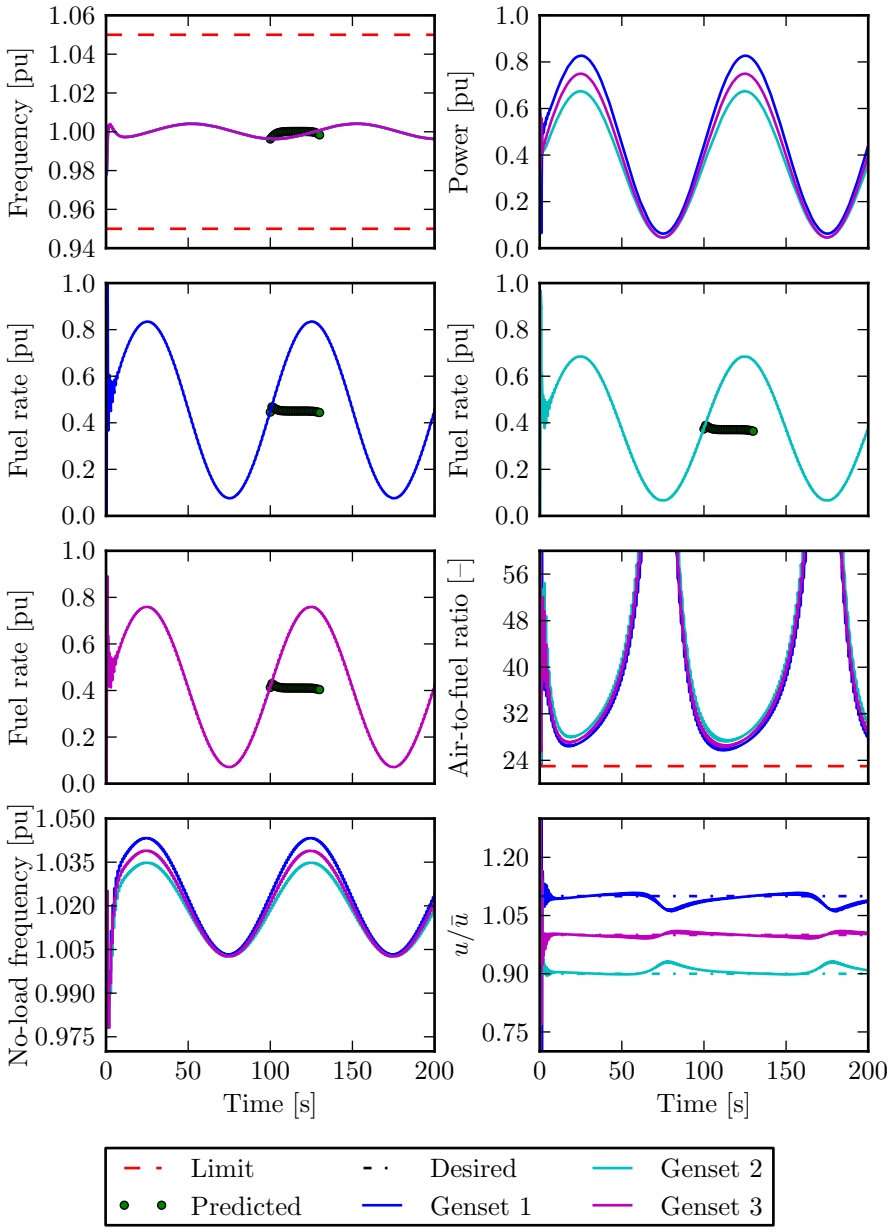

Figure 6.9: Results from simulation with slow periodic load. Note that the prediction of the load is that it will stay constant.

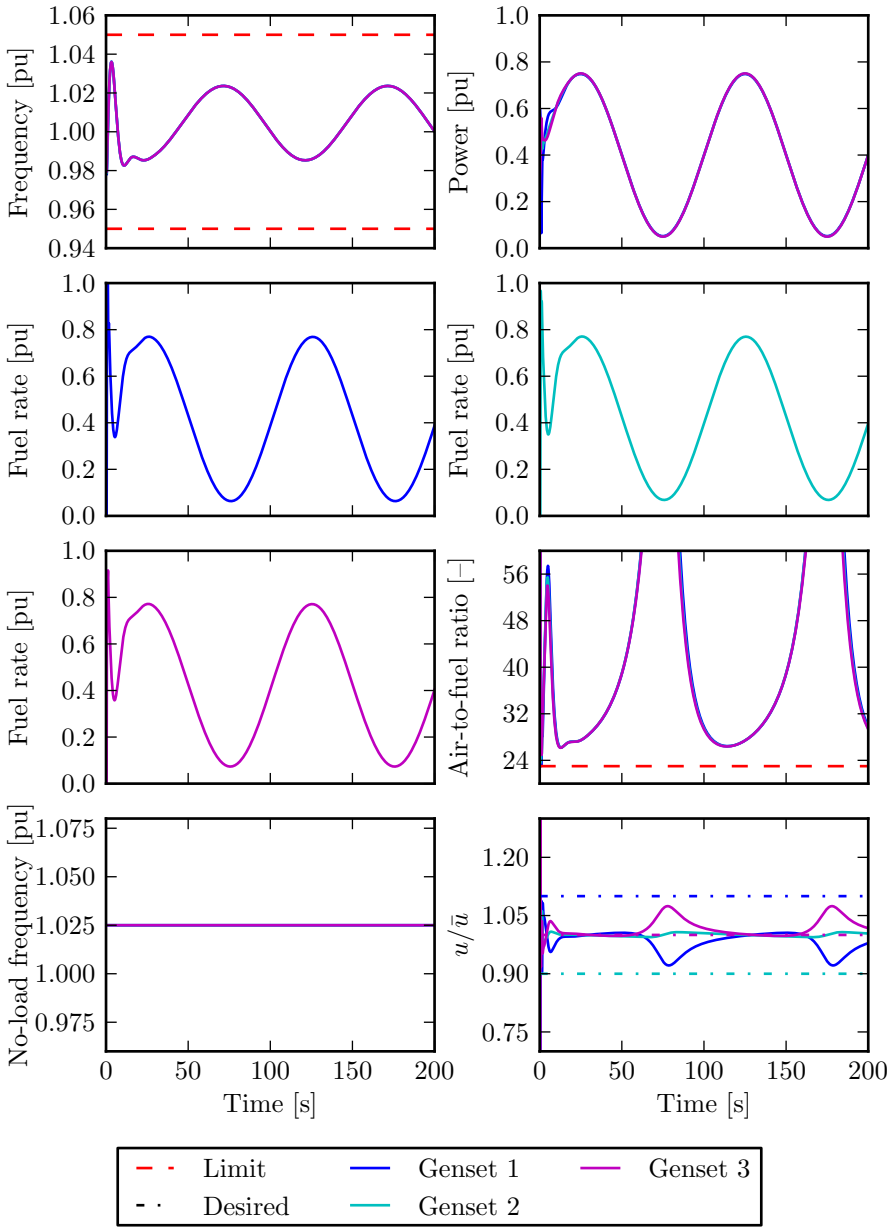

Figure 6.10: Results from simulation with slow periodic load and constant no-load frequency.

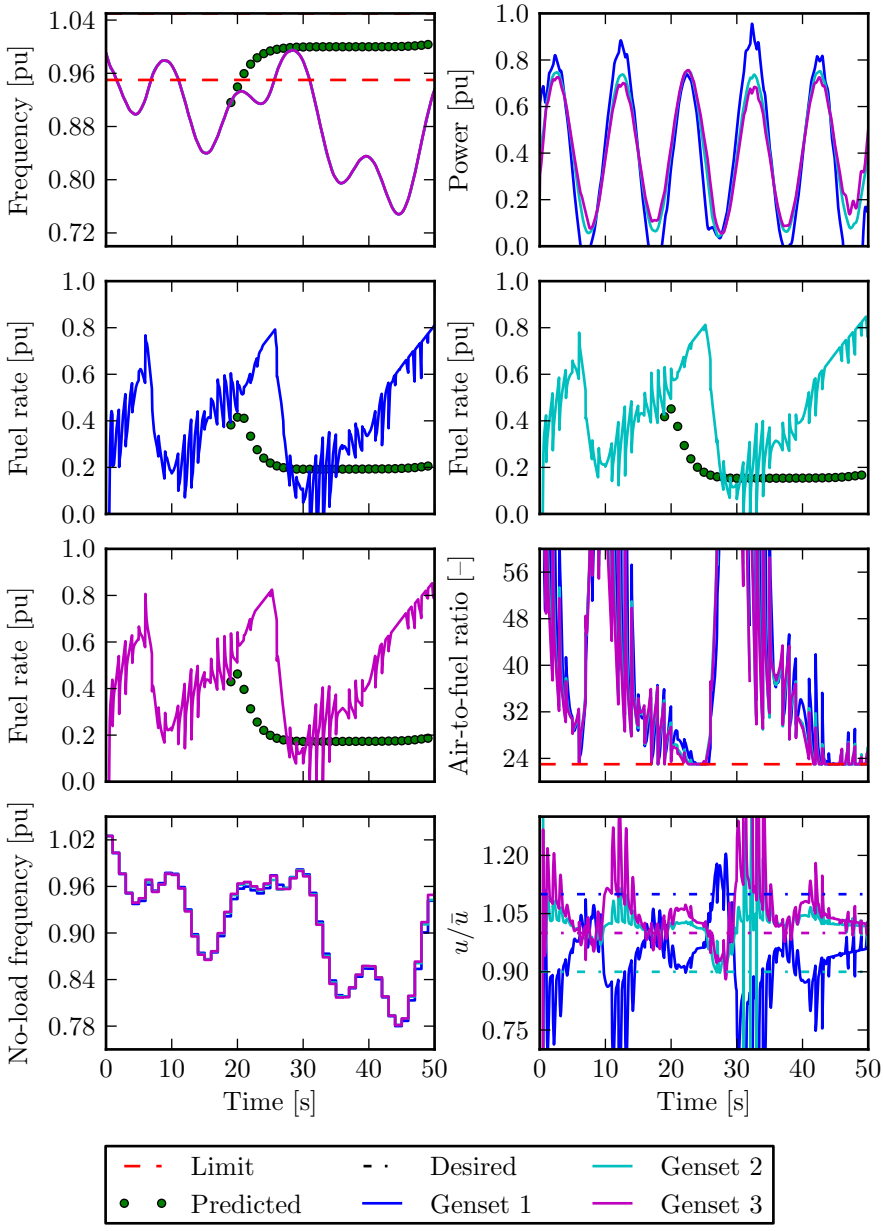

Figure 6.11: Results from simulation with fast periodic load and rate based fuel rate constraint. The ramp time of the load is shorter than the ramp time given as fuel rate constraints for the MPC.

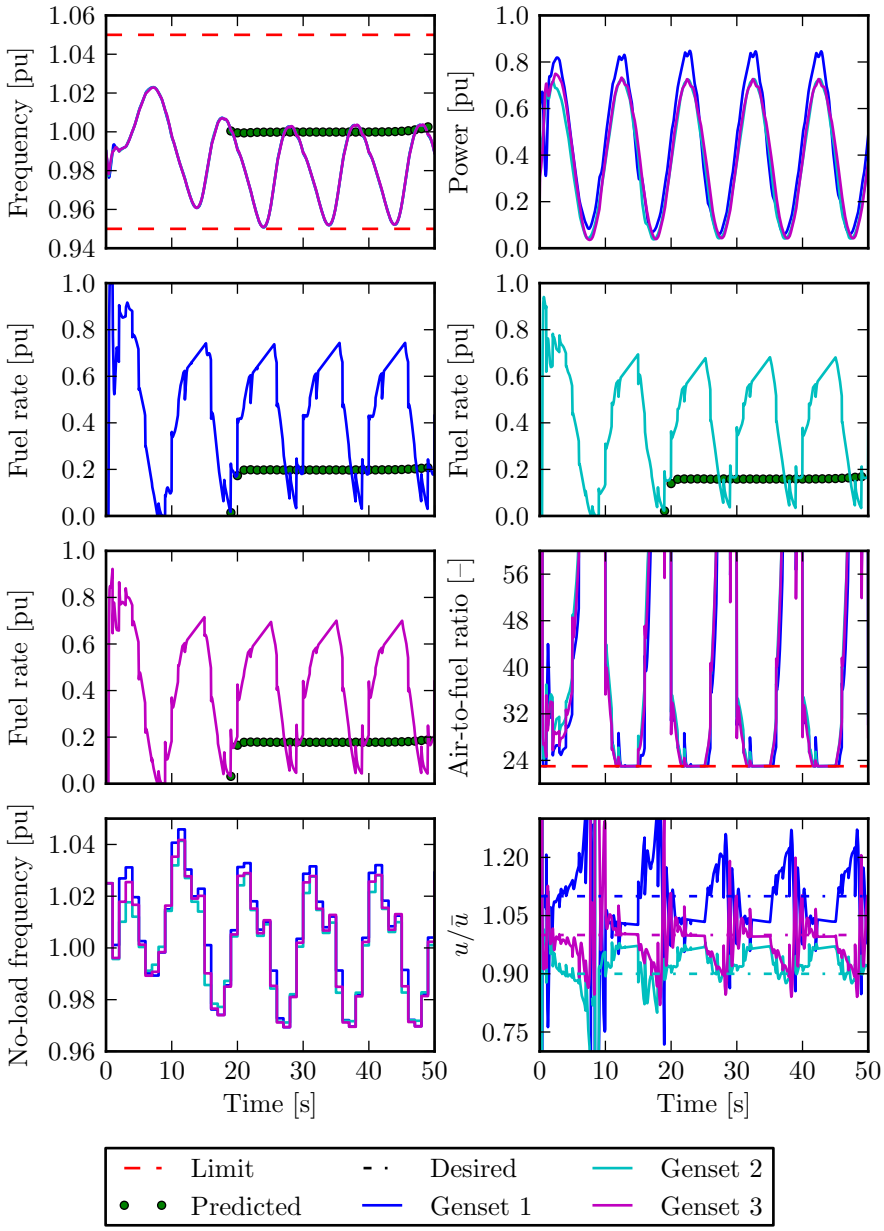

Figure 6.12: Results from simulation with fast periodic load, with air dependent fuel rate constraints. Note that there is much air available at the periods of low loads, this can be used to increase the average frequency.

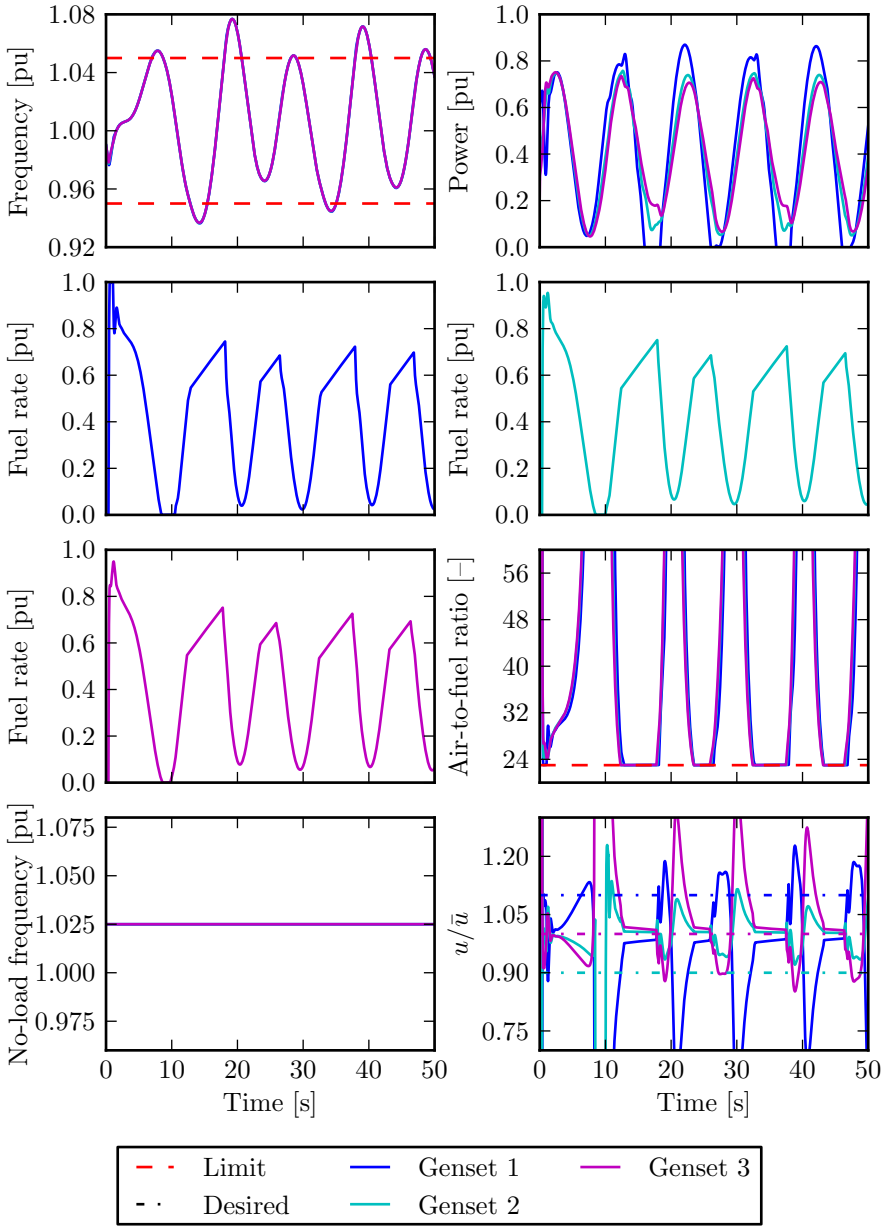

Figure 6.13: Results from simulation with fast periodic load, with constant no-load frequency.

6.3 Frequency Cost

The designed controller has a cost function where the error between the frequency and the rated frequency is penalized. In Figure 6.14, a simulation is done without any penalty on frequency error, and a similar simulation is shown in Figure 6.15, with a large penalty on frequency errors.

It is clear that with no penalty, the frequency is chosen as low as possible, but high enough to satisfy the failure case constraints. However, with big penalty the frequency stays close to the rated frequency.

Both these behaviors could be desired. For example if a new genset is synchronized to the bus, a constant frequency makes it easier to synchronize. However, during some operation it is more important to have less variation on the fuel rate than frequency. The variations in frequency can then be used as energy storage to reduce some of the variations on the fuel rate.

6.4 Tuning of Fuel Rate Constraint

To tune the rate based fuel rate constraints, the load is increased from 0% to 100% in a ramp. The ramp is set so steep that the constraints in the turbocharger are only active for short amounts of time, see Figure 6.16. The simulated ramp has a ramp time of 30 seconds. Only some saturation of the fuel rate occurs at the end, so this ramp time seems to be the minimum.

Note that the fuel rate and frequency decreases at the end of the prediction. This happens since the total fuel rate does not give energy balance (i.e., more power is consumed than supplied). The controller tries to achieve the desired fuel rate; this gives the decrease of fuel rate and frequency. This effect can be removed by adding an end cost to the cost function.

In Figure 6.17, the air dependent fuel rate constraint is tuned. The test simulation is started with a step, to utilize the maximum fuel rate. After this the fuel rate is increased with the same ramp as above. The resulting air-to-fuel ratio is in this case closer to (but always above) the minimum air-to-fuel ratio, this means that more of the potential of the diesel engine is used.

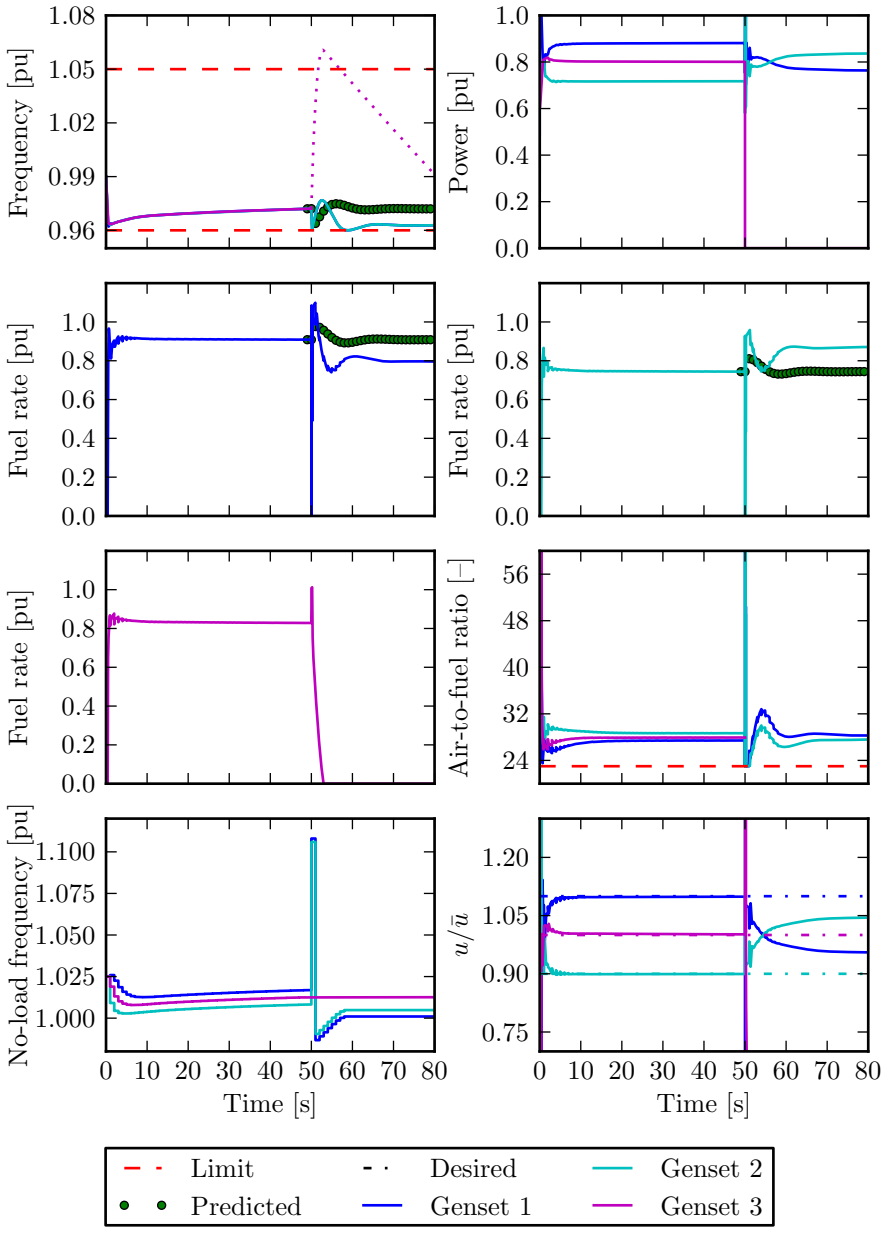

Figure 6.14: Results from simulation with disconnection of Genset 3, without any penalty on frequency error. The dotted line denotes the frequency of Genset 3 after disconnection.

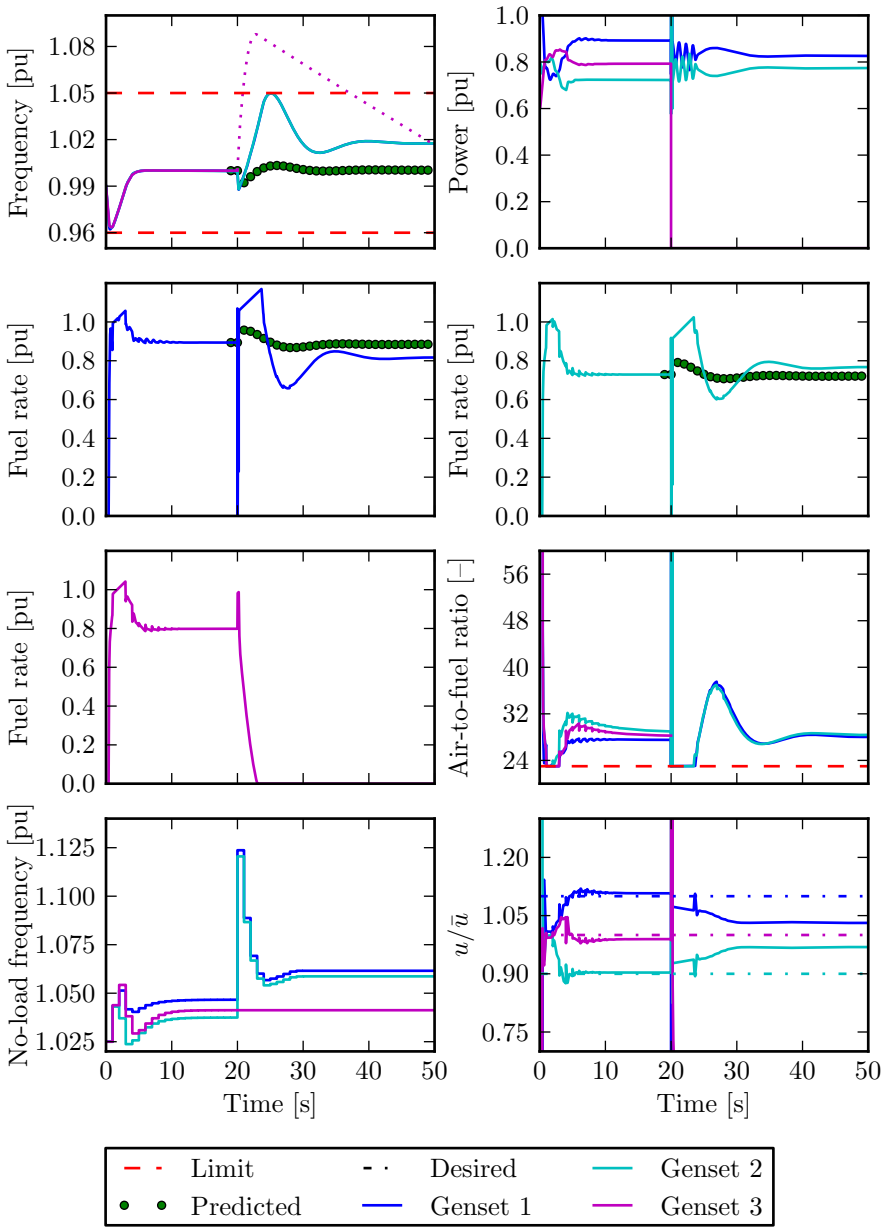

Figure 6.15: Results from simulation with disconnection of Genset 3, with high penalty on frequency error. The dotted line denotes the frequency of Genset 3 after disconnection.

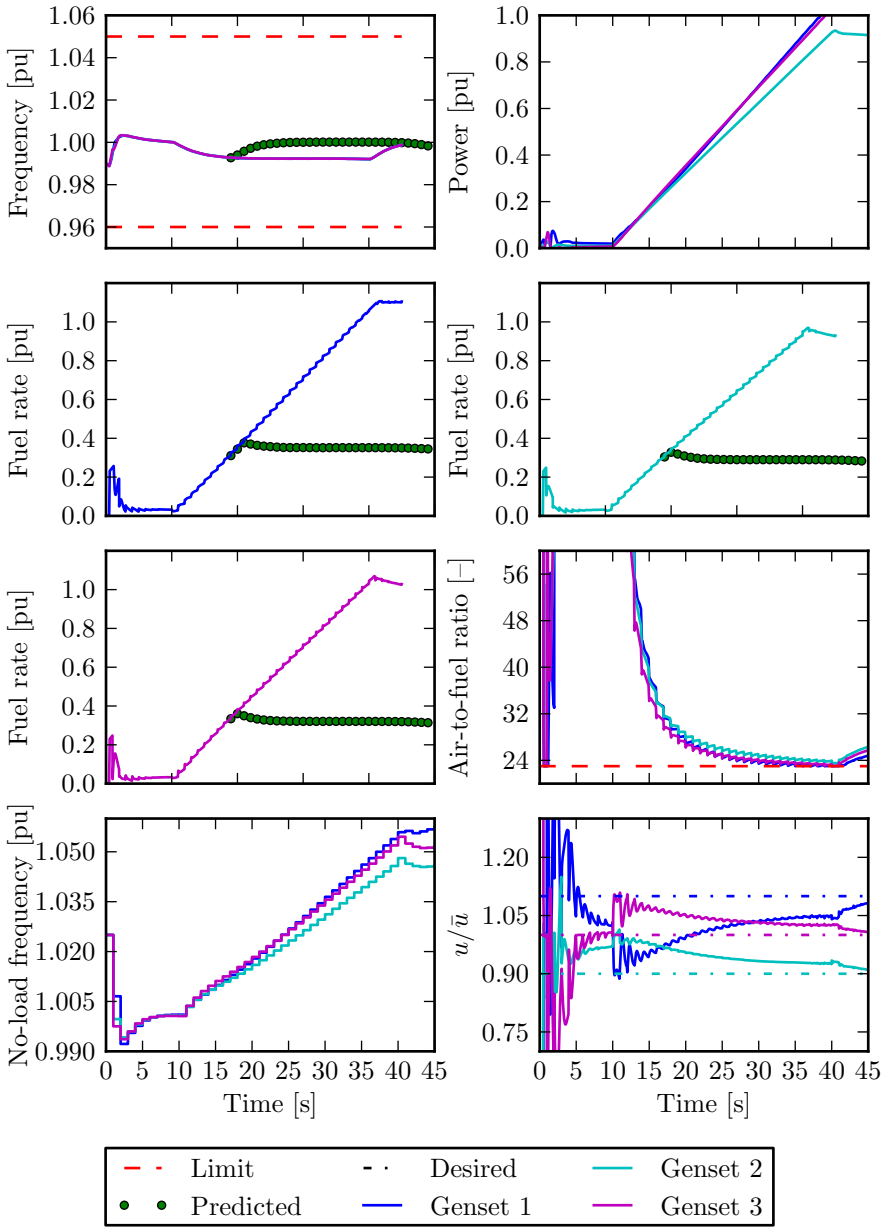

Figure 6.16: Simulation for estimation fuel rate ramp time. The load is increased with a ramp and only some saturation of fuel rate is registered.

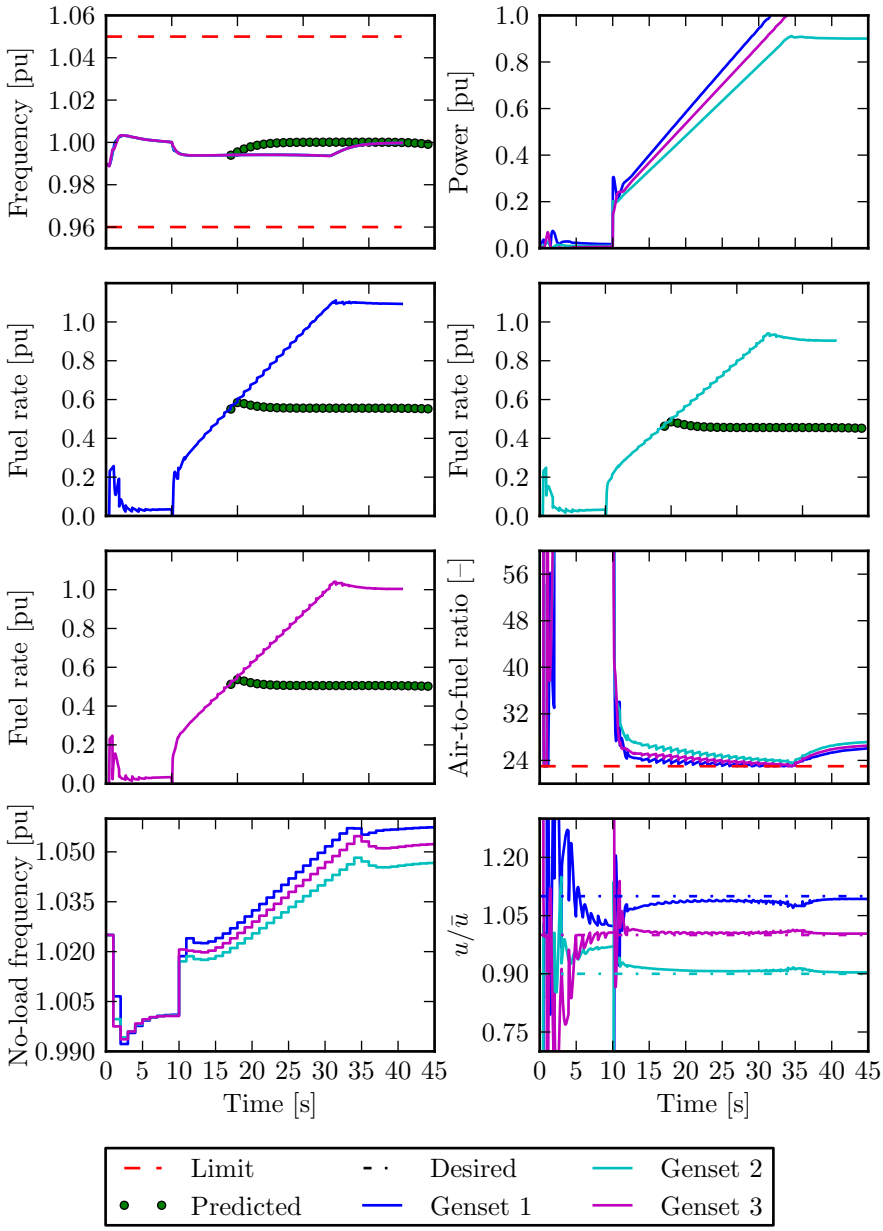

Figure 6.17: Simulation for estimation of fuel rate ramp time using air dependent fuel rate constraints. The load is increased first as a step and then as a ramp. Only some saturation of fuel rate is registered in the simulation.

6.5 Update Frequency and Prediction Horizon

The update frequency must be so fast that it can handle the fastest dynamics. In Figure 6.18, a disconnection is done with constant no-load frequency, this is done to estimate the time scales of the process. The fastest dynamics seems to operate in a time scale of seconds. It seems therefore reasonable to set the update frequency to 1 second.

From the figure the length of the control horizon can also be chosen. The rule of thumb is that the length should at least be comparable with the time scale of the slowest dynamics. From the figure it is clear that most of the dynamics dies out after 20 seconds. To be safe the horizon is set to 30 seconds.

The change of no-load frequency gives a jagged fuel rate, this is shown in Figure 6.19. To minimize this, the update frequency can be increased, since this gives smaller changes of the no-load frequency.

In Figure 6.20 and 6.21, the simulation is repeated with update interval of 0.5 seconds and 0.3 seconds. For all cases the prediction horizon is set constant to 30 samples, equivalent to 15 and 9 seconds.

Note that with shorter update interval the changes of fuel rate are smaller. Also the frequency converges faster to the rated value. The faster convergence can be due to the interpretation of the cost function. When the update frequency is increased, different time samples of the errors are penalized, and the prediction horizon is decreased. It is therefore reasonable that this effect is only due to the cost function. A similar improvement of convergence can be achieved by tuning the cost function.

6.6 Check of Fuel Rate Optimization

One of the control objectives for the controller is to achieve any given load sharing. This could be used to achieve better fuel efficiency of the plant, or to burn off soot by increasing the load share on one genset. In Figure 6.22, fuel rates are compared with the desired fuel rate. All costs on the failure case are removes, to avoid that the load sharing is affected by the failure case.

The figure shows that the fuel rates converge to the desired values. This is also clear from the previous cases, where the fuel rates converges in all of the cases except for the cases where the FLR is turned off and the cases with fast varying load. From this it is concluded that the control objective for load sharing is satisfied.

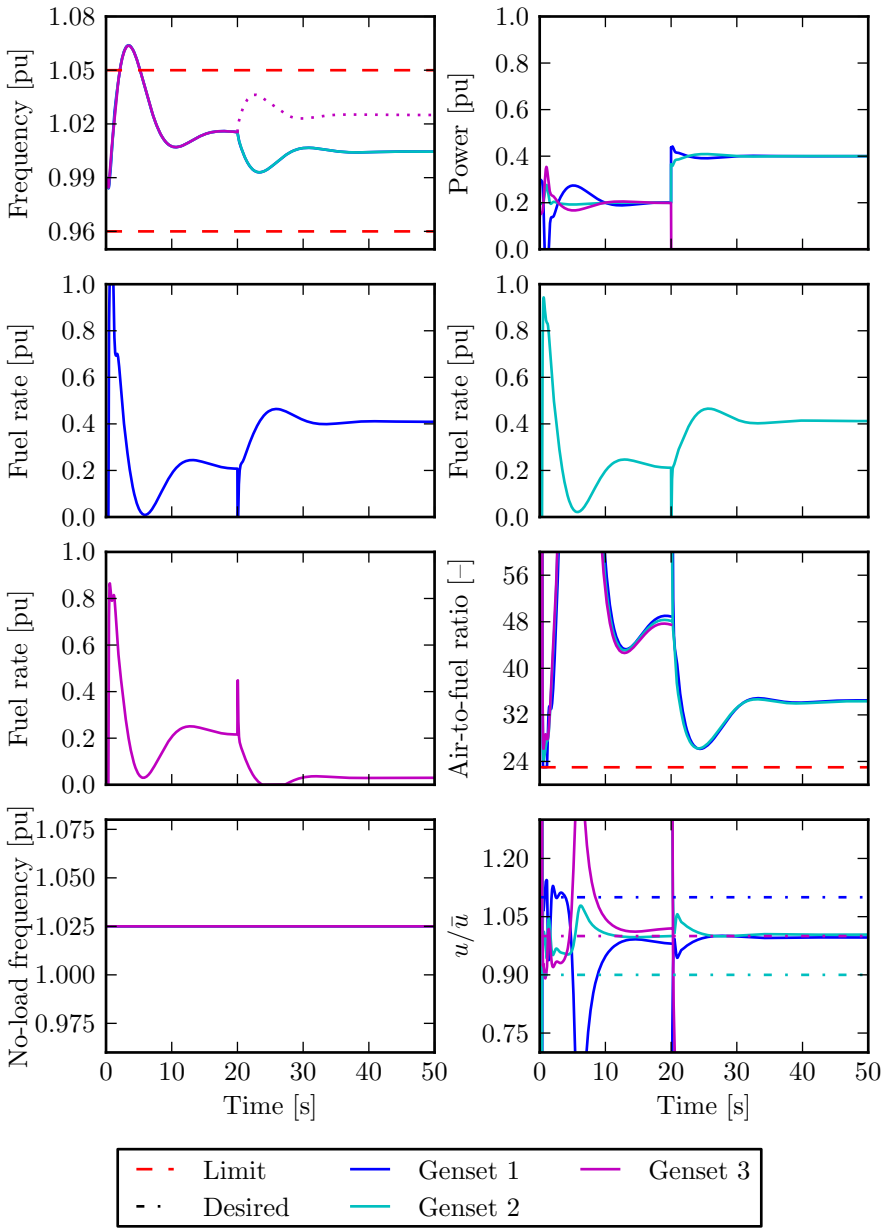

Figure 6.18: Simulation done without MPC for estimation of time constant for the plant. Note that the smallest time constant seems to be of order of seconds. The dynamics also seems to die out after around 15 seconds. The dotted line denotes the frequency of Genset 3 after disconnection.

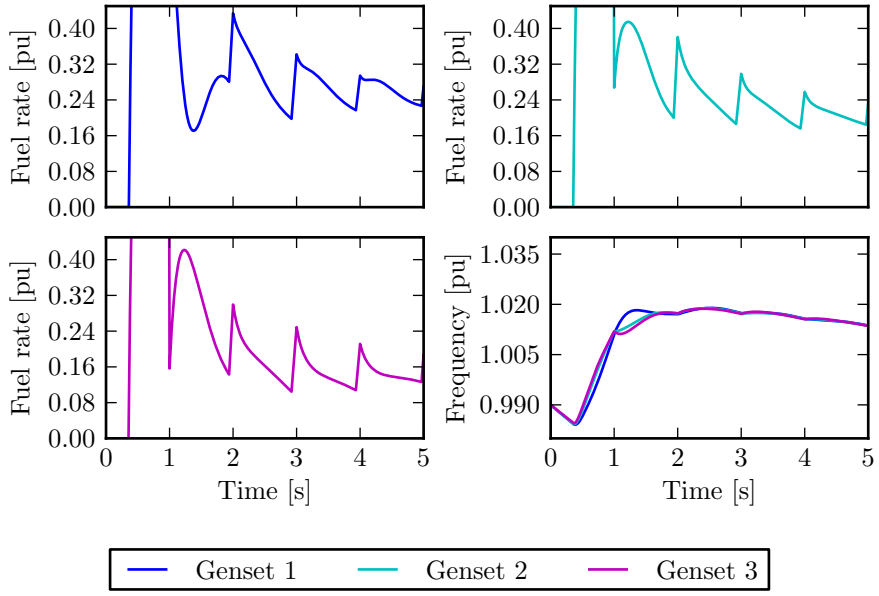

Figure 6.19: Simulation done with update interval of 1 second for MPC.

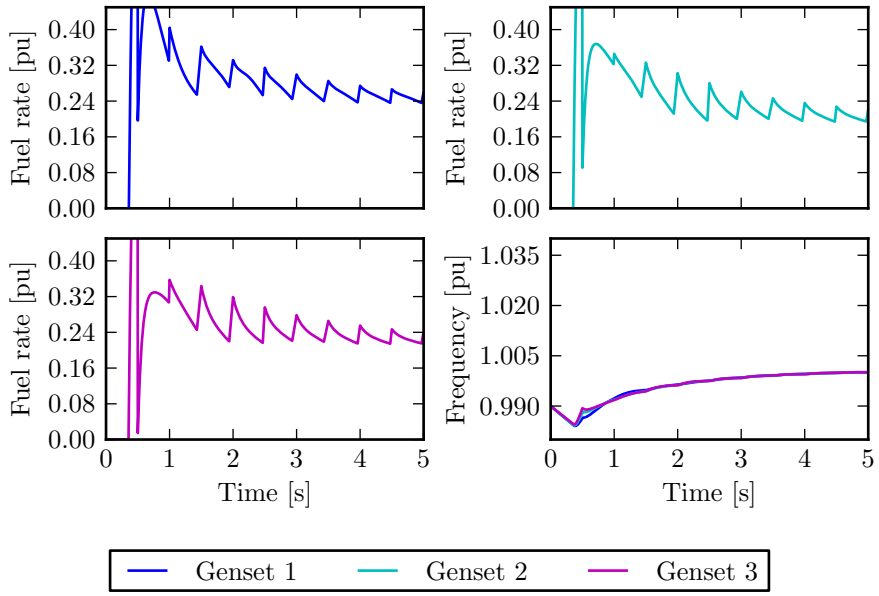

Figure 6.20: Simulation done with update interval of 0.5 seconds for MPC.

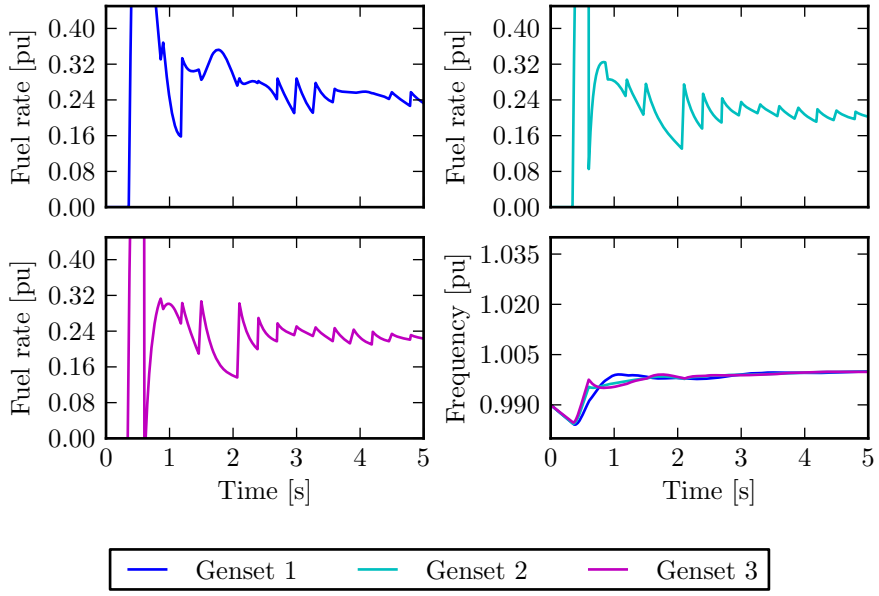

Figure 6.21: Simulation done with update interval of 0.3 seconds for MPC.

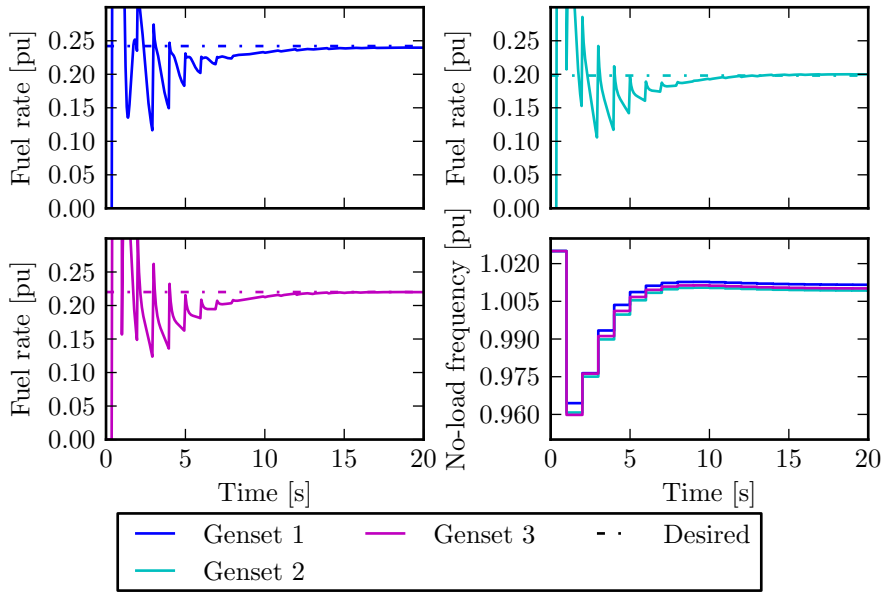

Figure 6.22: Fuel rates compared with the desired values.

Chapter 7

Discussion and Recommendations

In this chapter, recommendations for improvements of the controller are given.

From the case study it is clear that the controller works well, as long as the air dependent fuel rate constraints are used. The linearized model used in the model predictive control (MPC) gives accurate predictions as long as the predictions for the constraints are good and the values are close to the linearization point.

With the air dependent fuel rate constraints the MPC performs well. The predictions are reliable for the failure case, in the sense that when it predicts that the frequency will stay within the given limits after a disconnection, it also manages to keep it so after an actual disconnection. However, if the timing is not as predicted, the frequency can go below the given limits, so a safety margin is needed. It also manages to control the fuel rates to desired values. However, a trade of between failure tolerant load sharing and desired load sharing, moves the load sharing away from the desired load sharing in some cases. Lastly it is seen that this controller achieves smaller variations in frequencies than conventional droop control during load variations.

With the rate based fuel rate constraints the MPC performs unsatisfactorily. It gets confused by small decreases of fuel rates, which results in too low constraints on the fuel rate. This method is mainly included to show that the linear control plant model gives accurate predictions; however, the performance is so poor that it should not be used any further.

7.1 Computation Time

The computational speed of the controller is good, as it is around 0.1 seconds (Intel core i5 2.60GHz). The simulations of the closed loop system are quite fast, where it uses around 0.2 seconds computation time per simulated second.

To achieve the fast computation time of the simulation, some values are low-pass filtered in the process plant to avoid problem with algebraic loops. The time constant for such filters are typically set to a millisecond, which is in all cases much faster than the affected dynamics.

7.2 Include Efficiency

In the controller a desired load sharing is set to be proportional to the consumed power. However, this is set arbitrary to show that the controller manages to achieve any desired load sharing. The next step for a more fuel efficient power plant is to use actual efficiencies in the cost function, so that the overall efficiency is maximized. The process plant should also include the efficiency, so that the benefits can be estimated.

7.3 Better Process Plant Model

The long term goal of this work is that the controller can be developed further and at the end be implemented in a real plant. To make this possible it is important that the controller is tested as much as possible. A more realistic process plant is therefore needed. Things that may be done to improve the process plant are:

- Add process and measurement noise.
- Output only measured values (internal variables such as states of governors must be estimated).
- Use different parameters in controller and process plant.
- Include more details in turbocharger/air dynamics in the diesel engine.
- Model consumers (e.g., DP, drilling and hive compensators), which gives a better description of the time evolution of the loads.

7.4 Governor

In this thesis the controller manipulates the no-load frequency of governors with droop. This gives a peak each time the frequency is changed. To avoid this effect

the no-load frequency must be made continuous. This can be achieved by using predictive first-order hold.

Another possibility is to use other types of governors. Isochronous load sharing seems to be a good alternative (see Section 2.2). The MPC can then adjust the power sharing and the common reference frequency. Isochronous load sharing has also better properties than droop during step changes of the load. While a droop controller will for a short amount of time reduce its reference speed, and hence the fuel rate, will a isochronous governor react instantly. However, the droop controller is generally believed to have better failsafe properties than isochronous since it does not depend on a common load sharing line that may fail and lead to common mode failure.

The best solution may be to develop a new type of governor tailor made for this problem. The governor could be based on MPC and utilize prediction given by the overall Power Management System (PMS)-controller. However, this is longer into the future than the alternatives mentioned above.

7.5 Linear Model Predictive Control

This controller is based on linear model predictive control. An alternative is to use nonlinear model predictive control. The linear MPC is chosen since this method generally has lower computational time than nonlinear methods. In the development process the model has been validated by running simulations with the linearized control plant model in parallel with the nonlinear process plant model (not shown here). The linearized model is accurate as long as the values are close to the linearization point, when the difference is large the estimates are still fairly accurate.

It should also be considered to linearize along a trajectory instead of linearizing around the current value. If the linearization is done around the prediction from last time step (see Figure 7.1) the prediction will be better. This improvement may be especially large for the failure cases. At the time instant when the failure occurs, the states may be far from an equilibrium. The current linearization may give wrong equilibrium and may degrade the performance of the controller. However, the predictions will converge to the true solution if the prediction for the failure case from the previous update is used for linearization, since the model gets better after each update.

7.6 Include Turbocharger in Control Plant

As seen in the previous chapter, the rate based constraint gives good predictions but the constraints are too conservative. The air dependent constraint gives good performance, but not as good predictions.

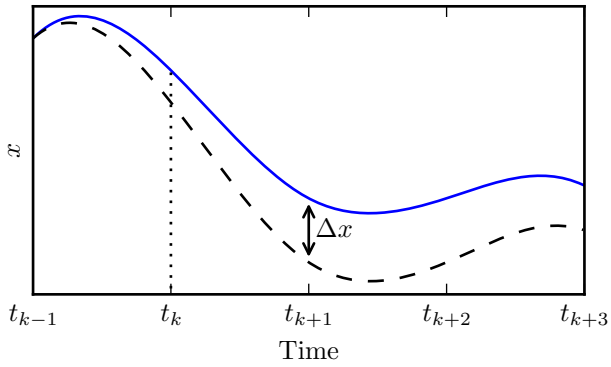

Figure 7.1: Illustration of an alternative linearization, where the linearization is done around the prediction from last update (dashed line). The actual value is the blue line.

A better way of calculating these constraints are to use the turbocharger model used in the process plant, in the control model. Both the model and the constraint are linear, so it should give good estimates. This will give better predictions of how fast the fuel rate can increase during critical periods, hence less conservative predictions of the failure cases.

7.7 Constraints for Failsafe

The MPC will make decisions on wrong assumptions if a sensor fails in the power plant. This may lead the MPC to give no-load frequencies that drives the system into an unsafe condition.

To address this problem, the no-load frequency should be constrained to a range of safe no-load frequency, such that the controller cannot drive the system in to a blackout. To find such a bound may be a study in itself. As a start a large bound can be set, for example a bound for per unit no-load frequency may be 90% to 115%, if 5% droop is used.

7.8 Predictions of Load

In this study the controller predicts that the load will stay constant. However, for marine power plants the consumed load is seldom constant. In rigs the load will often vary with the waves, due to heave compensators and dynamic positioning (DP). These variations will propagate to both the fuel rate and the frequency. If knowledge of how the load varies is obtained and used, these fluctuations can be

reduced. However, erroneous predictions can in worst case drive the system to an unsafe state. This risk can be reduced by using the method outlined in Section 7.7 and by using sets of different load predictions.

7.9 Fast Load Reduction After Disconnection

The Fast Load Reduction (FLR) is not modeled after a disconnection in the MPC, since the period where this is needed is very short (i.e., only from disconnection till the loads are reduced). However, this implementation gives in some cases unwanted, but not fatal, consequences. To remove this effect the FLR should be modeled also after a disconnection. This will give better predictions and performance.

7.10 Frequency Margin

After a failure the problem is often to avoid underfrequency. It is therefore important to have as large as possible margins on the frequency.

To increase the margin, a cost for the largest deviation of frequency during the prediction horizon can be added to the cost function. This can be done by using a slack variable that is the largest deviation from the rated frequency during the prediction horizon. It can be implemented by adding constraints and a slack variable:

$$\omega_d - \epsilon \leq \omega[k+i] \leq \omega_d + \epsilon \tag{7.1}$$

$$0 \leq \epsilon, \tag{7.2}$$

where $1 \leq i \leq m-1$. This is equivalent to:

$$\epsilon = \max_i |\omega[k+i] - \omega_d| \tag{7.3}$$

7.11 Soft Constraints on Change of Fuel Rate

In diesel engines there is an internal controller, it sets the limit of how fast the fuel rate can be increased. However, some internal controllers have different modes, for example can the internal limit be increased if it runs in *emergency mode*. To utilize this mode, a soft limit can be set at the limit for normal operation, while a hard limit is set at the limit for emergency mode. With suitable tuning the MPC will use the limit for the normal mode as long as possible, but when it needs more transient capacity it will automatically use the emergency mode.

7.12 More Failure Cases

As shown in Section 6.1.1, it is not optimal to only use one failure case in the MPC. Since this will make the MPC *think* that only one certain genset could disconnect. In a power plant it is seldom known which generator that will disconnect. Therefore, it is suggested that a disconnection case for each genset is calculated, as long as there is no good reason to believe that one certain generator will disconnect (e.g., a pre-warning for a genset is given).

Other cases could be calculated as well, for example:

- Step increase of load (may give underfrequency).
- Step decrease of load (may give overfrequency).
- Defect governor (may give overload or inverse power).
- Switchboard short circuits, with separation of connected switchboards (i.e., loss of several gensets).

7.13 Faster Sampling Rate for Failure Cases

After a disconnection the load is reduced by the FLR after around 200 milliseconds. This gives a decreasing frequency until the FLR reduces the load, after this time the frequency will typically increase again. This means that the minimum frequency occurs at around 200 milliseconds; however, in the calculation of the failure case the sampling rate is 1 second. This means that the calculated minimum frequency, could be much higher than the actual minimum (this effect is simulated but not shown). This can either be handled with a safety margin, as used in this study, or the sampling rate can be increased for the calculations of the failure case.

It can also be considered to reduce the length of the prediction horizon, since it often is clear if a blackout will happen after only a few seconds after the failure.

7.14 Monitoring of the Slack Variables

The slack variables connected to frequency of the failure case can be used by warning systems and automatic safety features. An underfrequency or overfrequency is predicted to happen during the failure case if these slack variables get too high. This information can be used to take action for reducing the risks. Such actions can also be to start standby genset, using jet assist, or reducing the power consumption. An alarm can also be sent to the operator, to inform that the plant is not in a safe condition.

Conclusion

In this thesis a controller based on model predictive control has been developed. The controller gives settings to governors, while the governors are in charge of the low-level control. To handle failures the controller calculates both a normal case and a failure case. The failure case used to illustrate the method is a disconnection of the largest genset.

To constraint the fuel rate an air dependent fuel rate constraint is used. It allows the fuel rate to step up to the maximum fuel rate that gives complete combustion, and afterwards the fuel rate can increase linearly. A rate based fuel rate constraint is also implemented, where the fuel rate can increase linearly but without a step at the beginning.

The controller is verified by a simulation study, where different cases are simulated. With the air dependent constraint the performance is good during all the simulated cases. However, the predictions are often conservative. During periods when the load varies greatly, this controller reduces the variations of frequency compared with standard droop implementations.

The use of failure case seems to work very well. The failure case gives in practice a constraint on the frequency for the normal case. This constraint makes sure that the frequency during the failure case does not go below a given limit. However, the frequency did go under the given limit when the timing of the disconnection was changed. It is therefore recommended to have some safety margins on the frequency limits.

The controller is also able to achieve any desired load sharing. This can be used to increase the efficiency of the plant.

Simulations was also done with the rate based fuel rate constraints, this gave good predictions in some cases. However, this method sets too strict constraints on the fuel rate when the fuel rate decreases for a short amount of time. This lead to blackout in some cases. This method for constraining the fuel rate is therefore not recommended. The method is included to show that the control plant model gives accurate predictions if the predictions of the fuel rate constraints are good.

Recommendations for further improvements of the performance are discussed in

Chapter 7. It is recommended that a simple model of the turbocharger is included in the control plant model. This will give better predictions of the fuel rate constraints than the air dependent fuel rate constraint; hence it will give better performance and predictions of the control outputs.

When the no-load frequency is change, a jagged response of the fuel rate occurs. However, one of the goals with the controller is to get a smoother fuel rate. To remove this effect, the changes of settings in the governor must be made continuous. The recommendation is therefore to use predictive first-order hold for changes of the no-load frequency, instead of zero-order hold.

It is also clear from simulation that multiple cases should be calculated. During the simulation with only one case, the controller tries to avoid only the given case. For example it reduces the load on the genset that is expected to disconnect. However, there are no reasons to believe that the other gensets cannot disconnect. Therefore a case for each generator should be used.

Other recommendations are:

Better process plant, for better validation of the controller.

Soft constraints on changes of fuel rates, for utilizing of emergency modes of the gensets.

Failsafe constraints, give a range for values of settings for governor, to ensure that the governors cannot be set to settings that can drive the system into blackouts.

Increase the number of failure cases, for assuring that the plant handles even more failures.

Add efficiency to both models, for optimizing of the fuel consumption.

Change type of governor, for better performance.

The potential of the new controller seems to be large. With further development, where the recommended improvements are implemented, this controller is expected to give significant better safety, reduced operational costs, and lower emissions.

Bibliography

ABB (2012). Breakthrough order for dc technology, http://www.abb.com/cawp/seitp202/eed2d9bfd017d66dc12579ac0035469e.aspx. Online; accessed 22-02-2012.

Arfolini, R. and Bloisi, V. (2007). *On optimal control of the wastegate in a turbocharged si engine*, Master's thesis, Kungliga Tekniska högskolan.

Bø, T. I. (2011). Development of a diesel-electric simulation model and nonlinear control of power load-sharing, *Technical report*, Project Thesis, Norwegian University of Science and Technology.

Blanke, M. (1981). *Ship Propulsion Losses Related to Automatic Steering And Prime Mover Control*, PhD thesis, Technical University of Denmark (DTU).

ComAp (2009). *MainsCompact NT, Mains controller for the InteliCompact genset controllers, Reference Guide*, ComAp. http://cdn.comap.cz/files/manuals/MainsCompact-NT-1.0-Reference%20Guide.pdf. Online; accessed 02-06-2012.

Djagarov, N., Bonev, M. and Grozdev, Z. (2011). Study of the work of ship electrical power station at anchor-mooring device operation, *Environment and Electrical Engineering (EEEIC), 2011 10th International Conference on*, pp. 1 –4.

Ådnanes, A. K. (2003). *Maritime Electrical Installations And Diesel Electric Propulsion*, Department of Marine Technology, NTNU.

DNV (2012). Rules for classification of ships. Det Norske Veritas, April 2012.

Florián, M., Macek, J., Polášek, M., Steinbauer, P., Šika, Z., Takats, M., Vaculín, O., Valášek, M., Vávra, J., Vítek, O. et al. (2006). Improving the engine transient performance using model-based predictive control, *THIESEL Conference on Thermo and Fluid Dynamic Processes in Diesel Engines*.

Gill, P. E., Murray, W. and Saunders, M. A. (2008). *User's Guide for SQOPT Version 7*, University of California, San Diego.

Guzzella, L. and Amstutz, A. (1998). Control of diesel engines, *Control Systems, IEEE* **18**(5): 53 –71.

Hansen, J. F. (2000). *Modelling and Control of Marine Power System*, PhD thesis, Norwegian University of Science and Technology.

Hansen, J. F., Lindtjørn, J. O. and Vanska, K. (2011). Onboard dc grid for enhanced dp operation in ships, *Dynamic Positioning Conference 2011*, ABB.

Imsland, L. (2007). Introduction to model predictive control. Note from TTK4135 at NTNU.

Jiang, J. (1994). Optimal gain scheduling controller for a diesel engine, *Control Systems, IEEE* **14**(4): 42 –48.

Khalid, M. and Savkin, A. (2010). A model predictive control approach to the problem of wind power smoothing with controlled battery storage, *Renewable Energy* **35**(7): 1520 – 1526.

Krause, P. C., Wasynczuk, O. and Sudhoff, S. D. (2002). *Analysis of electric machinery and drive systems*, second edn, IEEE Press.

Kundur, P., Balu, N. and Lauby, M. (1994). *Power system stability and control*, Vol. 4, McGraw-hill New York.

Kuraoka, H., Ohka, N., Ohba, M., Hosoe, S. and Zhang, F. (1990). Application of h-infinity design to automotive fuel control, *Control Systems Magazine, IEEE* **10**(3): 102 –106.

Maciejowski, J. M. (2002). *Predictive Control with Constraints*, 1 edn, Pearson Education Limited.

Mathiesen, E. (2012). Discussion on fast load reduction. Personal communication, 2012-04-12.

McGowan, D., Morrow, D. and Fox, B. (2006). Integrated governor control for a diesel-generating set, *Energy Conversion, IEEE Transactions on* **21**(2): 476 – 483.

Nord, T. (2006). *Voltage stability in an electric propulsion system for ships*, Master's thesis, Royal Institute of Technology in Sweden.

Ouroua, A., Domaschk, L. and Beno, J. (2005). Electric ship power system integration analyses through modeling and simulation, *Electric Ship Technologies Symposium, 2005 IEEE*, pp. 70 – 74.

Pedersen, T. A. (2009). *Bond Graph Modeling of Marine Power Systems*, PhD thesis, Norwegian University of Science and Technology.

Radan, D. (2008). *Integrated Control of Marine Electrical Power System*, PhD thesis, Norwegian University of Science and Technology.

Rizzoni, G. (2007). *Principles and Applications of Electrical Engineering*, 5th edn, McGraw-Hill.

Rolls-Royce (2011). The HSG concept, http://www.rolls-royce.com/Images/hsg_factsheet_tcm92-18297.pdf. Online; accessed 09-December-2011.

Sebastián, R. and Alzola, R. P. (2010). Effective active power control of a high penetration wind diesel system with a ni-cd battery energy storage, *Renewable Energy* **35**(5): 952 – 965.

Skjetne, R. (2010). Modeling a diesel-generator power plant, Lecture note in TMR4290 at NTNU.

TOMLAB (2011). Tomlab 7.8, Tomlab Optimization, http://www.tomopt.com/tomlab. Computer software.

Veksler, A., Johansen, T. A. and Skjetne, R. (2012). Transient power control in dynamic positioning - governor feedforward and dynamic thrust allocation, *Manoeuvring and Control of Marine Craft, 2012 9th IFAC Conference on*. Submitted for acceptance.

Woodward (2011). *Governing Fundementals and Power Management*, Woodward. http://www.woodward.com/pdf/ic/26260.pdf. Online; accessed 08-12-2011; Manual 26260.

Xiros, N. (2002). *Robus control of diesel ship propulsion*, 1 edn, Springer-Verlag London Limited.

Appendix A

Process Plant Model

In this appendix a more details of the process plant model are presented than given in Section 4.1. For details about the governor and Automatic Voltage Regulator (AVR), see Section 4.1.3.

A.1 Mechanical Equations for Genset

A diesel engine is a rotating machine, Newton's second law for rotation is therefore relevant.

$$J_m \dot{\omega}_m = \sum T_i, \tag{A.1}$$

where J_m is the moment of inertia of the diesel engine and generator, ω_m is the angular velocity of the engine, and T_i are torques.

The equation can be made per unit (pu) by introducing some new variables. Per unit angular velocity, $\omega = \frac{\omega_m}{\omega_{m,b}}$; per unit torque, $t_i = \frac{T_i}{T_b}$; base torque, T_b; and the inertia constant (Krause et al.; 2002):

$$H = \frac{J_m \omega_{m,b}^2}{2S_b} = \frac{J_m \omega_{m,b}}{2T_b}. \tag{A.2}$$

The per unit equation of (A.1) can now be found as:

$$2\frac{H\dot{\omega}_m}{\omega_{m,b}} = 2H\dot{\omega} = \sum \frac{T_i}{T_b} = \sum t_i. \tag{A.3}$$

The mechanical torque, t_m, is the torque produced by the burning of fuel in the diesel engine. It is mainly dependent on the amount of fuel burned. Veksler et al.

(2012) suggest the following model for turbocharger and mechanical torque:

$$(\mathrm{A/F}) = \frac{m_{a,0} + (1 - m_{a,0})\omega_t}{u}(\mathrm{A/F})_n \tag{A.4}$$

$$\eta_c = \begin{cases} 1 & (\mathrm{A/F}) \geq (\mathrm{A/F})_{high} \\ \dfrac{(\mathrm{A/F}) - (\mathrm{A/F})_{low}}{(\mathrm{A/F})_{high} - (\mathrm{A/F})_{low}} & (\mathrm{A/F})_{low} < (\mathrm{A/F}) < (\mathrm{A/F})_{high} \\ 0 & (\mathrm{A/F}) \leq (\mathrm{A/F})_{low} \end{cases} \tag{A.5}$$

$$\dot{\omega}_t = -\frac{1}{T_t}(\omega_t - t_m) \tag{A.6}$$

$$t_m = \eta_c u, \tag{A.7}$$

where the symbols are:

$(\mathrm{A/F})$	Air-to-fuel ratio, the ratio between the mass flow of air and fuel into the engine.
$(\mathrm{A/F})_{low}$	Lower air-to-fuel ratio for any combustion.
$(\mathrm{A/F})_{high}$	Lower air-to-fuel ratio for full combustion.
$(\mathrm{A/F})_n$	Air-to-fuel ratio at rated power and maximum turbocharger speed.
η_c	Combustion efficiency.
$m_{a,0}$	Ratio between the air flow into the engine when the turbocharger is at zero speed and when it is running at full speed.
ω_t	Per unit speed of the turbocharger.
T_t	Time constant of the turbocharger.

If the air-to-fuel ratio becomes lower than $(\mathrm{A/F})_{high}$, the torque drops, since less fuel is burned. Saturation is added to the fuel rate with the constraint that the air-to-fuel ratio should not go below $(\mathrm{A/F})_{high}$.

The damping due to friction and windage, can be expressed as (Skjetne; 2010):

$$t_D = D_f \omega \tag{A.8}$$

This can now be combined to:

$$2H\dot{\omega} = t_m - D_f\omega - t_e, \tag{A.9}$$

where t_e is the electrical torque, the torque from the generator.

Also define electrical rotor angle, θ, and mechanical rotor angle, θ_m:

$$\dot{\theta} = \omega\omega_b \tag{A.10}$$

$$\theta_m = \frac{2}{N}\theta, \tag{A.11}$$

where N is the number of poles in the generator.

A.2 Load Sharing

In this section a model for the electrical system is derived using complex-phasors form (Rizzoni; 2007). The values are all given in complex number, where the length denotes the root mean square (rms) value and the argument denotes the phase angles. The following equations are given under these assumptions:

1. The electrical system is in steady-state. This means that the frequencies of all generators are close and the electrical system is in a normal state (i.e., not short circuits).
2. The generators have round rotors.

Under these assumptions the equations for a generator in steady-state are given as (Krause et al.; 2002):

$$\tilde{E} = \omega V_f e^{j\delta} \tag{A.12}$$

$$\tilde{e} = \omega v_f e^{j\delta} \tag{A.13}$$

$$\tilde{V} = -\sqrt{3} Z \tilde{I}_{as} + \tilde{E}, \tag{A.14}$$

where the tilde denotes that the variables are given as complex phasors. The symbols denote:

δ	Load angle.
$\tilde{e}$	Per unit complex induced voltage.
$\tilde{E}$	Complex induced voltage.
$\tilde{I}_{as}$	Complex current out of stator winding a.
v	Per unit line-to-line bus voltage, absolute value.
$\tilde{V}$	Line-to-line complex bus voltage.
V_b	Base voltage.
v_f	Per unit field induced voltage.
V_f	Field induced voltage.
Z	Generator impedance.

The generator impedance is defined as:

$$Z = (R_s + j\omega X_s)z = r_s + jx_s, \tag{A.15}$$

where R_s/r_s is the resistance in the stators and X_s/x_s is the synchronous reactance.

The load angle is defined as:

$$\delta = \theta_i - \theta_0, \tag{A.16}$$

where θ_i is the electrical angle of genset i, from (A.10), and θ_0 is the electrical angle of the bus, which is found from load sharing.

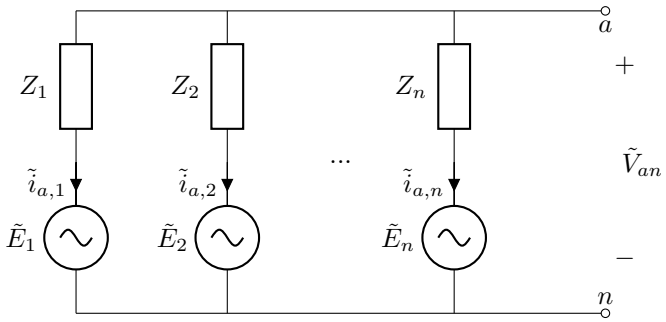

Figure A.1: Circuit diagram of phase a for the producer side of power plant with n gensets.

Equivalent Circuit

To analyze the circuit, the producer side of the circuit is rearranged to a Thévenin-equivalent circuit. The Thévenin-voltage is found by calculating the open-circuit voltage for the circuit shown in Figure A.1.

For each generator and phase the voltages are given from (A.14):

$$\tilde{E}_i - \sqrt{3} Z_i \tilde{I}_{as,i} = \tilde{V}_T, \tag{A.17}$$

where $\tilde{V}_T$ is the Thévenin-voltage. Since the circuit is open, the sum of current out of the gensets must be zero:

$$\sum \tilde{I}_{as,i} = 0. \tag{A.18}$$

Or in per unit:

$$\tilde{e}_i - \sqrt{3} z_i \tilde{i}_{as,i} = \tilde{v}_T \tag{A.19}$$

$$\sum \tilde{i}_{as,i} S_{b,i} = 0. \tag{A.20}$$

For a power plant with n generators, we get this system:

$$\begin{bmatrix} 0 & S_{b,1}/S_b & S_{b,2}/S_b & \dots & S_{b,n}/S_b \\ 1 & \sqrt{3} z_1 & 0 & \dots & 0 \\ 1 & 0 & \sqrt{3} z_2 & & 0 \\ \vdots & \vdots & & \ddots & \vdots \\ 1 & 0 & 0 & \dots & \sqrt{3} z_n \end{bmatrix} \begin{bmatrix} \tilde{v}_T \\ \tilde{i}_{as,1} \\ \tilde{i}_{as,2} \\ \vdots \\ \tilde{i}_{as,n} \end{bmatrix} = \begin{bmatrix} 0 \\ \tilde{e}_1 \\ \tilde{e}_2 \\ \vdots \\ \tilde{e}_n \end{bmatrix}. \tag{A.21}$$

where S_b and $S_{b,i}$ are base apparent power for respectively the bus and Genset i. This matrix can always be inverted, since each row cannot be written as a linear combination of the others. The Thévenin-voltage can therefore be found by solving the linear equations.

The Thévenin-impedance is found by nulling all sources ($\tilde{E}_{a,i} = 0$) in Figure A.1 and calculating the impedance of the remaining circuit. It is easy to see that the Thévenin-impedance must be:

$$Z_T = \left(\sum_i \frac{1}{Z_i} \right)^{-1}. \tag{A.22}$$

In per unit:

$$z_T = S_b \left(\sum_i \frac{S_{b,i}}{z_i} \right)^{-1}. \tag{A.23}$$

The impedance of the load can be calculated from the consumed active and reactive power, by assuming that the impedance doesn't change with change of voltage. Since the voltage is dependent on the impedance and the impedance is calculated from the voltage, the calculation of the impedance is done by using the voltage from the previous time step. The load impedance can therefore be found by:

$$P_{load} + jQ_{load} = \sqrt{3}\tilde{V}\tilde{I}^* \tag{A.24}$$

$$\tilde{I} = \frac{P_{load} - jQ_{load}}{\sqrt{3}\tilde{V}^*} \tag{A.25}$$

$$Z_L = \frac{\tilde{V}}{\sqrt{3}\tilde{I}} = \frac{\tilde{V}\tilde{V}^*}{P_{load} - jQ_{load}} = \frac{|\tilde{V}|^2}{P_{load} - jQ_{load}} \tag{A.26}$$

$$z_L = \frac{|\tilde{v}^2|}{p_{load} - jq_{load}}, \tag{A.27}$$

where P_{load}/p_{load} and Q_{load}/q_{load} are respectively the active and reactive power consumed by the loads. The asterisk denotes complex conjugate and Z_L/z_L is the equivalent impedance of all loads connected to the bus for each phase.

The current through each phase in the complete system can now be calculated as:

$$\frac{\tilde{V}_T}{\sqrt{3}} = (Z_T + Z_L)\tilde{I}_{as} \tag{A.28}$$

$$\tilde{I}_{as} = \frac{\tilde{V}_T}{\sqrt{3}(Z_T + Z_L)}, \tag{A.29}$$

and the bus voltage is:

$$\tilde{V} = \sqrt{3}Z_L\tilde{I}_{as} = \frac{Z_L}{Z_T + Z_L}\tilde{V}_T. \tag{A.30}$$

In per unit:

$$\tilde{v} = \frac{z_L}{z_T + z_L}\tilde{v}_T. \tag{A.31}$$

The current through Generator i can now be calculated, by using (A.14) and solve for $\tilde{I}_{as,i}$

$$\tilde{I}_{as,i} = \frac{\tilde{E}_i - \tilde{V}}{\sqrt{3}Z_i}. \tag{A.32}$$

The complex power delivered from Generator i is therefore:

$$S_i = \sqrt{3}\tilde{V}\tilde{I}^*_{as,i} = \tilde{V}\left(\frac{\tilde{E}_i - \tilde{V}}{Z_i}\right)^* \tag{A.33}$$

$$s_i = \tilde{v}\left(\frac{\tilde{e}_i - \tilde{v}}{z_i}\right)^*. \tag{A.34}$$

This can be divided into active power for Genset i, P_i/p_i, and reactive power, Q_i/q_i.

$$P_i = \mathrm{Re}(S_i) \tag{A.35}$$

$$p_i = \mathrm{Re}(s_i) \tag{A.36}$$

$$Q_i = \mathrm{Im}(S_i) \tag{A.37}$$

$$q_i = \mathrm{Im}(s_i). \tag{A.38}$$

A.3 Electrical Equations for Generator

A static model is used for the generator. From energy balance, the torque from the generator is:

$$T_e = \frac{P + P_{loss}}{\omega_m}, \tag{A.39}$$

where P is the power delivered from the generator and P_{loss} are the electrical losses in the generator.

The loss in the generator is mainly due to resistance in the stator windings:

$$P_{loss} = 3R_s|\tilde{I}_{as}|^2 = 3R_s\left(\frac{|\tilde{S}|}{\sqrt{3}|\tilde{V}|}\right)^2 = R_s\frac{S_b^2(p^2+q^2)}{V_b^2 v^2} = S_b r_s\frac{p^2+q^2}{v^2}, \tag{A.40}$$

The torque from the generator, is therefore:

$$T_e = \frac{P + P_{loss}}{\omega_m} = \frac{S_b}{\omega\omega_{m,b}}\left(p + r_s\frac{p^2+q^2}{v^2}\right) = \frac{1}{\omega}T_b\left(p + r_s\frac{p^2+q^2}{v^2}\right) \tag{A.41}$$

$$t_e = \frac{1}{\omega}\left(p + r_s\frac{p^2+q^2}{v^2}\right). \tag{A.42}$$

Next, k_u is defined such that $u = 1$ at rated values (i.e., $p = 1$, $v = 1$....) and zero reactive power:

$$k_u = 1 + D_f + r_s. \tag{A.43}$$

Appendix B

Linearization

In this appendix the linearized state space equations are derived. These equations are used in the model predictive control (MPC) controller as control plant model.

The goal of the linearization is to get a system on the form:

$$\boldsymbol{\Delta}\dot{\boldsymbol{x}} = A\boldsymbol{\Delta}\boldsymbol{x} + B\boldsymbol{\Delta}\boldsymbol{\omega}_{NL} + \boldsymbol{f}_k, \tag{B.1}$$

where the state vector and input vector are:

$$\boldsymbol{\Delta}\boldsymbol{x} = \begin{bmatrix} \Delta p_{bus} \\ \Delta q_{bus} \\ \Delta\phi_1 \\ \Delta\omega_1 \\ \Delta\xi_{\omega,1} \\ \Delta\xi_{v,1} \\ \vdots \\ \Delta\phi_n \\ \Delta\omega_n \\ \Delta\xi_{\omega,n} \\ \Delta\xi_{v,n} \end{bmatrix} \tag{B.2}$$

$$\boldsymbol{\Delta}\boldsymbol{\omega}_{NL} = \begin{bmatrix} \Delta\omega_{NL,1} & \dots & \Delta\omega_{NL,n} \end{bmatrix}^\top, \tag{B.3}$$

p_{bus} and q_{bus} are per unit (pu) active and reactive consumed power. ϕ_i is an angle and is defined in (4.17). $\xi_{\omega,i}$ and $\xi_{v,i}$ are integral values in the PID-controllers of the governor and Automatic Voltage Regulator (AVR).

This derivation is done by first finding the equations for the local controllers, the governors and AVRs. Then the state space equations for the genset are found, with no-load frequency and produced power as inputs. Next, is the produced power found as a function of the state variables. This function is inverted and

inserted into the state space equation, so that the only inputs to the state space equation are the no-load frequencies. Lastly the control outputs are found as a linear combination of the state variables and no-load frequencies.

B.1 Governor

As described in Section 4.2.2 is the governor an ideal PID-controller with droop. The equation for reference frequency, (2.2), are:

$$\omega_{ref,i} = \omega_{NL,i}(1 - \text{Droop}_i p_i). \tag{B.4}$$

The equations for an ideal PID-controller are:

$$e_i = \omega_{ref,i} - \omega_i \tag{B.5}$$
$$\dot{\xi}_i = e_i \tag{B.6}$$
$$u = K_{P,i}e + K_{I,i}\xi_i + K_{D,i}\dot{e}_i. \tag{B.7}$$

For simplicity the time derivative of the frequency error is approximated to:

$$\dot{e}_i \approx -\dot{\omega}_i. \tag{B.8}$$

This gives:

$$u = K_{P,i}e + K_{I,i}\xi_i + K_{D,i}\dot{\omega}_i. \tag{B.9}$$

Further the states are linearized to the form: $x(t) \approx \Delta x(t) + x(t_k)$. This gives:

$$\Delta\omega_{ref,i} = (1 - \text{Droop}_i p_i)|_{t=t_k}\Delta\omega_{NL,i} - \omega_{NL,i}\text{Droop}_i|_{t=t_k}\Delta p_i \tag{B.10}$$
$$\Delta e_i = \Delta\omega_{ref,i} - \Delta\omega_i \tag{B.11}$$
$$\Delta\dot{\xi}_i = \Delta e_i + e_i(t_k) \tag{B.12}$$
$$= \Delta\omega_{ref,i} - \Delta\omega_i + (\omega_{ref,i} - \omega_i)|_{t=t_k} \tag{B.13}$$
$$= (1 - \text{Droop}p_i)\Delta\omega_{NL,i} - \omega_{NL,i}\text{Droop}\Delta p_i - \Delta\omega_i + (\omega_{ref,i} - \omega_i)|_{t=t_k} \tag{B.14}$$
$$\Delta u_i = K_{P,i}\Delta e_i + K_{I,i}\Delta\xi_i - K_{D,i}\Delta\dot{\omega}_i \tag{B.15}$$
$$u_i(t) \approx u_i(t_k) + K_{P,i}\Delta e_i(t) + K_{I,i}\Delta\xi_i(t) - K_{D,i}\Delta\dot{\omega}_i(t). \tag{B.16}$$

B.2 Automatic Voltage Regulator

The AVR is modeled as a PI-controller, with droop. The per unit bus voltage at zero reactive power is set to unity. The droop curve is assumed to be constant.

The reference voltage is given by the droop equation:

$$v_{ref,i} = (1 - \text{Droop}_{AVR} q_i) \tag{B.17}$$
$$\Delta v_{ref,i} = -\text{Droop}_{AVR} \Delta q_i. \tag{B.18}$$

The equations for the AVR are:

$$e_{v,i} = v_{ref,i} - v \tag{B.19}$$
$$= 1 - \text{Droop}_{AVR} q_i - v \tag{B.20}$$
$$\dot{\xi}_{v,i} = 1 - \text{Droop}_{AVR} q_i - v \tag{B.21}$$
$$\Delta\dot{\xi}_{v,i} = -\text{Droop}_{AVR} \Delta q_i - \Delta v \tag{B.22}$$
$$v_{f,i} = K_{vP,i} e_{v,i} + K_{vI,i} \xi_{v,i} \tag{B.23}$$
$$\Delta v_{f,i} = K_{vP,i} \Delta e_{v,i} + K_{vI,i} \Delta \xi_{v,i} \tag{B.24}$$
$$\Delta v_{f,i} = K_{vP,i}(-\text{Droop}_{AVR} \Delta q_i - \Delta v) + K_{vI,i} \Delta \xi_{v,i}. \tag{B.25}$$

B.3 Genset

Combining the equations for genset, (A.9), (A.39), and (B.9), and solving for $\dot{\omega}$ gives:

$$\dot{\omega}_i = \frac{1}{2H_i}\left[- D_{f,i}\omega_i + k_u u - \frac{1}{\omega_i}\left(p_i + r_i \frac{p_i^2 + q_i^2}{v^2}\right)\right] \tag{B.26}$$
$$= \frac{1}{2H_i}\Bigg[- D_{f,i}\omega_i + k_u(K_P(\omega_{ref} - \omega_i) + K_I \xi - K_D \dot{\omega}) - \frac{1}{\omega_i}\left(p_i + r_i \frac{p_i^2 + q_i^2}{v^2}\right)\Bigg] \tag{B.27}$$
$$= \frac{1}{k_u K_D + 2H_i}\Bigg[(-D_{f,i} - k_u K_P)\omega_i + k_u K_P \omega_{ref} + k_u K_I \xi - \frac{1}{\omega_i}\left(p_i + r_i \frac{p_i^2 + q_i^2}{v^2}\right)\Bigg]. \tag{B.28}$$

Linearize the angular velocity with respect to the state variables, no-load frequency,

power, and voltage, gives:

$$\begin{aligned}\Delta\dot{\omega}_i \approx & \dot{\omega}_i(t_k) + \alpha_{\omega,i}\Delta\omega_i \\ & + h_i\Bigg[-\frac{1}{\omega_i}\left(1+2\frac{p_i r_i}{v^2}\right)\Delta p_i - \frac{2q_i r_i}{v^2\omega_i}\Delta q_i + 2r_i\frac{p_i^2+q_i^2}{\omega_i v^3}\Delta v \\ & + k_u K_p \Delta\omega_{ref} + k_u K_I \Delta\xi_{\omega i}\Bigg] \qquad \text{(B.29)} \\ = & \dot{\omega}_i|_{t=t_k} + \alpha_{\omega,i}\Delta\omega_i \\ & + h_i\Bigg[-\frac{1}{\omega_i}\left(1+2\frac{p_i r_i}{v^2}\right)\Delta p_i - \frac{2q_i r_i}{v^2\omega_i}\Delta q_i + 2r_i\frac{p_i^2+q_i^2}{\omega_i v^3}\Delta v \\ & + k_u K_p((1-p_i\text{Droop}_i)\Delta\omega_{NL,i} - \omega_{NL,i}\text{Droop}_i\Delta p_i) \\ & + k_u K_I \Delta\xi_{\omega i}\Bigg] \qquad \text{(B.30)} \\ = & \dot{\omega}_i(t_k) + \alpha_{\omega,i}\Delta\omega_i + \alpha_{p,i}\Delta p_i + \alpha_{q,i}\Delta q_i + \alpha_{v,i}\Delta v + k_p\Delta\omega_{NL,i} + k_I\Delta\xi_{\omega i}, \qquad \text{(B.31)}\end{aligned}$$

where the symbols are defined as:

$$h_i = \frac{1}{2H_i + k_u K_D} \qquad \text{(B.32)}$$

$$\alpha_{\omega,i} = h_i\left[-D_{f,i} + \frac{1}{\omega_i^2}\left(p_i + r_i\frac{p_i^2+q_i^2}{v^2}\right) - k_u K_p\right] \qquad \text{(B.33)}$$

$$\alpha_{p,i} = -\frac{h_i}{\omega_i}\left(1+2\frac{p_i r_i}{v^2}\right) - h_i k_u K_p \omega_{NL,i}\text{Droop}_i \qquad \text{(B.34)}$$

$$\alpha_{q,i} = -\frac{h_i}{\omega_i}\left(2\frac{q_i r_i}{v^2}\right) \qquad \text{(B.35)}$$

$$\alpha_{v,i} = 2\frac{h_i(p_i^2+q_i^2)r_i}{\omega_i v^3} \qquad \text{(B.36)}$$

$$k_{P,i} = h_i k_u K_P(1-p_i\text{Droop}_i) \qquad \text{(B.37)}$$

$$k_{I,i} = h_i k_u K_I. \qquad \text{(B.38)}$$

This can be arranged on the matrix form:

$$\boldsymbol{\Delta\dot{x}} = \tilde{A}\boldsymbol{\Delta x} + B\boldsymbol{\Delta\omega}_{NL} + \boldsymbol{f}_k + K\boldsymbol{\Delta p} \qquad \text{(B.39)}$$

For a case with two engines, the matrices and vectors are:

$$\boldsymbol{\Delta x} = \begin{bmatrix} \Delta p_{bus} \\ \Delta q_{bus} \\ \Delta \phi_1 \\ \Delta \omega_1 \\ \Delta \xi_{\omega,1} \\ \Delta \xi_{v,1} \\ \Delta \phi_2 \\ \Delta \omega_2 \\ \Delta \xi_{\omega,2} \\ \Delta \xi_{v,2} \end{bmatrix} \tag{B.40}$$

$$\boldsymbol{\Delta \omega}_{NL} = \begin{bmatrix} \Delta \omega_{NL,1} & \Delta \omega_{NL,2} \end{bmatrix}^\top \tag{B.41}$$

$$\boldsymbol{\Delta p} = \begin{bmatrix} \Delta \phi_0 & \Delta v & \Delta p_1 & \Delta q_1 & \Delta p_2 & \Delta q_2 \end{bmatrix}^\top \tag{B.42}$$

$$A = \begin{bmatrix} 0 & 0 & 0 & 0 & 0 & 0 & 0 & 0 & 0 & 0 \\ 0 & 0 & 0 & 0 & 0 & 0 & 0 & 0 & 0 & 0 \\ 0 & 0 & 0 & \frac{1}{2}\omega_b & 0 & 0 & 0 & -\frac{1}{2}\omega_b & 0 & 0 \\ 0 & 0 & 0 & \alpha_{\omega,1} & k_{I,1} & 0 & 0 & 0 & 0 & 0 \\ 0 & 0 & 0 & -1 & 0 & 0 & 0 & 0 & 0 & 0 \\ 0 & 0 & 0 & 0 & 0 & 0 & 0 & 0 & 0 & 0 \\ 0 & 0 & 0 & -\frac{1}{2}\omega_b & 0 & 0 & 0 & \frac{1}{2}\omega_b & 0 & 0 \\ 0 & 0 & 0 & 0 & 0 & 0 & 0 & \alpha_{\omega,2} & k_{I,2} & 0 \\ 0 & 0 & 0 & 0 & 0 & 0 & 0 & -1 & 0 & 0 \\ 0 & 0 & 0 & 0 & 0 & 0 & 0 & 0 & 0 & 0 \end{bmatrix} \tag{B.43}$$

$$B = \begin{bmatrix} 0 & 0 \\ 0 & 0 \\ 0 & 0 \\ k_{P,1} & 0 \\ (1 - \text{Droop}_1 p_1) & 0 \\ 0 & 0 \\ 0 & 0 \\ 0 & k_{P,2} \\ 0 & (1 - \text{Droop}_2 p_2) \\ 0 & 0 \end{bmatrix} \tag{B.44}$$

$$\boldsymbol{f}_k = \begin{bmatrix} 0 \\ 0 \\ \frac{1}{2}\omega_b(\omega_1 - \omega_2) \\ \dot{\omega}_1 \\ \omega_{ref,1} - \omega_1 \\ (1 - \text{Droop}_{AVR} q_1) - v \\ \frac{1}{2}\omega_b(-\omega_1 + \omega_2) \\ \dot{\omega}_2 \\ \omega_{ref,2} - \omega_2 \\ (1 - \text{Droop}_{AVR} q_2) - v \end{bmatrix} \tag{B.45}$$

$$K = \begin{bmatrix} 0 & 0 & 0 & 0 & 0 & 0 \\ 0 & 0 & 0 & 0 & 0 & 0 \\ 0 & 0 & 0 & 0 & 0 & 0 \\ 0 & \alpha_{v,1} & \alpha_{p,1} & \alpha_{q,1} & 0 & 0 \\ 0 & 0 & -\omega_{NL,1}\text{Dr}_1 & 0 & 0 & 0 \\ 0 & -1 & 0 & -\text{Dra} & 0 & 0 \\ 0 & 0 & 0 & 0 & 0 & 0 \\ 0 & \alpha_{v,2} & 0 & 0 & \alpha_{p,2} & \alpha_{q,2} \\ 0 & 0 & 0 & 0 & -\omega_{NL,2}\text{Dr}_2 & 0 \\ 0 & -1 & 0 & 0 & 0 & -\text{Dra} \end{bmatrix}, \tag{B.46}$$

where Droop = Dr and Dra = Droop_{AVR}.

B.4 Load Sharing

As mentioned in Section 4.2.6, the equations for load sharing are:

$$\sum_i p_i \frac{S_{b,i}}{S_b} = p_{bus} \tag{B.47}$$

$$\sum_i q_i \frac{S_{b,i}}{S_b} = q_{bus} \tag{B.48}$$

$$p_i = \frac{e_i v}{x_s \omega_i} \sin\delta_i = \frac{v_{f,i} v}{x_s} \sin\delta_i \tag{B.49}$$

$$q_i = \frac{v}{x_s}\left(v_{f,i}\cos\delta_i - \frac{v}{\omega_i}\right), \tag{B.50}$$

where v_f is field voltage. The linearization is done with respect to the variables in $\boldsymbol{\Delta p}$ and $\boldsymbol{\Delta x}$. First v_f is substituted by using equations from Section B.2. The load angle is substituted by using $\delta_i(t) = \phi_i(t) - \phi_0(t)$. For readability v_f is substituted back after linearization and the equations are written on matrix form. For a case

with two gensets, this gives:

$$E\boldsymbol{\Delta p} = F\boldsymbol{\Delta x} \tag{B.51}$$

$$E = \begin{bmatrix} 0 & 0 & S_{b1}/S_b & 0 & S_{b2}/S_b & 0 \\ 0 & 0 & 0 & S_{b1}/S_b & 0 & S_{b2}/S_b \\ \gamma_{Z,1} & \gamma_{v,1} & 1 & \gamma_{q,1} & 0 & 0 \\ \beta_{Z,1} & \beta_{v,1} & 0 & \beta_{q,1} & 0 & 0 \\ \gamma_{Z,2} & \gamma_{v,2} & 0 & 0 & 1 & \gamma_{q,2} \\ \beta_{Z,2} & \beta_{v,2} & 0 & 0 & 0 & \beta_{q,2} \end{bmatrix} \tag{B.52}$$

$$\boldsymbol{\Delta p} = \begin{bmatrix} \Delta\phi_0 & \Delta v & \Delta p_1 & \Delta q_1 & \Delta p_2 & \Delta q_2 \end{bmatrix}^\top \tag{B.53}$$

$$F = \begin{bmatrix} 1 & 0 & 0 & 0 & 0 & 0 & 0 & 0 & 0 & 0 \\ 0 & 1 & 0 & 0 & 0 & 0 & 0 & 0 & 0 & 0 \\ 0 & 0 & \gamma_{\phi,1} & 0 & 0 & \gamma_{\xi_v,1} & 0 & 0 & 0 & 0 \\ 0 & 0 & \beta_{\phi,1} & \beta_{\omega,1} & 0 & \beta_{\xi_v,1} & 0 & 0 & 0 & 0 \\ 0 & 0 & 0 & 0 & 0 & 0 & \gamma_{\phi,2} & 0 & 0 & \gamma_{\xi_v,2} \\ 0 & 0 & 0 & 0 & 0 & 0 & \beta_{\phi,2} & \beta_{\omega,2} & 0 & \beta_{\xi_v,2} \end{bmatrix} \tag{B.54}$$

$$\gamma_{Z,i} = \frac{v_{fi} v}{x_s} \cos(\delta_i) \tag{B.55}$$

$$\beta_{Z,i} = -\frac{v_{fi} v}{x_s} \sin(\delta_i) \tag{B.56}$$

$$\gamma_{v,i} = \frac{K_{vP} v - v_{fi}}{x_s} \sin(\delta_i) \tag{B.57}$$

$$\beta_{v,i} = -\frac{v_{fi}}{x_s} \cos(\delta_i) + \frac{2v}{\omega_i x_s} + \frac{v}{x_s} K_{vP} \cos(\delta_i) \tag{B.58}$$

$$\gamma_{q,i} = K_{vP} \text{Droop}_{AVR} \frac{v}{x_s} \sin(\delta_i) \tag{B.59}$$

$$\beta_{q,i} = 1 + \frac{v}{x_s} K_{vP} \text{Droop}_{AVR} \cos(\delta_i) \tag{B.60}$$

$$\gamma_{\phi,i} = v_{fi} \frac{v}{x_s} \cos(\delta_i) \tag{B.61}$$

$$\beta_{\phi,i} = -v_{fi} \frac{v}{x_s} \sin(\delta_i) \tag{B.62}$$

$$\beta_{\omega,i} = \frac{v^2}{x_s \omega_i^2} \tag{B.63}$$

$$\gamma_{\xi_v,i} = K_{vI} \frac{v}{x_s} \sin(\delta_i) \tag{B.64}$$

$$\beta_{\xi_v,i} = \frac{v}{x_s} K_{vI} \cos(\delta_i). \tag{B.65}$$

In the next section the inverse of E is needed, it is therefore important to know if E is invertible. It is hard to find the requirements for the matrix to be invertible. However, some special cases where it is not invertible are easy to spot.

- If the frequency droops to zero, multiple terms get singular, and the matrix becomes singular. Protection relays will make sure that this never occurs.

- If all the engines are at the pull-out torque ($\delta = 90°$), the matrix is singular. This is avoided by overload protection.
- If the bus voltage is zero, the matrix is singular. However, this is handled by under voltage protection.

Another approach is to look on the nonlinear equations, (B.47) to (B.50). It is clear that each equation cannot be written as a function of the others, even for the equations that are given for each generator, (B.49) and (B.50). It is also clear that there is a solution to the problem as long as:

- $|\delta| \neq 90°$ for any gensets.
- $\omega \neq 0$ for all genset.
- $v \neq 0$, this implies $v_f \neq 0$ for any gensets.

These are the same requirements as listed before.

During the case study it never did occur that E was singular and the power system in a physical state (i.e., within the limits of the protection relays). It seems therefore plausible that as long as the system is within the limits of the protection relays, E is invertible. However, a check of the singularity of E should be implemented, with a fail-to-safe if E is singular. A test of the determinant E can be the used and the fail-to-safe strategy can be to freeze the no-load frequency.

B.5 Complete State Space Equations

At last the mechanical and electrical system can be combined to a complete state space model. This is done by combining (B.1) and (B.51):

$$\boldsymbol{\Delta}\dot{\boldsymbol{x}} = \tilde{A}\boldsymbol{\Delta}\boldsymbol{x} + K\boldsymbol{\Delta}\boldsymbol{p} + B\boldsymbol{\Delta}\boldsymbol{\omega}_{NL} + \boldsymbol{f}_k \tag{B.66}$$

$$\boldsymbol{\Delta}\dot{\boldsymbol{x}} = (\tilde{A} + KE^{-1}F)\boldsymbol{\Delta}\boldsymbol{x} + B\boldsymbol{\Delta}\boldsymbol{\omega}_{NL} + \boldsymbol{f}_k \tag{B.67}$$

$$A = \tilde{A} + KE^{-1}F \tag{B.68}$$

$$\boldsymbol{\Delta}\dot{\boldsymbol{x}} = A\boldsymbol{\Delta}\boldsymbol{x} + B\boldsymbol{\Delta}\boldsymbol{\omega}_{NL} + \boldsymbol{f}_k \tag{B.69}$$

This means that the state space is only dependent of the no-load frequency.

B.6 Control Output

B.6.1 Mean Frequency

One of the control output is the electrical frequency, this is approximated to be the mean frequency of the gensets.

It is easily found by averaging the frequency from the state vector:

$$\bar{\omega}[k+i] = \bar{\omega}[k] + C_\omega \boldsymbol{\Delta x}[k+i] \tag{B.70}$$

$$C_\omega = \begin{bmatrix} 0 & 0 & 0 & 1/n & 0 & 0 & \dots & 0 & 1/n & 0 & 0 \end{bmatrix}. \tag{B.71}$$

B.6.2 Fuel rate

The other control output is fuel rate. The goal of this derivation is to find a equation for the fuel rate on this form:

$$\boldsymbol{u} = \boldsymbol{u}(t = t_k) + C_u \boldsymbol{x} + D_u \boldsymbol{\omega}_{NL}. \tag{B.72}$$

The power and time derivative of frequency are given from (B.39) and (B.51):

$$\boldsymbol{\Delta p} = H_{\Delta p} E^{-1} F \boldsymbol{\Delta x} \tag{B.73}$$

$$\boldsymbol{\Delta \dot{\omega}} - \boldsymbol{\Delta \dot{\omega}}|_{t=t_k} = H_{\dot{\omega}}(A \boldsymbol{\Delta x} + B \boldsymbol{\Delta \omega}_{NL}), \tag{B.74}$$

For a case with two gensets $H_{\Delta p}$ and $H_{\dot{\omega}}$ are:

$$H_{\Delta p} = \begin{bmatrix} 0 & 0 & 1 & 0 & 0 & 0 \\ 0 & 0 & 0 & 0 & 1 & 0 \end{bmatrix} \tag{B.75}$$

$$H_{\dot{\omega}} = \begin{bmatrix} 0 & 0 & 0 & 1 & 0 & 0 & 0 & 0 & 0 & 0 \\ 0 & 0 & 0 & 0 & 0 & 0 & 0 & 1 & 0 & 0 \end{bmatrix}. \tag{B.76}$$

Each term in PID-controller can now be derived. For a case with two gensets it becomes:

$$\boldsymbol{\Delta u} = \boldsymbol{\Delta u}_P + \boldsymbol{\Delta u}_I + \boldsymbol{\Delta u}_D \tag{B.77}$$

$$\boldsymbol{\Delta u}_P = K_P \boldsymbol{\Delta e} \tag{B.78}$$

$$= C_{u_P} \boldsymbol{\Delta x} + D_{u_P} \boldsymbol{\Delta \omega}_{NL} \tag{B.79}$$

$$C_{u_P} = -\operatorname{diag}(\boldsymbol{K_P \omega}_{NL} \mathbf{Droop}) H_{\Delta p} E^{-1} F - K_P H_{\Delta \omega} \tag{B.80}$$

$$H_{\Delta \omega} = H_{\dot{\omega}} \tag{B.81}$$

$$D_{u_P} = K_P \begin{bmatrix} (1 - p_1 \mathrm{Droop}_1) & 0 \\ 0 & (1 - p_2 \mathrm{Droop}_2) \end{bmatrix} \tag{B.82}$$

$$\boldsymbol{\Delta u}_I = K_I \boldsymbol{\Delta \xi} = C_{u_I} \boldsymbol{\Delta x} \tag{B.83}$$

$$C_{u_I} = K_I \begin{bmatrix} 0 & 0 & 0 & 0 & 1 & 0 & 0 & 0 & 0 & 0 \\ 0 & 0 & 0 & 0 & 0 & 0 & 0 & 0 & 1 & 0 \end{bmatrix} \tag{B.84}$$

$$\boldsymbol{\Delta u}_D = -K_D H_{\dot{\omega}} A \boldsymbol{\Delta x} - K_D H_{\dot{\omega}} B \boldsymbol{\Delta \omega}_{NL} \tag{B.85}$$

$$C_{u_d} = -K_D H_{\dot{\omega}} A \tag{B.86}$$

$$D_{u_d} = -K_D H_{\dot{\omega}} B \tag{B.87}$$

$$C_u = C_{u_P} + C_{u_I} + C_{u_D} \tag{B.88}$$

$$D_u = D_{u_P} + D_{u_D}. \tag{B.89}$$

Appendix C

Equations for MPC

In this chapter equations for the controller are presented. These equations are discrete, in contrast to those given in the previously appendixes, which are continuous. For simplicity the state matrices are now given for discrete time, with sampling frequency equal to the update frequency of the model predictive control (MPC) and zero-order hold element is used on the inputs.

C.1 Cost Function

Define output variable:

$$\boldsymbol{z}[k+i] = \begin{bmatrix} \bar{\omega}[k+i] \\ \boldsymbol{u}[k+i] \end{bmatrix} = \boldsymbol{z}[k] + C\boldsymbol{\Delta x}[k+i] + D\boldsymbol{\Delta\omega}_{NL}[k+i-1]. \tag{C.1}$$

Note that $\boldsymbol{u}$ is the fuel rate right before the change of no-load frequency. The input variable is:

$$\boldsymbol{\Delta\omega}_{NL}[k+i] = \begin{bmatrix} \omega_{NL,1}[k+i] & \dots & \omega_{NL,n}[k+i] \end{bmatrix}^\top. \tag{C.2}$$

The discrete state variables can be calculated by converting the state matrices given in (B.69) to discrete time. This is done with MATLABs `c2d` function which calculates the discrete matrices, with zero-order hold on the input, exactly within

machine precision. The states are then given as:

$$\Delta \boldsymbol{x}[k+1] = A\boldsymbol{\Delta x}[k] + B\boldsymbol{\Delta \omega}_{NL}[k] + \boldsymbol{f}_k \tag{C.3}$$

$$\Delta \boldsymbol{x}[k+2] = A\boldsymbol{\Delta x}[k+1] + B\boldsymbol{\Delta \omega}_{NL}[k+1] + \boldsymbol{f}_k \tag{C.4}$$

$$= A(\Delta \boldsymbol{x}[k] + B\boldsymbol{\delta \omega}_{NL}[k] + \boldsymbol{f}_k) + B(\boldsymbol{\delta \omega}_{NL}[k] + \boldsymbol{\delta \omega}_{NL}[k+1]) + \boldsymbol{f}_k \tag{C.5}$$

$$= A\Delta \boldsymbol{x}[k] + (A+I)B\boldsymbol{\delta \omega}_{NL}[k] + B\boldsymbol{\delta \omega}_{NL}[k+1] + (A+I)\boldsymbol{f}_k \tag{C.6}$$

$$\Delta \boldsymbol{x}[k+3] = A\boldsymbol{\Delta x}[k+2] + B\boldsymbol{\Delta \omega}_{NL}[k+2] + \boldsymbol{f}_k \tag{C.7}$$

$$= A\left[A\Delta \boldsymbol{x}[k] + (I+A)B\boldsymbol{\delta \omega}_{NL}[k] + B\boldsymbol{\delta \omega}_{NL}[k+1] + (A+I)\boldsymbol{f}_k\right] + B(\boldsymbol{\delta \omega}_{NL}[k] + \boldsymbol{\delta \omega}_{NL}[k+1] + \boldsymbol{\delta \omega}_{NL}[k+2]) + \boldsymbol{f}_k \tag{C.8}$$

$$= A^2\Delta \boldsymbol{x}[k] + (I+A+A^2)B\boldsymbol{\delta \omega}_{NL}[k] + (I+A)B\boldsymbol{\delta \omega}_{NL}[k+1] + B\boldsymbol{\delta \omega}_{NL}[k+2] + (I+A+A^2)\boldsymbol{f}_k \tag{C.9}$$

$$\Delta \boldsymbol{x}[k+i] = A^i\boldsymbol{\Delta x}[k] + \sum_{l=0}^{i-1}\sum_{j=0}^{i-l} A^j B\boldsymbol{\delta \omega}_{NL}[k+l] + \sum_{j=0}^{i} A^j \boldsymbol{f}_k. \tag{C.10}$$

The control output can now be rewritten to:

$$\boldsymbol{z}[k+i] = \boldsymbol{z}[k] + C\boldsymbol{\Delta x}[k+i] + D\boldsymbol{\Delta \omega}_{NL} \tag{C.11}$$

$$= \boldsymbol{z}[k] + CA^i\boldsymbol{\Delta x}[k] + C\sum_{j=0}^{i} A^j \boldsymbol{f}_k + C\sum_{l=0}^{i-1}\sum_{j=0}^{i-l} A^j B\boldsymbol{\delta \omega}_{NL}[k+l] + \sum_{j=0}^{i-1} D\boldsymbol{\delta \omega}_{NL}[k+j]. \tag{C.12}$$

The prediction for the complete prediction horizon can now be established on

matrix form:

$$\boldsymbol{Z}[k] = \Phi[k] + \Psi[k]\boldsymbol{\delta\Omega}_{NL}[k] \tag{C.13}$$

$$\Phi[k] = \begin{bmatrix} C \\ CA \\ CA^2 \\ \vdots \\ CA^m \end{bmatrix} \boldsymbol{\Delta x}[k] + \begin{bmatrix} 0 \\ C \\ C + CA \\ \sum_{i=0}^{2} CA^i \\ \vdots \\ \sum_{i=0}^{m-1} CA^i \end{bmatrix} \boldsymbol{f}_k + \begin{bmatrix} \boldsymbol{z}[k] \\ \boldsymbol{z}[k] \\ \boldsymbol{z}[k] \\ \vdots \\ \boldsymbol{z}[k] \end{bmatrix} \tag{C.14}$$

$$\Psi[k] = \begin{bmatrix} 0 & 0 & 0 & 0 & \dots & 0 \\ C & 0 & 0 & 0 & \dots & 0 \\ C + CA & C & 0 & 0 & \dots & 0 \\ \sum_{i=0}^{2} CA^i & C + CA & C & 0 & \dots & 0 \\ \vdots & \vdots & & \ddots & & \vdots \\ \sum_{i=0}^{m-2} CA^i & \sum_{i=0}^{m-3} CA^i & & \dots & C & 0 \\ \sum_{i=0}^{m-1} CA^i & \sum_{i=0}^{m-2} CA^i & & \dots & & C \end{bmatrix} B + \begin{bmatrix} 0 & 0 & \dots & 0 \\ D & 0 & \dots & 0 \\ \vdots & \ddots & \ddots & \vdots \\ D & \dots & D & 0 \\ D & \dots & D & D \end{bmatrix}. \tag{C.15}$$

The cost function, (5.1), can be written as:

$$\begin{aligned} J[k] = \sum_{i=0}^{\infty} \big[& (\boldsymbol{z}_d[k+i] - \boldsymbol{z}[k+i])^\top Q[i] (\boldsymbol{z}_d[k+i] - \boldsymbol{z}[k+i]) \\ & + \boldsymbol{\delta\omega}_{NL}[k+i] R[i] \boldsymbol{\delta\omega}_{NL}[k+i] \big] \end{aligned} \tag{C.16}$$

$$= \boldsymbol{Z}^\top \mathcal{Q} \boldsymbol{Z} + \boldsymbol{\delta\Omega}_{NL} \mathcal{R} \boldsymbol{\delta\Omega}_{NL}. \tag{C.17}$$

The vectors are:

$$\boldsymbol{Z}[k] = \begin{bmatrix} \boldsymbol{z}^\top[k] & \boldsymbol{z}^\top[k+1] & \dots & \boldsymbol{z}^\top[k+m] \end{bmatrix}^\top \tag{C.18}$$

$$\boldsymbol{\delta\Omega}_{NL} = \begin{bmatrix} \boldsymbol{\delta\omega}_{NL}[k] & \boldsymbol{\delta\omega}_{NL}[k+1] & \dots & \boldsymbol{\delta\omega}_{NL}[k+m-1] \end{bmatrix}^\top \tag{C.19}$$

$$\mathcal{Q} = \operatorname{diag}(Q[0], Q[1], \dots, Q[m]) \tag{C.20}$$

$$\mathcal{R} = \operatorname{diag}(R[0], R[1], \dots, R[m]). \tag{C.21}$$

Define the error:

$$\boldsymbol{\varepsilon}[k+i] = \boldsymbol{z}_d - \boldsymbol{z}[k+i] \tag{C.22}$$

$$\boldsymbol{E}[k] = \begin{bmatrix} \boldsymbol{\varepsilon}[k] & \boldsymbol{\varepsilon}[k+1] & \dots & \boldsymbol{\varepsilon}[k+m] \end{bmatrix}^\top \tag{C.23}$$

$$\boldsymbol{E}[k] = \boldsymbol{Z}_d - \Phi[k] - \Psi[k]\boldsymbol{\delta\Omega}_{NL}[k] \tag{C.24}$$

$$= \mathcal{T}[k] - \Psi[k]\boldsymbol{\delta\Omega}_{NL}[k]. \tag{C.25}$$

Insert (C.25) into (C.17), gives:

$$J = \boldsymbol{\delta\Omega}_{NL}^{\top}(\mathcal{R} + \Psi^{\top}\mathcal{Q}\Psi)\boldsymbol{\delta\Omega}_{NL} - 2\mathcal{T}^{\top}\mathcal{Q}\Psi\boldsymbol{\delta\Omega}_{NL} + \mathcal{T}^{\top}\mathcal{Q}\mathcal{T}^{\top}. \tag{C.26}$$

C.2 Constraints

In Section 5.2 and 5.3, the constraints are listed. These constraints can be written in matrix form for a case with two gensets:

$$\begin{bmatrix} u_{L,1} \\ u_{L,2} \\ -\infty \\ -\infty \\ \omega_L \\ -\infty \\ 0 \end{bmatrix} \leq \begin{bmatrix} 0 & 0 & 0 & 0 & 0 & 1 & 0 & 0 \\ 0 & 0 & 0 & 0 & 0 & 0 & 1 & 0 \\ 0 & -1 & 0 & 0 & 0 & 1 & 0 & 0 \\ 0 & 0 & -1 & 0 & 0 & 0 & 1 & 0 \\ 0 & 0 & 0 & 0 & 1 & 0 & 0 & 1 \\ 0 & 0 & 0 & 0 & -1 & 0 & 0 & 1 \\ 0 & 0 & 0 & 0 & 0 & 0 & 0 & 1 \end{bmatrix} \begin{bmatrix} \bar{\omega}[l-1] \\ u_1[l-1] \\ u_2[l-1] \\ e[l-1] \\ \bar{\omega}[l] \\ u_1[l] \\ u_2[l] \\ e[l] \end{bmatrix} \leq \begin{bmatrix} u_{U,1} \\ u_{U,2} \\ ud_{u,1} \\ ud_{u,2} \\ \infty \\ \omega_U \\ \infty \end{bmatrix}. \tag{C.27}$$

When air dependent fuel rate constraints are used, $du_{max,now}$ must be added to relevant elements.

These constraints are copied for each predicted time and stacked together. The constraints must also be written as a function of the optimization variables, this is done by using (C.13).

$$g_L \leq G\boldsymbol{Z}' \leq g_U \tag{C.28}$$

$$g_L \leq G(\Phi' + \Psi'\boldsymbol{\delta\Omega}'_{NL}) \leq g_U \tag{C.29}$$

$$g - G\Phi' \leq G\Psi'\boldsymbol{\delta\Omega}'_{NL} \leq g_U - G\Phi', \tag{C.30}$$

where:

$$\boldsymbol{Z}' = \begin{bmatrix} \boldsymbol{z}[k]^{\top} & \epsilon[k] & \dots & \boldsymbol{z}[k+m]^{\top} & \epsilon[k+m] \end{bmatrix}^{\top} \tag{C.31}$$

$$\boldsymbol{\delta\Omega}'_{NL} = \begin{bmatrix} \boldsymbol{\delta\omega}_{NL}[k]^{\top} & \epsilon[k] & \dots & \boldsymbol{\delta\omega}_{NL}[k+m-1]^{\top} & \epsilon[k+m-1] \end{bmatrix}^{\top}. \tag{C.32}$$

Ψ' is Ψ augmented with rows and columns with zeros connected to ϵ, except on the diagonal where ones are inserted. Similarly Φ' is Φ augmented with rows of zeros for the slack variable.

C.3 LQ Problem

The slack variables need to be added to the cost function as well. A cost for the slack variable is therefore added to $\mathcal{Q}$, such the new matrix becomes:

$$\mathcal{Q}' = \begin{bmatrix} Q & 0 & 0 & 0 & \dots & 0 & 0 \\ 0 & \rho & 0 & 0 & \dots & 0 & 0 \\ 0 & 0 & Q & 0 & \dots & 0 & 0 \\ 0 & 0 & 0 & \rho & \dots & 0 & 0 \\ \vdots & \vdots & \vdots & \vdots & \ddots & \vdots & \vdots \\ 0 & 0 & 0 & 0 & \dots & Q & 0 \\ 0 & 0 & 0 & 0 & \dots & 0 & \rho \end{bmatrix}. \tag{C.33}$$

The $\mathcal{R}$ matrix is augmented with columns and rows with zeros and $\mathcal{T}$ is augmented with rows of zeros, for the slack variable in a similar way.

The cost function becomes:

$$J = \boldsymbol{\delta\Omega}'^{\top}_{NL}(\mathcal{R}' + \Psi'^{\top}\mathcal{Q}'\Psi')\boldsymbol{\delta\Omega}'_{NL} - 2\mathcal{T}'^{\top}\mathcal{Q}'\Psi'\boldsymbol{\delta\Omega}'_{NL} + \mathcal{T}'^{\top}\mathcal{Q}'\mathcal{T}'^{\top}. \tag{C.34}$$

This combined with the constraints (C.30) give the linear quadratic problem to be solved by MATLAB. From the solution, $\boldsymbol{\delta\omega}_{NL}[k]$ are found and it is used as the new configurations of the governors.

C.4 Failure Tolerant

The response for the failure case is also calculated. To denote the variable connected to the failure case, subscript w is added. The case simulates that the disconnection happens at $k+1$, this means the *next* time for update of the MPC. The states at that instant are:

$$\boldsymbol{\Delta x}[k+1] = \boldsymbol{f}_k + B\boldsymbol{\delta\omega}_{NL}[k]. \tag{C.35}$$

To have a model that is fairly good, the model is linearized at the power level that settles after the Fast Load Reduction (FLR) has reduced the load. This gives:

$$\boldsymbol{\Delta x}_w[k+1] = C_{n2w}\boldsymbol{\Delta x}[k+1] + \begin{bmatrix} p_{FLR} \\ 0 \\ \vdots \\ 0 \end{bmatrix} \tag{C.36}$$

$$= C_{n2w}\boldsymbol{\Delta x}[k+1] + \boldsymbol{p}_{FLR}, \tag{C.37}$$

where p_{FLR} is the per unit reduction of consumed power and C_{n2w} is a conversion matrix from the normal state space to the failure case state space:

$$C_{n2w} = \begin{bmatrix} I^{(4(n-1)+2)\times(4(n-1)+2)} & 0^{4\times4} \\ 0^{4\times4} & 0^{4\times4} \end{bmatrix}. \tag{C.38}$$

The states right before the FLR reduces the load are:

$$\begin{aligned}\boldsymbol{\Delta x}_w^-(t_{k+1}+t_{FLR}) =& A_{FLR}^- \boldsymbol{\Delta x}_w[k+1] + B_{FLR}^- \boldsymbol{\Delta\omega}_{NL,w}[k+1] + \boldsymbol{f}_{k,FLR}^- \quad \text{(C.39)}\\ =& A_{FLR}^- C_{n2w}(B\boldsymbol{\delta\omega}_{NL}[k] + \boldsymbol{f}_k) + A_{FLR}^- \boldsymbol{p}_{FLR}\\ &+ B_{FLR}^- \boldsymbol{\Delta\omega}_{NL}[k+1] + \boldsymbol{f}_{k,FLR}^-, \quad \text{(C.40)}\end{aligned}$$

where subscript FLR and superscript minus denotes that it is valid for the period from the time where the genset tripped, till the FLR reduces the load. This means that A_{FLR}^- is the state transition matrix from the update instant where the genset tripped, to the instant right before the FLR decreases the load. Superscript plus denotes that is it valid from the time the FLR decreases the load to next update of no-load frequency. Figure C.1 illustrates when the different transition matrices are used.

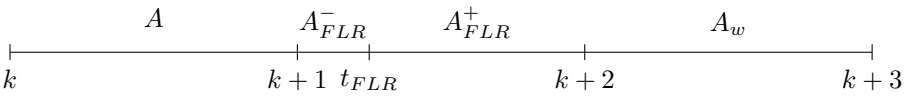

Figure C.1: Time line showing when the different state transition matrices should be used. Time k is the time when the MPC updates the no-load frequency, $k+1$ is the time when Genset 3 is predicted to disconnect. The load is reduces at t_{FLR}.

Right after the reduction of load the first element in the state vector is changed:

$$\boldsymbol{\Delta x}^+(t_{k+1}+t_{FLR}) = \boldsymbol{\Delta x}^-(t_k+t_{FLR}) - \boldsymbol{p}_{FLR}. \quad \text{(C.41)}$$

At the next time instant, the states are:

$$\begin{aligned}
\boldsymbol{\Delta x}_w[k+2] =& A^+_{FLR}\boldsymbol{\Delta x}^+_w(t_k+t_{FLR}) + B^+_{FLR}\boldsymbol{\Delta\omega}_{NL}[k] + \boldsymbol{f}^+_{k,FLR} \\
=& A^+_{FLR}(\boldsymbol{\Delta x}^-(t_k+t_{FLR}) - \boldsymbol{p}_{FLR}) \\
&+ B^+_{FLR}\boldsymbol{\Delta\omega}_{NL}[k+1] + \boldsymbol{f}^+_{k,FLR} && \text{(C.42)} \\
=& A^+_{FLR}\Big[A^-_{FLR}C_{n2w}(B\boldsymbol{\delta\omega}_{NL}[k] + \boldsymbol{f}_k) \\
&+ B^-_{FLR}\boldsymbol{\Delta\omega}_{NL}[k+1] + \boldsymbol{f}^-_{k,FLR} + (A^-_{FLR} - I)\boldsymbol{p}_{FLR}\Big] \\
&+ B^+_{FLR}\boldsymbol{\Delta\omega}_{NL}[k+1] + \boldsymbol{f}^+_{k,FLR} && \text{(C.43)} \\
=& A_w C_{n2w}(B\boldsymbol{\delta\omega}_{NL}[k] + \boldsymbol{f}_k) + A^+_{FLR}\boldsymbol{f}^-_{k,FLR} + \boldsymbol{f}^+_{k,FLR} \\
&+ (A_w - A^+_{FLR})\boldsymbol{p}_{FLR} \\
&+ (B^+_{FLR} + A^+_{FLR}B^-_{FLR})(\boldsymbol{\delta\omega}_{NL}[k] + \boldsymbol{\delta\omega}_{NL,w}[k+1]) && \text{(C.44)} \\
=& \boldsymbol{f}_{k,w} + A_w C_{n2w}\boldsymbol{f}_k + (A_w - A^+_{FLR})\boldsymbol{p}_{FLR} \\
&+ B_w(\boldsymbol{\delta\omega}_{NL}[k] + \boldsymbol{\delta\omega}_{NL,w}[k+1]) \\
&+ A_w C_{n2w}B\boldsymbol{\delta\omega}_{NL}[k] && \text{(C.45)} \\
=& \boldsymbol{f}_{k,w} + A_w C_{n2w}\boldsymbol{f}_k + (A_w - A^+_{FLR})\boldsymbol{p}_{FLR} \\
&+ (B_w + A_w C_{n2w}B)\boldsymbol{\delta\omega}_{NL}[k] + B_w\boldsymbol{\delta\omega}_{NL,w}[k+1]. && \text{(C.46)}
\end{aligned}$$

Note that:

$$A_w = A^+_{FLR}A^-_{FLR}. \tag{C.47}$$

At the next steps the states are:

$$\boldsymbol{\Delta x}_w[k+i] = A_w\boldsymbol{\Delta x}[k+i-1] + B_w\boldsymbol{\Delta\omega}_{NL}[k+i-1] + \boldsymbol{f}_{k,w}. \tag{C.48}$$

For the first two time steps (k and $k+1$) control outputs are equal for both cases,

they are therefore not included. The z variables are:

$$\boldsymbol{z}_w[k+i] = \boldsymbol{z}_w[k] + C_w \boldsymbol{\Delta x}_w[k+i] + D\boldsymbol{\Delta\omega}_{NL,w}[k+i] \tag{C.49}$$

$$\boldsymbol{Z}_w[k] = \begin{bmatrix}\boldsymbol{z}_w^\top[k+2] & \boldsymbol{z}_w^\top[k+3] & \dots \boldsymbol{z}_w^\top[k+m]\end{bmatrix}^\top \tag{C.50}$$

$$= \Phi_w[k] + \Psi_w[k]\boldsymbol{\delta\Omega}_{NL,w}[k] \tag{C.51}$$

$$= \begin{bmatrix} C_w A_w \\ C_w A_w^2 \\ \vdots \\ C_w A_w^{m-1} \end{bmatrix} \boldsymbol{\Delta x}[k+1] + \begin{bmatrix} C_w \\ C_w + C_w A_w \\ \sum_{i=0}^{2} C_w A_w^i \\ \vdots \\ \sum_{i=0}^{m-2} C_w A_w^i \end{bmatrix} \boldsymbol{f}_{k,w} + \begin{bmatrix} \boldsymbol{z}[k] \\ \boldsymbol{z}[k] \\ \boldsymbol{z}[k] \\ \vdots \\ \boldsymbol{z}[k] \end{bmatrix}$$

$$+ D\boldsymbol{\delta\omega}_{NL}[k] + D\boldsymbol{\delta\omega}_{NL,w}[k+1] + \hat{\Psi}_w[k+2]\boldsymbol{\delta\hat{\Omega}}_{NL,w}[k+2] \tag{C.52}$$

$$= \begin{bmatrix} C_w A_w \\ C_w A_w^2 \\ \vdots \\ C_w A_w^{m-1} \end{bmatrix} (\boldsymbol{f}_{k,w} + A_w C_{n2w} \boldsymbol{f}_k + (A_w - A_{FLR}^+)\boldsymbol{p}_{FLR} \tag{C.53}$$

$$+ (B_w + A_w C_{n2w} B)\boldsymbol{\delta\omega}_{NL}[k] + B_w \boldsymbol{\delta\omega}_{NL,w}[k+1]) \tag{C.54}$$

$$+ \begin{bmatrix} C_w \\ C_w + C_w A_w \\ \sum_{i=0}^{2} C_w A_w^i \\ \vdots \\ \sum_{i=0}^{m-2} C_w A_w^i \end{bmatrix} + \begin{bmatrix} \boldsymbol{z}[k] \\ \boldsymbol{z}[k] \\ \boldsymbol{z}[k] \\ \vdots \\ \boldsymbol{z}[k] \end{bmatrix}$$

$$+ D\boldsymbol{\delta\omega}_{NL,w}[k] + \hat{\Psi}_w[k+2]\boldsymbol{\delta\hat{\Omega}}_{NL,w}[k+2], \tag{C.55}$$

where $\hat{\Psi}_w$ is the Ψ matrices for dependency between $\boldsymbol{\delta\omega}_{NL,w}$ and $\boldsymbol{z}$ from $k+2$ to $k+m$. This mean that it corresponds to (C.15) but with the matrices for the failure case and for only $m-2$ steps.

$$\boldsymbol{\delta\hat{\Omega}}_{NL,w} = \begin{bmatrix}\boldsymbol{\delta\omega}_{NL,w}[k+2]^\top & \boldsymbol{\delta\omega}_{NL,w}[k+3]^\top & \dots & \boldsymbol{\delta\omega}_{NL,w}[k+m-1]^\top\end{bmatrix}^\top. \tag{C.56}$$

The matrices can now be rearranged to:

$$\begin{aligned}\Phi_w[k] = &\begin{bmatrix} C_wA_w \\ C_wA_w^2 \\ \vdots \\ C_wA_w^{m-1} \end{bmatrix} C_{n2w}\boldsymbol{f}_k + \begin{bmatrix} C_w \\ C_wA_w \\ C_wA_w^2 \\ \vdots \\ C_wA_w^{m-2} \end{bmatrix} (A_w - A_{FLR}^+)\boldsymbol{p}_{FLR} \\ &+ \begin{bmatrix} C_w \\ C_w + C_wA_w \\ \sum_{i=0}^{2} C_wA_w^i \\ \vdots \\ \sum_{i=0}^{m-1} C_wA_w^i \end{bmatrix} \boldsymbol{f}_{k,w} + \begin{bmatrix} \boldsymbol{z}[k] \\ \boldsymbol{z}[k] \\ \boldsymbol{z}[k] \\ \vdots \\ \boldsymbol{z}[k] \end{bmatrix}\end{aligned} \tag{C.57}$$

$$\begin{aligned}\Psi_w[k] = &\begin{bmatrix} C_w & C_w & 0 & 0 & \dots & 0 \\ \sum_{i=0}^{1} C_wA_w^i & \sum_{i=0}^{1} C_wA_w^i & C_w & 0 & \dots & 0 \\ \vdots & & & \ddots & \ddots & \vdots \\ \sum_{i=0}^{m-2} C_wA_w^i & \sum_{i=0}^{m-2} C_wA_w^i & \sum_{i=0}^{m-3} C_wA_w^i & \dots & C_w & 0 \\ \sum_{i=0}^{m-1} C_wA_w^i & \sum_{i=0}^{m-1} C_wA_w^i & \sum_{i=0}^{m-2} C_wA_w^i & \dots & & C_w \end{bmatrix} B_w \\ &+ \begin{bmatrix} C_wA_wC_{n2w}B & 0 & \dots & 0 \\ C_wA_w^2C_{n2w}B & 0 & \dots & 0 \\ & \vdots & & \\ C_wA_w^mC_{n2w}B & 0 & \dots & 0 \end{bmatrix} \\ &+ \begin{bmatrix} D_w & D_w & 0 & & \dots & 0 \\ D_w & D_w & D_w & 0 & \dots & 0 \\ \vdots & & & \ddots & \ddots & \vdots \\ D_w & D_w & & \dots & D_w & 0 \\ D_w & D_w & & \dots & D_w & D_w \end{bmatrix}\end{aligned} \tag{C.58}$$

$$\boldsymbol{\delta\Omega}_{NL,w}[k] = \begin{bmatrix} \boldsymbol{\delta\omega}_{NL}[k] \\ \boldsymbol{\delta\omega}_{NL,w}[k+1] \\ \boldsymbol{\delta\omega}_{NL,w}[k+2] \\ \dots \\ \boldsymbol{\delta\omega}_{NL,w}[k+m-1] \end{bmatrix}. \tag{C.59}$$

Note that the first matrix in Ψ_w is two matrices multiplied. The notation is a bit incorrect, what is meant is that each sub matrix should be multiplied with B_w. The notation is used to fit the equation into the page.

The matrices and vectors are further augmented with slack variables. Nest the matrices and vectors for the normal case and failure case are stacked together. Note that the first control inputs are equal for both cases, so the first columns of

the Ψ matrices are stacked, while the rest are put on the block diagonal:

$$\Psi = \begin{bmatrix} \Psi_1 & \Psi_{2-n} \end{bmatrix} \tag{C.60}$$

$$\Psi_{tot} = \begin{bmatrix} \Psi_{normal,1} & \Psi_{normal,2-n} & 0 \\ \Psi_{failure,1} & 0 & \Psi_{failure,2-n} \end{bmatrix}. \tag{C.61}$$

C.4.1 Load Sharing After Disconnection

Right after the disconnection of Genset 3 a new load sharing will take place. The load sharing is calculated from the equations given in Section 5.4.2. However, the field voltage and load angles must also be calculated. This is done by using the equation for load sharing that is used in the process plant (see Section A.2).

From (A.34)

$$\tilde{s}_i = \tilde{v} \left(\frac{\tilde{e}_i - \tilde{v}}{z_i} \right)^*. \tag{C.62}$$

Solve for $\tilde{e}_i$ gives:

$$\tilde{e}_i = \frac{\tilde{s}_i^*}{\tilde{v}^*} z_i + \tilde{v}. \tag{C.63}$$

The field voltage and load angle is given by (A.13):

$$v_{f,i} = \frac{\text{abs}(\tilde{e}_i)}{\omega_i} \tag{C.64}$$

$$\delta_i = \arg(\tilde{e}_i). \tag{C.65}$$